UNIVERSITÀ DEGLI STUDI DI MILANO
DIPARTIMENTO DI FISICA

CORSO DI DOTTORATO DI RICERCA IN
FISICA, ASTROFISICA E FISICA APPLICATA
CICLO XXVIII

Effects of spin value and topology on the spin dynamics of antiferromagnetic molecular rings unravelled by ^{1}H NMR

Settore Scientifico disciplinare <FIS/03>

Tesi di Dottorato di:

Fatemeh Adelnia

Supervisore: Prof. Alessandro Lascialfari

Coordinatore: Prof. Francesco Ragusa

A.A. 2015-2016

Commission of the final examination:

External Referee:
Prof. Paolo Santini

External Member:
Prof. Pietro Carretta

External Member:
Prof. Alberto Parola

Final examination:
May 13th 2016
Dipartimento di Fisica, Università degli Studi di Milano, Milano, Italy.

To my parents;

My Mam and My Dad ...

Cover illustration:
The Molecular structure of “open” and “closed” Antiferromagnetic rings, in a background of the NMR apparatus.

Design:
This document was typed by using Microsoft Word 2010.

MIUR subjects:
FIS/03

PACS:
75.50.Xx, 76.60.Es, 76.60.-k, 76.90.+d

Contents

Overview and Introduction

It was the early 90's when chemists discovered the interesting properties of molecular compounds comprising a finite number of magnetic ions and characterized by a ground state with S = 10, the so called Mn_{12} [1-3] and Fe_8 [4]. These systems present a regular arrangement of a finite number of metallic atoms surrounded by an organic shell, which prevents the magnetic interaction between different molecules thus allowing the study of single molecule magnetic properties. For this reason this family of molecules is called Single Molecule Magnets (SMMs). Due to their mesoscopic size, they are placed among individual spins and multidomain magnetic particles (Figure 1), a condition that attracted the attention of the scientific community since their early discovery.

The first important phenomenon showed by these molecules was the slow relaxation of the magnetization at low temperature due to their superparamagnetism, with a typical relaxation time of the order of months at 2 K. As a consequence, at these temperatures, if a single molecule is magnetized by an applied field it retains the magnetization for days and a magnetic hysteresis arises, important condition for storing information in a particle. A further scientific interest in these systems arose from the occurrence of quantum effects, like the quantum tunneling of the magnetization (QTM) [5-8] observed at very low temperature where the classical reversal of the magnetization through the energy barrier, typical of superparamagnetic systems, is prohibited.

Another class of molecular magnets that stimulated the scientific community, was the one of high-symmetry antiferromagnetic (AFM) rings that, once connected by different moieties containing metal ions, have been proposed as quantum devices for quantum information processing.

Nowadays, chemists are able to prepare a great variety of molecular clusters with a good control of the most important physical parameters [9-13]:

1) the total spin value of the cluster, ranging from high "classical" values down to low "quantum" ones, with dominating exchange interactions among different magnetic ions like Fe^{3+} and Mn^{2+} (s = 5/2), Mn^{3+} (s = 2), Cr^{3+} and Mn^{4+} (s = 3/2), V^{3+} (s = 1), Cu^{2+} and V^{4+} (s = 1/2);
2) the kind of exchange interaction, which can be Ferromagnetic (FM) or Antiferromagnetic (AFM) with an exchange coupling constant J value going from few Kelvin up to 1000 K;
3) the spin topology of the magnetic core of the molecule, going from highly symmetric like in AFM rings or clusters like Fe_{30} to low symmetry like Fe_8.

4) the form of the spin Hamiltonian resulting from all the above reported properties. Here the exchange interaction can be of isotropic Heisenberg type, easy axis or easy plane, and the anisotropic terms derives from single ion and/or dipolar-induced local anisotropy.

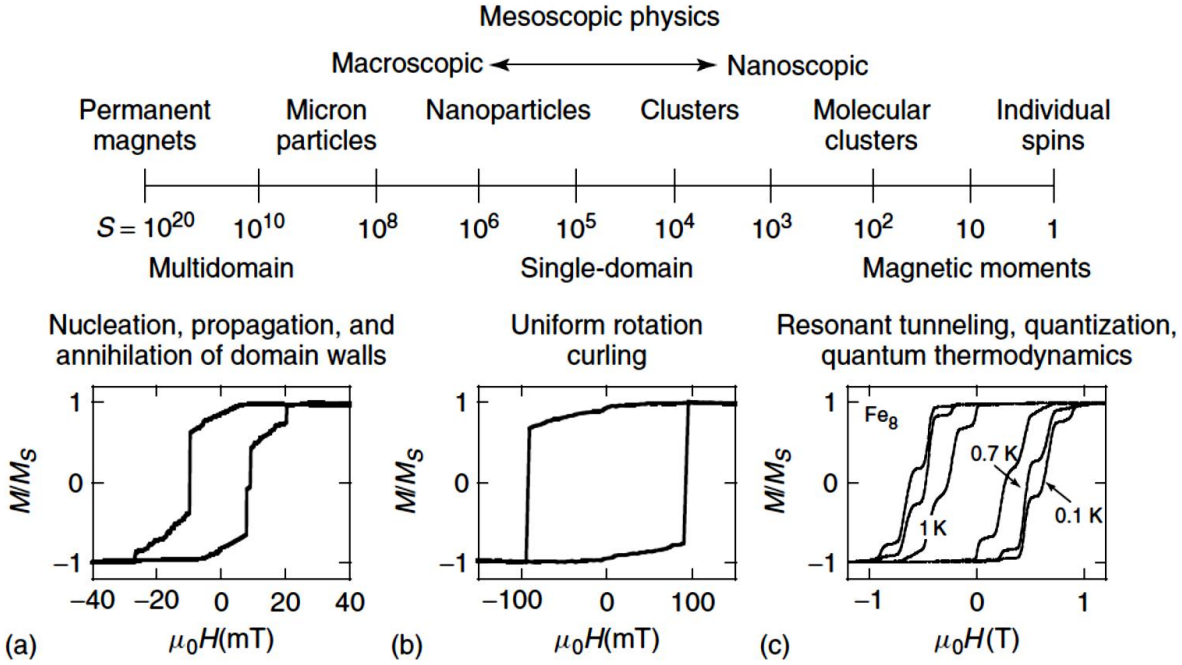

Figure 1: Scale of systems' size, from macroscopic down to nanoscopic one. The scale unit is the number of magnetic moments in a magnetic system (roughly correspond to the number of atom). The hysteresis loops show typical examples of magnetization reversal via nucleation, propagation, and annihilation of domain walls (a), via uniform rotation (b), and via quantum tunneling (c) [14].

The possibility to control the physical properties of a great variety of compounds allowed scientists to study many fundamental problems in magnetism like the transition from quantum to classical behavior, the effects of spin topology, the discrete energy levels structure, and new quantum phenomena like the above-mentioned quantum resonant tunneling of the magnetization, the Berry phase and the tunneling of the Neel vector [15-18]

The phenomena observed in SMMs are mainly investigated by using the superconducting quantum interference device (SQUID), Neutron Scattering, the synchrothron light sources, light/IR spectroscopies, Magnetic Resonance (MR) techniques and so on. Among different MR techniques, Electron Spin Resonance and Nuclear Magnetic Resonance (NMR) have been proved to be a very successful tool in addressing some special features in low dimensional magnetic systems and particularly SMMs [19].

The experimental results regarding the temperature and field behavior of the main NMR parameters for different MNMs, can be analyzed by looking at three different temperature regimes [19]. These regimes could be established by evaluating the ratio among the thermal energy k_BT and the exchange coupling constant J, i.e. k_BT/J. In the high temperature regime, i.e. $k_BT >> J$, the individual spin

moments in the molecule behave as almost independent/weakly correlated paramagnetic ions. In the low temperature regime, $k_BT << J$, the individual spin moments are locked into a collective quantum state characterized by a total spin S. In the intermediate temperature regime, i.e. $k_BT \sim J$, the individual spins start to develop strong correlations in a way similar to what happen for magnetic phase transitions in three dimensional systems.

In this thesis we focus on a subgroup of molecular magnets, the so called Antiferromagnetic (AFM) molecular rings, and their spin dynamics in different temperature regions. As the name itself suggest, in general AFM rings are constituted by molecules with a highly symmetric magnetic core composed of an even or odd number of uniformly spaced paramagnetic metal ions arranged in a planar ring. The interest for studying the AFM rings lies in the fact that they can be used in several applications such as the olefin polymerization catalysis, the magnetic regrigeration and quantum computing [14, 17]. Here, in particular, we study: (a) semi-integer spin Cr-based AFM rings, namely Cr_8, Cr_9, Cr_8Zn, and Cr_7Cd; (b) integer spin V-based AFM rings, namely V_7Ni and V_7Zn.

The outline of the thesis is the following:

Chapter 1 In the first part of chapter 1, the spin Hamiltonian approach used to describe the magnetic properties of AFM rings, is presented. In the second part, an introduction to the semi-integer spin Cr-based AFM rings is presented with a particular attention to the quantum "energy level crossing" phenomenon, whose effects are evidenced at low temperature. The last part of chapter 1 is devoted to integer-spin AFM rings and their magnetic properties.

Chapter 2 In this chapter the Nuclear Magnetic Resonance (NMR) technique is introduced along with the physical quantities that one can study, such as the absorption spectra and the spin-lattice and spin-spin relaxation rates. Theoretical models, included semi-phenomenological ones, are then introduced in order to explain the temperature and field dependence of the experimental data presented in Chapter 3.

Chapter 3 New experimental NMR data for both integer and semi-integer spin AFM rings are presented, along with an interpretation of the results by using the theoretical models previously discussed in chapter 2.

Chapter 4 The conclusions reached after the theoretical analysis of the experimental data are here summarized.

Finally, it should be noted that the NMR results on semi-integer spin AFM rings presented in this thesis are reported mostly in published papers (both in recent papers involving the author of the thesis and in previous papers by different authors), while the NMR results on integer spin AFM rings are presented in this thesis for the first time and are unpublished. This justifies the fact that the data analyses are often incomplete and qualitative. A quantitative analysis in collaboration with theorists is planned for the next future.

1. Molecular Antiferromagnetic (AFM) rings

Molecular Antiferromagnetic (AFM) rings are a particular subgroup of Molecular NanoMagnets (MNMs), which are formed by a set of N transition-metal ions arranged in an almost cyclic coplanar structure and interacting mainly via strong nearest-neighbor antiferromagnetic exchange interaction, J. These complexes are classified in two categories: the first one is called homometalic rings and contains just one type of magnetic ion; the second one, called heterometalic rings, are composed of different kinds of magnetic and/or nonmagnetic ions.

A prototype of AFM ring with the general formula $[M_8F_8(OOC^tBu)_{16}]$, was reported by the Molecular Magnetism group in Manchester in 1990 [1]. Starting by a homometallic ring structure, namely Cr_8, and by substituting different metallic ions in place of the transition metal magnetic ions, one can manipulate the spin dynamics and the physical properties like e.g. the exchange interaction constant J [2], and the local anisotropy. Normally, homometallic AFM rings with even number of magnetic ions have a singlet magnetic ground state with total spin $S_T = 0$. On the other hand, some heterometalic rings, due to an incomplete cancellation of spin moments, result in non-zero ground state ($S_T \neq 0$), a circumstance which is of particular interest since they could be used as qubits for quantum information processing [3].

A more recent use of rings is in the generation of supra-molecular assemblies where long organic molecules are threaded through the center of one or more rings [4, 5]. These so-called rotaxanes are of huge interest to chemists working in the field of bottom-up molecular machines. Recently, a new generation of AFM rings has been synthesized by replacing the trivalent Chromium (III) metal with other metals, like e.g. vanadium (III), iron (III), aluminum (III) and gallium (III). Given the large anisotropy expected in octahedral Vanadium (III), the rings including V(III) ions are particularly interesting for the study of the effects of local anisotropies and exchange interactions on the magnetic properties of the system. In addition to that, integer spin systems formed by V^{3+} (s = 1) magnetic ions can be considered a model system to study a spin-1 Haldane "finite" system, although it is thought that the Haldane behavior fully emerges for a number of interacting ions greater than 10-12.

In this chapter we first present the Hamiltonian of AFM rings in section 1.1. Then we introduce selected AFM rings that are studied in this manuscript showing their structure, magnetic properties and energy levels diagram.

1.1 Spin Hamiltonian

The formalism needed to describe the magnetic properties of AFM rings, makes use of the spin Hamiltonian approach. It is worth noticing that the spin Hamiltonian approach eliminates all the orbital coordinates needed to define the system, and replaces them with spin coordinates, taking advantage of the symmetry properties of the system [6]. The spin Hamiltonian can be expressed as:

$$\mathcal{H} = \mathcal{H}_{ex} + \mathcal{H}_{cf} + \mathcal{H}_{dip} + \mathcal{H}_{hf} + \mathcal{H}_{z} \tag{1.1}$$

The first term is the Heisenberg exchange interaction. The formal expression for this interaction is given by:

$$\mathcal{H}_{ex} = -\sum_{i>j} J_{ij} \boldsymbol{s}_i \cdot \boldsymbol{s}_j \tag{1.2}$$

where $J_{ij}$is the exchange parameter and can take positive or negative value depending on the type of interaction ($J > 0$ for ferromagnetic and $J < 0$ for antiferromagnetic). $\mathbf{s}_i$ and $\mathbf{s}_j$ are the spins of an isolated magnetic ion in the ring. Since the magnitude of J_{ij} decreases quite rapidly with the distance between the sites i and j, only the nearest neighboring pairs are generally taken into account. Consequently the exchange Hamiltonian can be reduced to

$$\mathcal{H}_{ex} = -\sum_{i=1}^{N} J_i \boldsymbol{s}_i \cdot \boldsymbol{s}_{i+1} \tag{1.3}$$

where only the first-neighbor interactions are considered, N is the number of magnetic ions in the spin system and $N + 1 \equiv 1$ for periodic boundary conditions. The second term in Equation (1.1) is the crystal field (cf) Hamiltonian. This Hamiltonian describes the breaking of degeneracy of electron states due to possible interactions between the electronic orbitals of the magnetic ions (d-orbitals in the case of transition metal ions) and a surrounding charge distribution, e.g. ligands. The leading interactions are second-order in the spin components and can be expressed as

$$\mathcal{H}_{cf} = \sum_{i=1}^{N} \boldsymbol{s}_i \cdot \widetilde{\boldsymbol{D}}_i \cdot \boldsymbol{s}_i \tag{1.4}$$

where D is a real symmetric tensor called fine structure tensor or zero field splitting tensor. In fact, in the strong-exchange limit the crystal field Hamiltonian is responsible for splitting of the (2S+1) degenerate level of the total-spin multiplet, in the absence of an external magnetic field. Equation (1.4) can also be rewritten as the sum of an axial and a rhombic term:

$$\mathcal{H}_{cf} = \sum_{i=1}^{N} \boldsymbol{s}_i \cdot \widetilde{\boldsymbol{D}}_i \cdot \boldsymbol{s}_i = \sum_{i=1}^{N} \left\{ d_i \left[s_{zi}^2 - \frac{s_i(s_i+1)}{3} \right] + e_i \left[s_{ix}^2 - s_{iy}^2 \right] \right\} \tag{1.5}$$

where d_i and e_i are the local axial and rhombic cf parameters, respectively. Since the rhombic parameters are negligible in the cyclic molecule, the first term of Equation (1.5) well approximate the crystal field Hamiltonian for AFM rings. The local anisotropy axis z can be assumed to be the same on all ions, and it is typically perpendicular to the ring plane.

The $\mathcal{H}_{dip}$ term in Equation (1.1) represents the magnetic dipolar interaction. This interaction in classical form is given by

$$\mathcal{H}_{dip} = \frac{g^2\mu_B^2}{2}\sum_{i>j}\left[\frac{(\boldsymbol{s}_i \cdot \boldsymbol{s}_j)}{r_{ij}^3} - 3\frac{(\boldsymbol{s}_i \cdot \boldsymbol{r}_{ij})(\boldsymbol{s}_j \cdot \boldsymbol{r}_{ij})}{r_{ij}^5}\right] \tag{1.6}$$

where $\mathbf{r}_{ij}$ is the vector connecting spins i-th and j-th. The term $\mathcal{H}_{hf}$, in Equation (1.1), is called hyperfine contribution and this is the most important interaction in NMR. Generally any type of magnetic interaction between nuclei and electrons are known as hyperfine interactions. These interactions are named direct hyperfine interactions in the case of magnetic moments belonging to the same atom, and transferred hyperfine interactions in the case of nuclear and electron magnetic moments belonging to different atoms. Their origin is rather complex, but the essential principle can be understood in the following way [7]. Consider a nuclear magnetic moment $\boldsymbol{\mu}$ which sits in a magnetic field $B_{electron}$ which is produced by the motion and the spins of all the electrons. This produces an energy term $\boldsymbol{\mu}\cdot\mathbf{B}_{electron}$ and is expected to be proportional to the total angular momentum of all the electrons, **S** in our case. Therefore, more generally the Hamiltonian for the hyperfine interaction can be written as

$$\mathcal{H}_{hf} = \sum_{ij} \boldsymbol{I}_i \cdot \widetilde{\boldsymbol{A}}_{ij} \cdot \boldsymbol{s}_j \tag{1.7}$$

where $\boldsymbol{I}$ is the nuclear angular momentum and A is an interaction tensor called "Hyperfine interaction tensor". The precise form of the hyperfine interaction is complicated in a complete system. However, in general, Equation (1.7) is given by the sum of two[1] different contributions, namely the contact and the dipolar term. The contact term is given by the electron spin density on the magnetic nucleus, and the dipolar term is given by the magnetic dipolar interaction between the electron and the nuclear spins (see Equation (1.5) and section 2.3). These interactions lead to energy levels splittings in absence of external magnetic field, which are even smaller than the fine structure due to spin-orbit interaction.

Finally, the last term $\mathcal{H}_z$ in Equation (1.1) represents the Zeeman interaction. The Zeeman effect is characterized by the splitting of the S-multiplets by an applied magnetic field. In the Spin Hamiltonian approach, the Zeeman interaction is given by:

$$\mathcal{H}_z = \mu_B \sum_{i=1}^{N} \boldsymbol{H} \cdot \tilde{g} \cdot \boldsymbol{s_i} \tag{1.8}$$

[1]One more contribution "Pseudocontact term", due to the magnetic dipolar interaction between the orbital moment of the electron and the nuclear spin, can be added.

where μ_B is the Bohr magneton, H is the applied magnetic field, and g is a tensor connecting the magnetic field and the spins. Equation (1.8) can often be reduced to a simpler isotropic form i.e.

$$\mathcal{H}_z = \mu_B \sum_{i=1}^{N} g H_z s_{zi} \tag{1.9}$$

where z is the direction of the external field. In principle, the Zeeman interaction is present for both electron and nuclear spins; however, since the spin Hamiltonian, Equation (1.1), refers to the electronic spin system the nuclear Zeeman term is irrelevant.

Once the total spin Hamiltonian is written, one can calculate the energy levels of the system. However this is a rather difficult task. Firstly one has to rewrite all the Spin Hamiltonian contributions in terms of Irreducible Tensor Operators (ITOs) [8] to calculate their matrix elements on the total spin basis $|S, M\rangle$ using the Wigner-Eckart theorem and the decoupling technique. Once the Hamiltonian matrix is obtained, then, one can diagonalize it in order to obtain the energy spectrum of the molecule. Most times an important difficulty is constituted by the dimension of the matrix. Typically the dimension of the Hilbert space associated to a molecule containing N magnetic ions (and thus the dimension of the Hamiltonian matrix) is given by $(2s+1)^N$; therefore the calculation may require long computing times if N is large [9].

When the isotropic exchange interaction is the dominant term in Equation (1.1), one can estimate the ground state and the lowest lying excited states by means of the phenomenological Landè's rule [10]: $E(S) = (2J/N)S_T(S_T+1)$, where J is the exchange constant and S_T is the total spin value. In general, however, to analyze the experimental results the evaluation of the energy level structure from the solution of the complete spin Hamiltonian is necessary [11].

One important magnetic property which can be evaluated by using the eigenvalues of the Hamiltonian is the magnetic susceptibility, χ. This parameter can be calculated through the fundamental thermodynamic expressions;

$$\chi_{\alpha,\beta} = \frac{\partial M_\alpha}{\partial B_\beta} \tag{1.10}$$

where

$$M_\alpha = \frac{1}{\mathcal{Z}} \sum_{i=1}^{dim} -\frac{\partial E_i}{\partial B_\alpha} e^{-E_i/k_B T} \tag{1.11}$$

Equation (1.10) yields the Molar magnetic susceptibility, where M is the total magnetization, B is magnetic field, α, β = x, y, and z, dim is the dimension of the Hilbert space which corresponds to different energy levels and $\mathcal{Z}$ is the partition function. Assuming $\chi_{\alpha,\beta}$ is diagonal and the three dimensions x, y, z are equivalent, the molar susceptibility then reduces to

$$\chi_{\alpha,\beta} = \delta_{\alpha\beta}\chi = \frac{1}{B} \cdot \frac{\sum_{i=1}^{dim} g\mu_B J_i e^{-E_i/k_B T}}{\sum_{i=1}^{dim} e^{-E_i/k_B T}} \tag{1.12}$$

where J_i is the total angular momentum ($J_i = S_i + L_i$) for the i-th energy level. In the high temperature limit or when the interaction among magnetic moments can be neglected, the result obtained through Equation (1.12) is approximated by the simple Curie law

$$\chi = \frac{N g_J^2 \mu_B^2 J(J+1)}{3 k_B T} = \frac{C}{T} \tag{1.13}$$

where μ_B is Bohr magneton, N is the number of magnetic sites and J is quantum number (J = L+S). C in the second term is called Curie constant. In presence of magnetic interactions among the individual magnetic moments, it is often possible to describe the magnetic susceptibility by the so called Curie-Weiss law

$$\chi = \frac{C}{T - \theta} \tag{1.14}$$

where the correction term, θ, has the units of temperature, and is called the "Curie-Weiss constant", empirically evaluated from a plot of $1/\chi$ vs T ($\theta > 0$ for ferromagnetic and $\theta < 0$ for anti-ferromagnetic system). Assuming that the dominating contribution to θ comes from the interacting magnetic ions and applying the molecular field approximation, the expression of θ can be given by $\theta = (2zS(S+1)J)/3k_B$, where z is the number of interacting nearest-neighbors, S is the quantum number (L = 0), and J is the exchange interaction.

1.2 Semi Integer-Spin Cr_8Zn and Cr_8 AFM rings

1.2.1 Synthesis and characterization

One of the best characterized AFM ring nanomagnet is $[Cr_8F_8(O_2CC(CH_3)_3)_{16}]0.25C_6H_{14}$ abbreviated as Cr_8. In fact Cr_8 is the grandfather compound of the $[M_8F_8((OOC^tBu)_{16}]$ family, first reported in 1990 [1]. This complex is composed of eight chromium (III), $[Cr^{+3}] = [Ar]3d^3$, ions in a ring formation, where each adjacent pair is bridged by two pivalates along the outer periphery and a μ_2-bridging fluoride atom along the inner edge. Between each pair of adjacent metals, one of the bridging pivalates always lies in the plane of the wheel, while the other always lies approximately perpendicular to it. The exchange interaction between the nearest-neighbor Cr^{+3} (s=3/2) ions ($J_{Cr\text{-}Cr}$~16.9K) is antiferromagnetic which gives rise to a zero ground state $S_T = 0$ [12]. The magnetic interaction between spins connected to form a "closed" ring as schematically shown in Figure 1.1(a).

Cr_8 crystal are synthesized by heating up to 413 K and stirring a mixture of hydrated chromium (III) fluoride $CrF_3.4H_2O$ and an excess of Pivalic acid $(CH_3)_3CCOOH$ in a suitable solvent. Further details about the synthesis and purification procedure can be found in the literature [13]

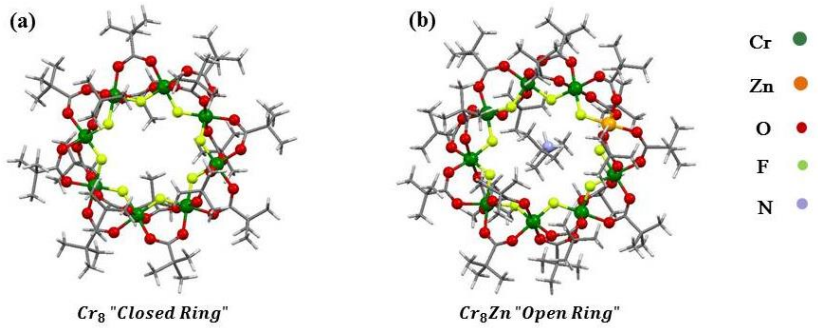

Figure 1.1: (a) Cr_8 molecular ring with the 16 pivalate ligands, Toluene is the solvent crystallization for Cr_8 and it is not shown here. (b) Cr_8Zn molecular ring with the 18 pivalate $(CH_3)_3CCOO^-$ bridging ligands and one Diisopropylamine molecule from crystallization solvent.

On the other hand, owing to the great success in synthesizing heterometallic AFM rings, it became possible to insert a dication M^{+2} into Cr_8 AFM ring; M = Cd, Ni, Zn. Therefore a monoanionic heterometallic species $[Cr_8MF_9Piv_{18}]^-$ is formed which can be separated from the homometallic compound because a cation-anion pair has different crystallization properties than a neutral species [14, 15]. One of the examples is $(Me_2CH)_2NH_2[Cr_8ZnF_9(O_2CC(CH_3)_3)_{18}]$ abbreviated as Cr_8Zn, where a Zn^{+2} (s = 0) ion is added to the eight Cr^{+3} ions of Cr_8. Since the Zn^{+2} ion has s = 0, AFM interaction between nearest-neighbor Cr^{+3} spins is suppressed by the Zn^{+2} ion as illustrated in Figure 1.1(b), and the resulting system can be regarded as an "open" ring. AFM interaction between the Cr^{+3} spins for Cr_8Zn is reported to be $J_{Cr\text{-}Cr} \sim 15.3$ K from inelastic neutron scattering and susceptibility measurements [16]. Both rings Cr_8 and Cr_8Zn are composed of eight Cr^{+3} spins with the only difference in the boundary conditions, thus making them ideal model systems to study how the spin dynamics and magnetic properties are affected by the spin topology. In the present work, we investigate this problem by means of proton nuclear magnetic resonance (^{1}H NMR) technique at intermediate temperature (see section 3.3). Furthermore, the Cr_8Zn "open" ring is an ideal model finite spin segment and it could possibly show spin diffusion behavior [17]. The most direct experimental verification for spin diffusion comes from the field dependence of the NMR spin-lattice relaxation at high temperature and the entire section 3.2 is devoted to this issue.

1.2.2 Magnetic properties

Following the theoretical discussion of section 1.1, we give here a brief description of the magnetic susceptibility and macroscopic magnetization in both Cr_8 and Cr_8Zn by reporting our experimental data. The magnetic susceptibilities χ have been measured by means of a superconducting quantum interference device (SQUID) magnetometer at two different external magnetic fields, $\mu_0 H = 0.47$ Tesla (Cr_8) and 0.5 Tesla (Cr_8Zn), in the temperature range $2 < T < 300$ K. The data were collected for Cr_8Zn on a single crystal with H oriented perpendicular to the molecular c-axis and on a powder sample for Cr_8.

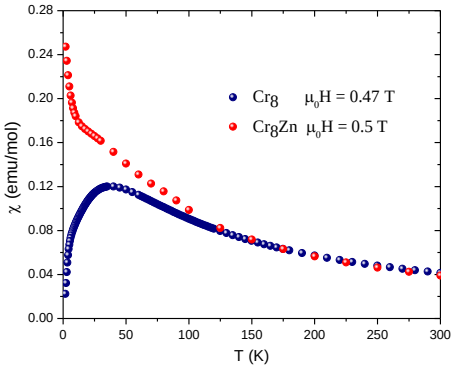

Figure 1.2: Temperature dependence of magnetic susceptibility of Cr_8Zn at μ_0H = 0.5 T and Cr_8 at μ_0H = 0.47 T (The magnetic field is oriented perpendicular to the molecular c-axis).

The temperature dependence of Cr_8Zn and Cr_8 magnetic susceptibility are shown in figure 1.2. Both open and closed rings feature the same behavior at high temperature (above 125 K) where all Cr^{3+} spins fluctuate independently. The magnetic susceptibility $\chi(T)$ of Cr_8Zn keeps increasing as the temperature drops down to 2 K, while $\chi(T)$ of the closed ring tends to zero below about 30 K. The different behavior of the two rings reflects the fact that, while both rings have a $S_T = 0$ ground state, the Cr_8Zn has a much smaller gap to the first excited magnetic state and thus the maximum in the susceptibility is expected around 2 K. The gap from the ground state to the first excited state has been determined from low-T magnetization measurements as shown in Figure 1.5 at the end of this section.

In the following we present an analysis of the magnetic susceptibility data using the expressions obtained from the Molecular Field Approximation (MFA). The values obtained for the exchange constant J and the g-factor will be compared with the results obtained directly from Inelastic Neutron Scattering and Electron Paramagnetic Resonance, respectively, in order to establish the reliability of MFA in the case of small number of magnetic ions.

In order to estimate the effective Curie constant ($C \sim \chi T$) parameter that was expressed by Equation (1.13), χT curves have been plotted as a function of temperature in Figure 1.3.

The χ is expressed as a molar susceptibility in AFM rings, therefore N is the number of magnetic ions per mole N_{mol} (= nN_A), where N_A is Avogadro number and n is the number of ionic sites in the molecular ring. The Quantum number J is reduced to S because in transition metal ions only d-orbital is partially occupied and the orbital angular momentum is completely quenched. The lower dashed lines for both Cr_8 and Cr_8Zn in Figure 1.3 correspond to the low- temperature limit of the Curie constant given by n = 8, g = 2 and S = 0, because the eight spins system occupy a collective ground state characterized by the total spin value S = 0 at low temperature. Vice versa, the upper dashed line represents the high temperature limit corresponding to an effective Curie constant in Equation (1.13) obtained by using n = 8 and s = 3/2 for both Cr_8 and Cr_8Zn and different g values, i.e. g = 2 for Cr_8 and g = 1.91 for Cr_8Zn as derived from the Curie constant, C, determined from the best fit in Figure 1.4 (see Table 1.1).

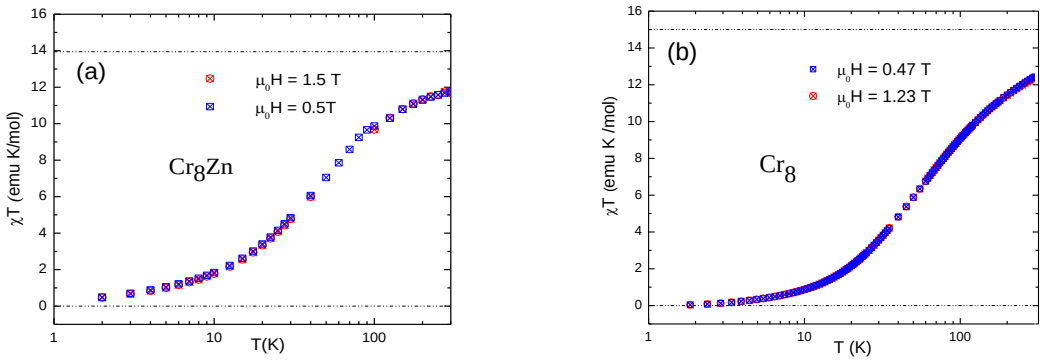

Figure 1.3: χT as a function of temperature at different external magnetic fields for (a) Cr_8Zn and (b) Cr_8. The dashed lines correspond to the low-temperature and high-temperature theoretical limits.

In order to estimate the nearest-neighbor exchange constant J, the inverse susceptibilities vs temperature are plotted in Figure 1.4. In both open and closed rings, the high-temperature results are fitted reasonably well by using the Curie-Weiss law, i.e. Equation (1.14).

Table 1.1 High and low temperature Curie constant limits and the Curie-Weiss temperature for Cr_8Zn "open" and Cr_8 "closed" rings.

Molecule	$\mathbf{C_{high\text{-}T\ limit}}$	$\mathbf{C_{low\text{-}T\ limit}}$	**Θ (K)**	$\mathbf{J/k_{B\ (SQUID\text{-}MFA)}}$	$\mathbf{J/k_{B\ (INS)}}$ [12,16]
Cr_8Zn	13.7 (0.3)	0	-43 (2.5)	19.6	15.3
Cr_8	15 (0.3)	0	-60 (3)	24.0	16.9

Since the J values obtained above correspond to a Hamiltonian for the Heisenberg model written as $\sum_{ij} -2J_{ij}S_i.S_j$, while the values of J given in molecular nanomagnets refer to a Hamiltonian in the form $\sum_{ij} J_{ij}S_i.S_j$, one should multiply these values by two and change the sign in order to compare them with the J constants that have been already reported in section 1.1. The results of this analysis are summarized in table 1.1, where the values of J have been renormalized as explained.

The comparison of the magnetic susceptibility measurements for the open and closed ring for T > 50 K reflects the difference in the exchange coupling constant J. The very different behavior of the susceptibility at low temperature shown in both Figures 1.4(a) and 1.4(b) can be explained on the basis of the different energy gap between the singlet ground state and the excited states for the two types of rings. This difference is in fact associated with the different spin topology [12] underlying the two spin systems, as a result of the energy levels structures.

The values of J in Table 1.1 determined from the fit of the magnetic susceptibility using the Molecular Field Approximation (MFA) (see Figure 1.4) are higher than the values obtained from Inelastic Neutron Scattering (INS) [12, 16]. Also the value of g = 1.91 for Cr_8Zn is anomalously low. In fact, the value of g for the two rings was measured directly by Electron Paramagnetic Resonance by Mozzati [18]. It was found g = 1.977(002) independently of crystal orientation with respect to the external magnetic field and the same for both rings within the experimental error. Both the

discrepancies in the J and g values indicate that the MFA is inadequate to describe quantitatively the collective effects in these small magnetic clusters.

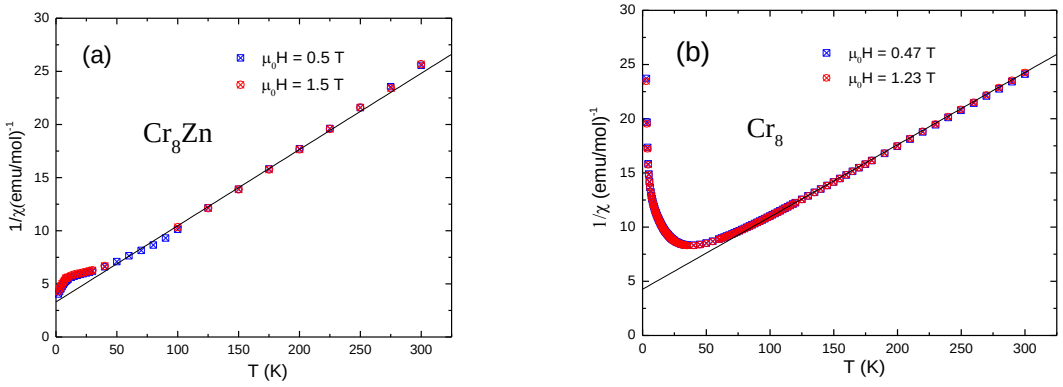

Figure 1.4: Inverse susceptibility as a function of temperature at two different external magnetic fields for (a) Cr_8Zn and (b) Cr_8. The solid lines are the best fit curves according to the Curie-Weiss law.

The magnetic field dependence of the magnetization M(H) at low temperature gives an estimate of the level crossings from which one can deduce the position of the low lying excited states. Measurements have been performed on polycrystalline sample of Cr_8 by using a pulsed magnet up to 35 T at T = 0.15K utilizing ^{3}He-^{4}He dilution refrigerator at the ISSP of the university of Tokyo [12]. For Cr_8Zn the M(H) curves have been measured on single crystal, with the magnetic field lying in the plane of the ring ($\theta = 90°$) by means of a cryomagnetic system with ^{3}He insert, that allows to reach temperatures as low as 0.3 K and a superconducting coil operating up to 7 T [19]. Figure 1.5(a) and 5(b) show the magnetization curves for Cr_8 and Cr_8Zn, respectively, for increasing magnetic field. The magnetization in the limit of zero field, M(0), is observed to be zero for both systems. This is a direct evidence of a singlet ground state. The M value rapidly increases on increasing the magnetic field with a peak in the dM/dH curves at the critical crossing field H_c. In fact, as external magnetic field is applied the ground state progressively switches from $S_T = 0$ to $S_T = 1$, and to $S_T = 2$ corresponding to critical field values H_{c1}, H_{c2}. The first ground state level crossing (LC) occurs around 7.4 Tesla for Cr_8, while occurs at only about 2.2 Tesla for Cr_8Zn. This indicates that there is a rather large gap (Δ = 9.365 K) between the ground state and the first excited state in Cr_8 and indeed at low temperature a rather high magnetic field is needed for measurable occupation of the first excited state, $S_T = 1$. The difference between closed and open ring in the case of the first critical magnetic field is qualitatively explained taking into account of the edge topological effects [12]. In fact, in order to flip one of the spins to create the $S_T = 1$ state in the closed ring, one needs an excitation energy corresponding to 2J, while in the case of open ring the excitation energy depends on the position of the spin. For example, the spin at the edge position is flipped with an energy cost of just J because the flipped spin is coupled to only a spin at one side.

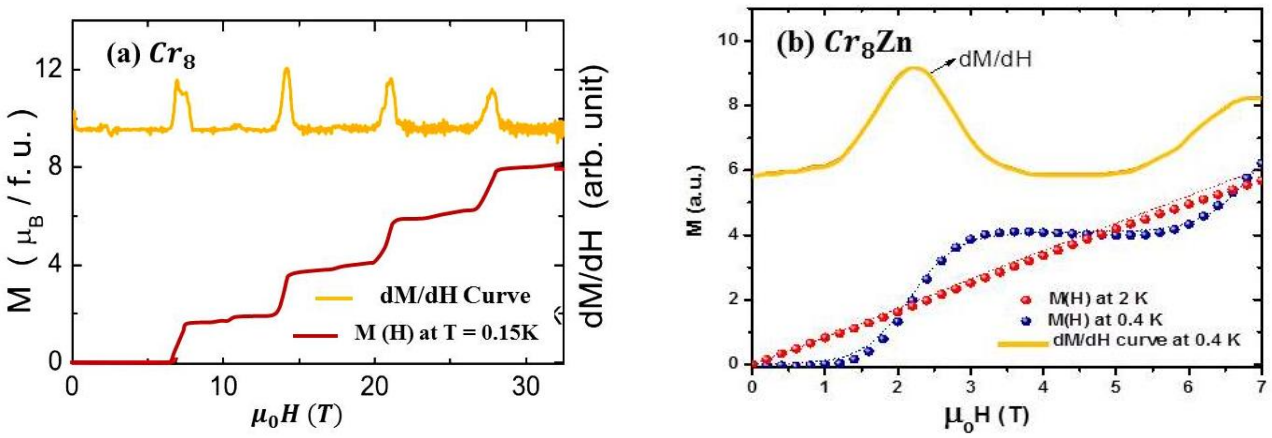

Figure 1.5: (a) Magnetization curve for Cr_8 at T = 0.15 K. The orange line is the experimental dM/dH. (b) Magnetization curves of Cr_8Zn measured at T = 0.4, and 2 K. Dashed lines show the theoretical calculations resulting from Equation (1.14), The experimental dM/dH curve is shown for T = 0.4 K.

The M (H) experimental results are theoretically reproducible by using a proper Hamiltonian. In the next subsection, we represent the energy structure of these two systems calculated by using χ(T) and M(H) experimental data.

1.2.3 Energy levels structure: Low-temperature level crossing

The energy levels structure of Cr_8 closed ring was already calculated solving the spin Hamiltonian. In addition, ^{1}H NMR experiments [20], as well as thermodynamic measurements like magnetization, specific heat and torque measurements [21], served to verify and modify those theoretical predictions. According to those results, the first and second ground state level crossing occur at $\mu_0 H$ = 7.43 T and $\mu_0 H$ = 14 T, respectively, as it is shown in Figure 1.6(a).

We now focus on the energy levels diagram of Cr_8Zn at low temperature. The microscopic picture of Cr_8Zn is represented by the following spin Hamiltonian:

$$\mathcal{H} = J_{Cr-Cr}\sum_{i=1}^{7} \boldsymbol{S}_i \cdot \boldsymbol{S}_{i+1} + d\sum_{i=1}^{8} S_{zi}^2 + e\sum_{i=1}^{8}\left(S_{xi}^2 + S_{yi}^2\right) + \sum_{i>j=1}^{8} \boldsymbol{S}_i \cdot \boldsymbol{D}_{ij} \cdot \boldsymbol{S}_j + g\mu_B \boldsymbol{H} \cdot \sum_{i=1}^{8} \boldsymbol{S}_i + G_z\sum_{i=1}^{7}\left(S_{xi}S_{yi+1} - S_{yi}S_{xi+1}\right) \quad (1.15)$$

where $\mathbf{S}_i$ is the spin operator of the ith Cr ion in the ring. It can be assumed that the site i = 9 is occupied by the Zn^{2+} ion. The first term in Equation (1.15) describes the isotropic Heisenberg exchange interaction between pairs of nearest neighboring Cr^{3+} ions, with strength $J_{Cr\text{-}Cr}$. The second and third terms account for single ion zero-field splitting anisotropy (with the z axis perpendicular to the plane of the ring) and the fourth one is the magnetic dipole-dipole interaction. The elements of the coupling tensor $\mathbf{D}_{ij}$ are calculated in the point-dipole approximation. The fifth term represents the Zeeman interaction with an external magnetic field $\mu_0\mathbf{H}$, and with isotropic and uniform g value for all Cr^{3+}

ions. Finally, the last term describes the Dzyaloshinskii-Moriya (DM) interaction where G_x and G_y components have not been included into the Hamiltonian for simplicity. The DM interaction determines the presence of a sizeable level anti-crossing which is not predictable by a simple Hamiltonian.

The minimal model introduced in Equation (1.15), with uniform exchange couplings and zero-field splitting tensors along the whole ring, is sufficient to provide a good description of thermodynamics and NMR nuclear spin-lattice relaxation rate (NSLR) experimental results [22]. It was found that the experimental data are well reproduced by assuming $J_{Cr\text{-}Cr}$ = 1.32(4) meV ≈ 15.31 K, d = -28(5) μeV ≈ 0.32 K, $|e|$ = 3(3) μeV ≈ 0.03 K and G_z =0.016(5) meV ≈ 0.18 K.

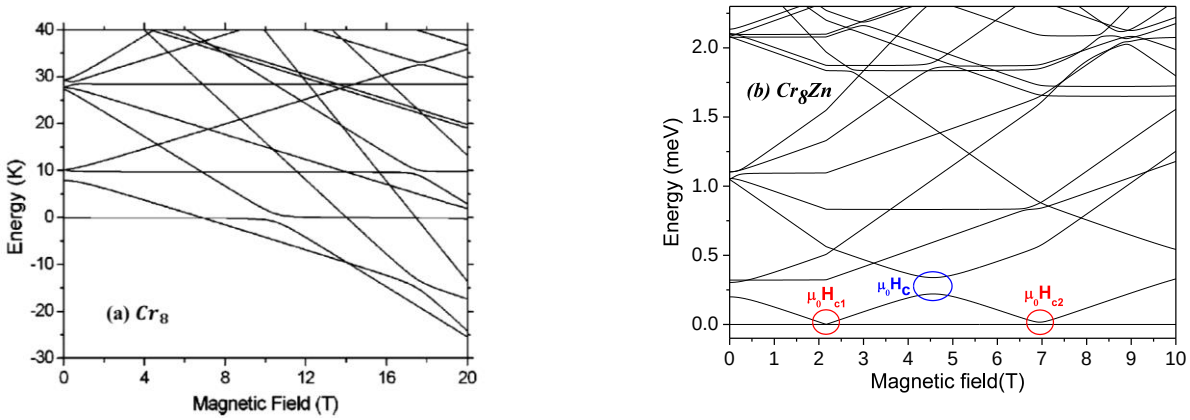

Figure 1.6: (a) Energy levels structure of Cr_8 [21]. (b) Magnetic field dependence of the low-lying energy levels of Cr_8Zn calculated according to Equation (1.14). The field lies in the plane of the ring. The two ground state level crossings fields μ_0H_{c1} and μ_0H_{c2} are indicated in red, while the excited states level anti-crossing μ_0H_c is indicated in blue. The energy of the ground state is set to zero for each value of the magnetic field.

With the calculated eigenstates and eigenvalues obtained by numerically diagonalizing the Hamiltonian, the field dependence of the energy levels was evaluated as it shown in Figure (1.6(b)). As can be seen, the external magnetic field lifts the degeneracy of the levels inducing level crossings between the ground and excited states. According to the results of the diagonalization of Equation (1.15) the first two ground state LCs are expected at μ_0H_{c1} = 2.15 T and μ_0H_{c2} = 6.95 T (red circles in Figure 6. (b)), where $|S = 0, M_s = 0>$ crosses $|S = 1, M_s = -1>$ and $|S = 1, M_s = -1>$ crosses $|S = 2, M_s = -2>$, respectively. The model yields a very small ground state anti-crossing at 2.15 T and a sizable one at 6.95 T. The excited state level anti-crossing, H_c = 4.4 T, shown by the blue circle of Figure 1.6(b) is also predicted by this theory and experimentally verified by specific heat and ^{1}H NMR measurements [22]. In this thesis, we investigate the multiple LCs between ground and excited states in a single crystal of Cr_8Zn at low temperature by means of ^{1}H NMR and spectroscopy (see section 3.4)

1.3 Integer-Spin V_7Zn and V_7Ni AFM rings

Recently, two different integer-spin AFM rings with the general formula $[\{(CH_3)_2NH_2\}V_7MF_8(O_2C^tBu)_{16}].2C_7H_8$, M = Ni and Zn, have been synthesized by the molecular magnetism group in Manchester [23]. In this section, we report the synthesis and structural characterization of these two compounds, along with magnetization and magnetic susceptibility measurements.

1.3.1 Synthesis and characterization

The same procedure, here briefly explained, was used to synthesize $[\{(CH_3)_2NH_2\}V_7ZnF_8(O_2C^tBu)_{16}].2C_7H_8$, abbreviated as V_7Zn, and $[\{(CH_3)_2NH_2\}V_7NiF_8(O_2C^tBu)_{16}].2C_7H_8$, abbreviated as V_7Ni. First, pivalic acid and dimethylammonium dimethylcarbamate are stirred at room temperature in a round bottomed flask until the solution becomes clear. $[Ni_2(\mu_2\text{-}OH_2)(\mu_2\text{-}O_2C^tBu)_4(HO_2C^tBu)_4]$ (Zinc powder in the case of V_7Zn) is then added to the mixture. Vanadium (III) fluoride is also added under inert conditions when the flask is thoroughly purged of all gases. This mixture is stirred under a steady flow of nitrogen at 160 ˚C for 24 h until a deep green solution reveals. The solution is then cooled to room temperature and dry acetonitrile is added. The dark green substance is precipitated by stirring the solution for 30 min. The revealed precipitate must be filtered under inert conditions and washed with dry acetonitrile. The powder is then dried under a steady flow of nitrogen and extracted into the minimum volume of dry toluene. Finally, large dark green single crystals form after a few days.

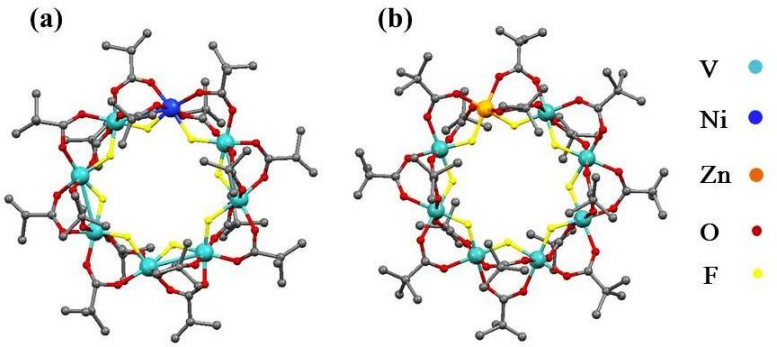

Figure 1.7: (a) V_7Ni and (b) V_7Zn molecular rings. Hydrogen atoms, dimethyl ammonium cation, and solvent toluene molecules are omitted for clarity.

The crystal data for both compounds were collected by means of X-Ray Crystallography[1] at 293 K. In both structures, the divalent metal M is disordered over all eight metal sites, and therefore each metal site had its occupancy fixed at 1/8 M and 7/8 vanadium. Crystallographic data show that both compounds crystallize in tetragonal space groups, with a C_4 axis perpendicular to the plane defined by the atoms within the ring. It is also found that all the rings in the unit cell lie in the *ab* crystallographic plane. Crystallographic data for both V_7Ni and V_7Zn AFM rings are listed in Table 1.2.

[1]The Bruker X8 Prospector 3-circle diffractometer with a Cukα microfocus source (λ = 1.54178 A˚) and an APEX2 II CCD detector.

Table 1.2: Crystallographic data for V_7M AFM rings.

	V_7Ni	**V_7Zn**
Formula	$C_{96}H_{168}F_8NO_{32}V_7Ni$	$C_{96}H_{168}F_8NO_{32}V_7Zn$
MW (g/mol)	2415.5426	2422.1582
Space.group	$P42_12$	$P4$
Cryst. Syst.	Tetragonal	Tetragonal
Cell. Lengths (Å)	***a*** 19.9861(3) ***b*** 19.9861(3) ***c*** 15.9170(3)	***a*** 20.0480(2) ***b*** 20.0480(2) ***c*** 16.0744(3)
Cell. Volume (Å^3)	6358.0(2)	6460.7(1)

1.3.2 Magnetic properties

Magnetic susceptibility of V_7M rings has been measured by means of SQUID magnetometry, at LAMM and Molecular Magnetism group of Florence (Italy), and the measurements were partially repeated in Pavia. In both cases, the measurements were performed on a single crystal sample with H oriented parallel and perpendicular to the molecular plane, at different external magnetic fields, in the temperature range $2 < T < 300$ K. Hysteresis curves at 2 K were also collected ($0 \leq \mu_0 H \leq 5$ Tesla). Figure 1.8 shows the temperature dependence of V_7Zn and V_7Ni magnetic susceptibility at $\mu_0 H = 0.1$ Tesla for $H \perp C$, where C is the molecular c-axis. Although the AFM interactions between nearest-neighbor, V^{3+} (s = 1) ions and between V^{3+} and the substituted ions (Zn^{2+} (s = 1) and Ni^{2+} (s = 1)) give rise to a different total spin ground state ($S_T = 0$ and $S_T = 1$ for V_7Ni and V_7Zn, respectively), both compounds show the same qualitative behavior of the susceptibility as a function of temperature as shown in Figure 1.8. The anisotropic effects can be observed from the hysteresis curve, i.e. M(H), as shown in Figure 1.9, where the curves are collected at T = 2 K in both directions. In the following we focus only on the susceptibility data collected for $H \perp C$ which is the same orientation used in our ^1H NMR measurements.

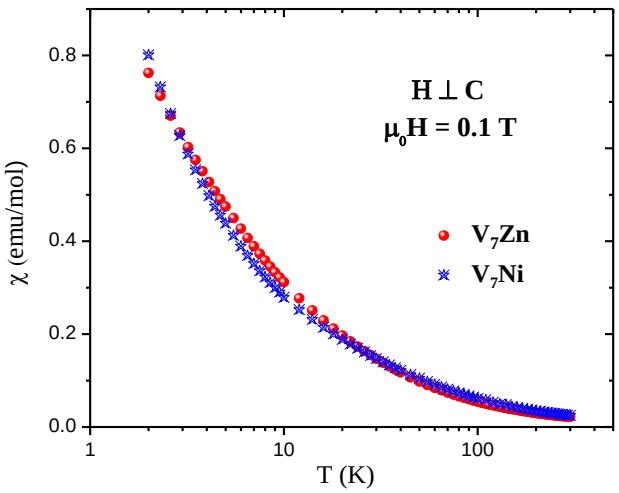

Figure 1.8: Temperature dependence of magnetic susceptibility of V_7Zn and V_7Ni at $\mu_0 H = 0.1$ Tesla for $H \perp C$.

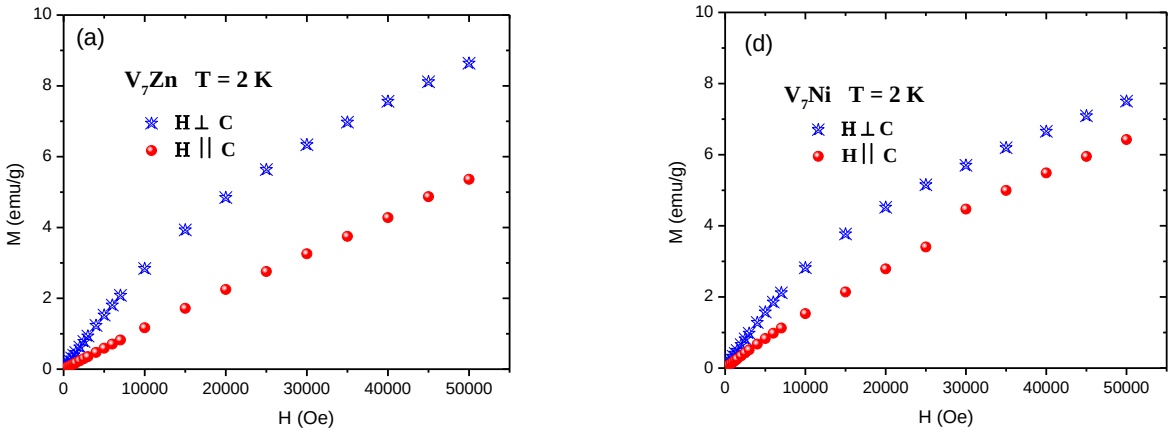

Figure 1.9: Hysteresis curves i.e. M vs. H, at T = 2 K collected in two different orientations H ⊥ C and H || C for (a) V_7Zn and (b) V_7Ni.

Although the Molecular Field Approximation (MFA) should be valid only in a system with large number of magnetic ions, it was previously found that magnetic constants such as the Curie and Curie-Weiss constants estimated from the analysis of the susceptibility data by MFA in molecular nanomagnets yield results which are within 20-25% of the more reliable values obtained by Inelastic Neutron Scattering and Electron Paramagnetic resonance. Thus, in zero order approximation we will rely on the analysis of the susceptibility data in the V rings to extract information about the thermodynamic magnetic properties. The Curie "C" and the Curie-Weiss "Θ" parameters obtained from susceptibility data by using the MFA can then be used to evaluate the exchange constant J for the V_7M rings.

The effective Curie constant parameter can be evaluated from the high temperature part of the $\chi \cdot T$ curves (shown in Figures 1.10(a) and 1.10(b) for V_7Zn and V_7Ni, respectively), by using Equation (1.13). The upper-dashed lines in Figures1.10 correspond to the high-temperature limit of the Curie constant: C = 7 and C = 8.217 for V_7Zn and V_7Ni, respectively, obtained by setting $g_v = 2$ for V^{3+} and $g_{Ni} = 2.2$ for Ni^{2+} as determined from the fit of the inverse susceptibility in Fig. 1.11 (the $g_{Ni} = 2.2$ value is expected for a Nickel ion in a tetragonal symmetry [24]). The lower-dashed lines correspond to the low-temperature limit of the Curie constant corresponding to S = 0 for V_7Ni and S = 1 for V_7Zn as a collective ground state spin value. It can be seen that in both samples the $\chi \cdot T$ curve agrees with the high and low T limiting values obtained by MFA.

To estimate the J value in MFA, the inverse susceptibilities plotted as a function of temperature (see Figures 1.11(a) and 1.11(b) for V_7Zn and V_7Ni, respectively) can be used. The high-temperature results for both vanadium rings are fitted well by Equation (1.14) as shown in Figure 1.10, with the fitting parameters $\theta = -25$ for V_7Zn and $\theta = -27$ for V_7Ni. It was shown previously (section 1.2.2) that from MFA one deduces $\theta = (2zs(s+1)J)/3k_B$, and from this formula the J constant can be extracted. It should be taken into account that the values reported in Table 1.3 have been multiplied by a factor of two and

changed in sign to compare them with the theoretical calculated values obtained by using a different starting Hamiltonian as explained in section 1.2.2.

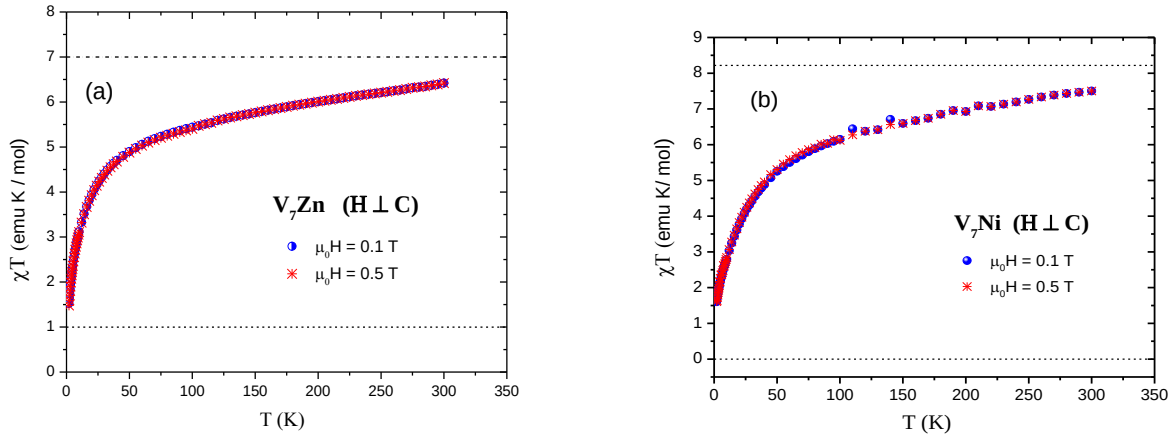

Figure 1.10: χT as a function of temperature for H ⊥ C, at different external magnetic fields μ_0H = 0.1, and 0.5 T for (a) V_7Zn and (b) V_7Ni. The dashed lines correspond to the high-temperature Curie constant limit.

The results of the fits for H ⊥ C orientation are summarized in Table 1.3. It is worth noticing that the experimental susceptibility (better to say M/H) data collected at higher magnetic fields, i.e. μ_0H = 1.5, 3, and 6 Tesla, were found to superimpose one each other for T > 80 K. It can also be observed that both compounds behave as a paramagnet down to a temperature T ~ 80 K, while for T < 80 K there is a deviation between the experimental data and the fitting curves obtained by using the MFA (see Figure 1.11).

Table 1.3: High and low temperature Curie constant limits, Curie-Weiss temperature and exchange constant (MFA approximation) for V_7Zn "open" and V_7Ni "closed" spin-1 AFM rings in H ⊥ C orientation.

Molecule	$C_{high\text{-}T\ limit}$	$C_{low\text{-}T\ limit}$	Θ (K)	$J/k_{B\ (MFA)}$
V_7Zn	6.99 (0.2)	0.998	-25 (3)	21.42
V_7Ni	8.2 (0.22)	0	-27 (2)	20.2

Since in the case of Antiferromagnetic (AFM) rings there is only a finite number of magnetic ions, we also tried to calculate, as a preliminary stage, the nearest-neighbor exchange constant J, by using the PHI software [25, 26] and a home-made software (calculations performed by Parma's group). In both calculations, the fitting of the χ·T curve have been done by using the results of the diagonalization of a simple (isotropic) spin Hamiltonian that includes both the Zeeman and the Heisenberg terms. The J value was estimated to be about ~ 4.64 K with g_v = 1.73 for V_7Zn and ~ 4.02 K with g = 1.93 for V_7Ni [26, 27]. It should be remarked that the used Hamiltonian has a very simple form that much probably does not represent the real system. In a future investigation the terms taking into account of the different kinds of magnetic anisotropy must be included.

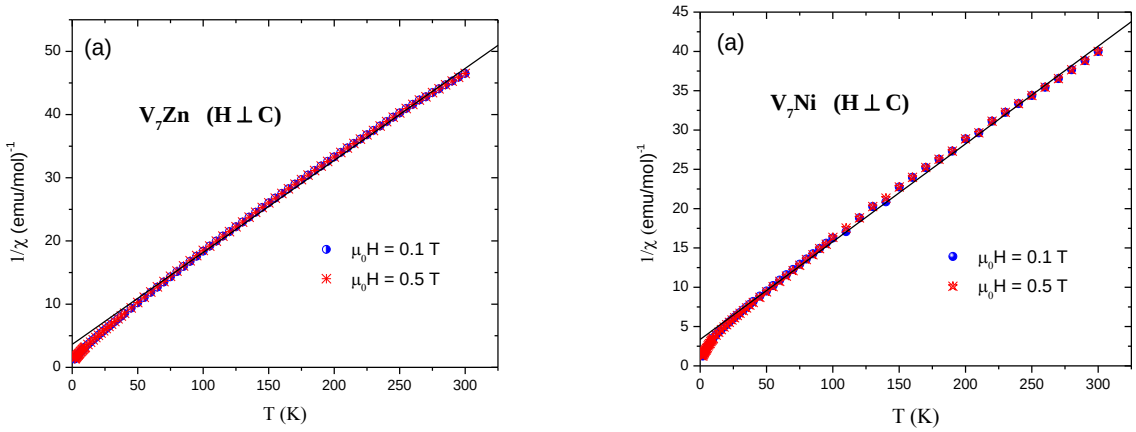

Figure 1.11: Inverse susceptibility as a function of temperature for H ⊥ C at $\mu_0 H = 0.1$ and 0.5 T for (a) V_7Zn and (b) V_7Ni. The solid lines are the best fit curves according to the Curie-Weiss law, i.e. Equation (1.13).

To conclude, a preliminary investigation of integer-spin AFM rings susceptibility by assuming an isotropic spin Hamiltonian, indicates that the nearest-neighbor exchange constant J is of the order of ~ 4 K for both V_7Zn and V_7Ni. This result seems in qualitative agreement with the results obtained for the temperature behavior of the nuclear spin lattice relaxation data, $1/T_1$. In fact the $1/T_1$ data vs. temperature reveals a peak in the temperature range 3.9 ÷ 4.5 K for different external magnetic fields (see section 3.3.2(ii)). Taking into account that in all other molecular rings the $1/T_1(T, H=const)$ anomaly appears at temperature of the order of J, the peak position and the estimated J appears roughly in agreement. On the other hand the MFA analysis of the susceptibility data leads to J values in complete disagreement with the theory and with the NMR results. This could indicate a total breakdown of the MFA for these integer spin molecular rings, due to the failure of the mean-field approximation and/or the presence of anisotropy.

1.3.3 Energy levels structure and low temperature level crossing: the case of V_7Ni

Here we present the magnetic energy levels structure of V_7Ni which was computed using the PHI software. For this purpose, a system made of eight spins s = 1 was defined in the input file. The g factor and the exchange constant were kept fixed to the value obtained from the susceptibility fit and the exchange Heisenberg and the Zeeman terms were assumed to be the only contributions to the spin Hamiltonian. Finally the external magnetic field was left to assume values from 0 to 7 Tesla in 250 steps. The calculated result is shown in Figure 1.12.

As one can see from Figure 1.12, the lowest-lying energy level corresponds to a spin ground state S = 0. The first excited level S = 1 lies at energy $E = 4\ cm^{-1} \approx 5.72$ K. The first level crossing between the ground state and the first excited states takes place around H = 3.5 T. It should be taken into account that the results shown in Figure 1.12 are just preliminary results, to be confirmed through more refined

theoretical calculations which include the anisotropy terms and further experimental data taken by NMR, Inelastic Neutron Scattering and specific heat measurements.

It should be remarked that the determination of the energy levels structure is crucial for the study of the level crossing and gives, for the first time, the possibility to investigate this phenomenon in integer spin systems.

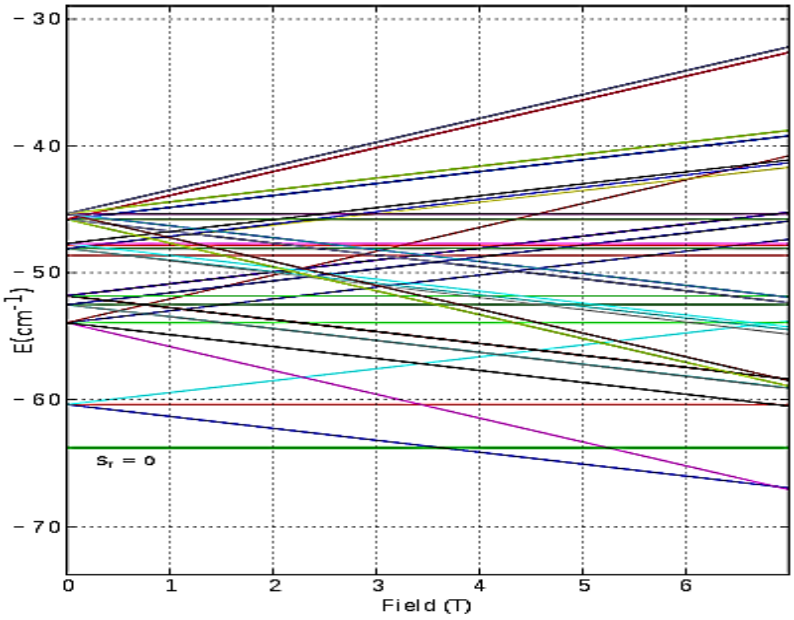

Figure 1.12: Energy levels structure of V_7Ni computed by PHI software by considering the Zeeman and the exchange Heisenberg contributions only.

The nature of the level crossings (true and/or anti level crossing), and of the related possible exchange of energy between the electrons and nuclei at the level crossing fields at low temperature ($k_BT << J$) have been investigated in the present thesis in the semi-integer AFM rings, where the proton NMR spin-lattice relaxation rate, $1/T_1(H)$, have been measured as a function of H at very low temperature (where the system is in the ground state) to gain information about the spin dynamics (see section 3.4). This study can be conducted on V_7M rings as well with the aim of investigating how the high local magnetic anisotropy in V_7M rings of the V^{3+} ions and the integer spin value (s = 1) of V^{3+} affect the spin dynamics at low temperature.

2. Nuclear Magnetic Resonance (NMR) as a probe of spin dynamics

The aim of this chapter is to recall some basic aspects of Nuclear Magnetic Resonance (NMR). Since we are mostly interested in probing the electronic spin dynamics in molecular magnets by using NMR, we will recall in some details the theory which connects the NMR measured parameters (mainly the spin-lattice and the spin-spin nuclear relaxation rates) to the spin dynamics of the molecular magnets.

2.1 NMR at a glance

NMR involves detailed manipulation of nuclear spins. The nucleus consists of many particles coupled together so that the nucleus possesses a total nuclear magnetic moment **μ**:

$$\boldsymbol{\mu} = \gamma\hbar\boldsymbol{I} \tag{2.1}$$

where γ is the gyromagnetic ratio and $\hbar\boldsymbol{I}$ is the nuclear angular momentum. The application of a static magnetic field $\mathbf{H_0}$ (necessary for NMR technique) produces the Zeeman splitting of the low-lying levels, through an interaction represented by the simple Hamiltonian:

$$\mathcal{H} = -\gamma\hbar\boldsymbol{I}\cdot\boldsymbol{H_0} \tag{2.2}$$

Taking the field H_0 to be along the z direction, one finds

$$\mathcal{H} = -\gamma\hbar H_0 I_z \tag{2.3}$$

The corresponding eigenvalues are:

$$E = -\gamma\hbar m H_0 \qquad\qquad m = -I, -I+1, \dots, I-1, I \tag{2.4}$$

as shown, for example, in Figure 2.1(a) for the case I = 3/2. As can be seen, the levels are equally spaced, the distance between adjacent ones being $\gamma\hbar H_0$. A time dependent perturbation of the Zeeman Hamiltonian can induce a transition between the energy levels. The most commonly used perturbation to produce such a transition (the case of NMR) is an alternating magnetic field applied perpendicularly to the static field H_0. By assuming a time dependent alternating magnetic field along x axis ($\boldsymbol{H_1} = H_1\cos(\omega t)\hat{x}$) the perturbing term in the Hamiltonian is given by [1]:

$$\mathcal{H}_{pert} = -\gamma\hbar I_x H_1 \cos(\omega t) \tag{2.5}$$

The operator I_x has matrix elements between the two different states of the transition, which vanish unless $m' - m = \pm 1$. Consequently the allowed transitions are between levels adjacent in energy, $\Delta E = \gamma\hbar H_0 = \hbar\omega$.

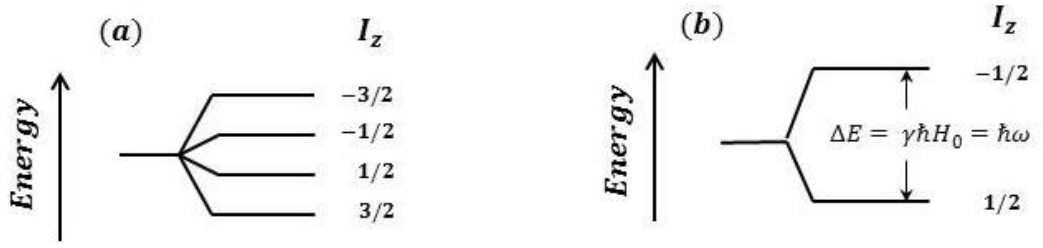

Figure 2.1(a) The four levels resulting from Zeeman splitting for a I = 3/2 nucleus. (b) Energy levels for the hydrogen nucleus ^{1}H, I = ½. The two nuclear resulting levels are separated by an energy gap $\Delta E = \gamma\hbar H_0 = \hbar\omega$; the lower (upper) level corresponds to the nuclear magnetic moment lying parallel (antiparallel) to the external magnetic field

We now wish to go a step further to consider what happens if one has a macroscopic sample in the field $\boldsymbol{H} = \boldsymbol{H_0} + \boldsymbol{H_1}$. Since we are interested in ^{1}H NMR measurements, let's consider a system whose nuclei possess spin ½. The application of an alternating field $\boldsymbol{H_1}$ causes the nuclear spins to change the energy state (see Figure 2.1(b)). We can now denote the transition probability per second of a spin (from I = +1/2 to a state with I = -1/2) by $W_{+\to-}$, and the one of the inverse transition by $W_{-\to+}$[1].We can then write a differential equation for the change of the population of the lower state N_+ and N_- as

$$\frac{dN_+}{dt} = N_- W_{-\to+} - N_+ W_{+\to-} \tag{2.6}$$
$$\frac{dN_-}{dt} = N_+ W_{+\to-} - N_- W_{-\to+}$$

Equation (2.6) represents the so-called "Master equation" [2], in the case of spin ½. It is convenient to introduce the variables $N = N_+ + N_-$ and $n = N_+ - N_-$. Thus by replacing n and N into Equations (2.6) it is obtained

$$\frac{dn}{dt} = \frac{n_0 - n}{T_1} \tag{2.7}$$

where

$$n_0 = N\left(\frac{W_{-\to+} - W_{+\to-}}{W_{-\to+} + W_{+\to-}}\right) \qquad and \qquad \frac{1}{T_1} = (W_{-\to+} + W_{+\to-})$$

---

[1]It can be considered that $W_{-\to+} = W_{+\to-} \equiv W$; in the framework of the time dependent perturbation theory for the probability per unit time [1].

[2]More generally, the master equations are denoted by $\frac{dN_m}{dt} = \sum_n (N_n W_{nm} - N_m W_{mn})$ where N_m is the population of the energy level E_m, and W_{mn} is the transition rate probability.

As can be seen, n_0 represents the thermal equilibrium population difference, and T_1 is a characteristic time associated with the thermal equilibrium recovery, called spin-lattice relaxation time. In order to gain a general view about the NMR technique, we first present a semi-classical model in the following section which sheds light onto the concept of the relaxation rates in NMR.

2.2 Semi-classical model of NMR

In the semi-classical model (called also vectorial model) only the net magnetization arising from the nuclei in the sample and its behavior in the applied magnetic fields is considered. This model also provides a convenient picture of the effect of the perturbation Hamiltonian, which is an alternating magnetic field in the case of NMR (see section 2.3).

If the spins don't interact, then the experimentally measured bulk nuclear magnetization is simply the vectorial sum of all the individual magnetic moments in presence of the static magnetic field $\mathbf{H_0}$ directed along z (see Figure 2.2(a)):

$$\boldsymbol{M} = \sum_i \boldsymbol{\mu}_i \tag{2.8}$$

The equation of motion of the magnetization vector is found by equating the torque with the rate of change of the net nuclear angular momentum (that is proportional to the net magnetization $\boldsymbol{M} = \gamma\hbar\boldsymbol{I}$) and is given by

$$\frac{d\boldsymbol{M}}{dt} = \gamma(\boldsymbol{M} \times \boldsymbol{H_0}) \qquad (non-interacting\ nuclei) \tag{2.9}$$

Equation (2.9) predicts that **M** precesses around the magnetic field $\mathbf{H_0}$ at a constant rate $\omega = \gamma H_0$. The frequency with which the magnetization precesses around this field is the Larmor frequency $\omega_0 = \gamma H_0$. The alternating magnetic field $\mathbf{H}_1$, the so-called radio frequency (rf) field, needs to be added perpendicularly to the static magnetic field in order to tip **M** from its equilibrium direction. If the duration of $\mathbf{H_1}$ is limited (μs ÷ ms), i.e. one uses pulsed NMR, the rotated magnetization will start to go back to the equilibrium condition when the rf field is switched off [2] (see Figure 2.2(c))[1].

In this case we can define the total magnetization relaxation times through the phenomenological Bloch equations that describe the evolution of the nuclear magnetization components, i.e. M_x, M_y, and M_z.

[1]Since in NMR technique the sample is placed inside a coil then, according to the Faraday-Lenz law, the decay of the transverse magnetization will induce an alternating electromotive force (emf) which represents the effective NMR signal. This signal contains all the information of the spin system and is called "free induction decay" [2, 3].

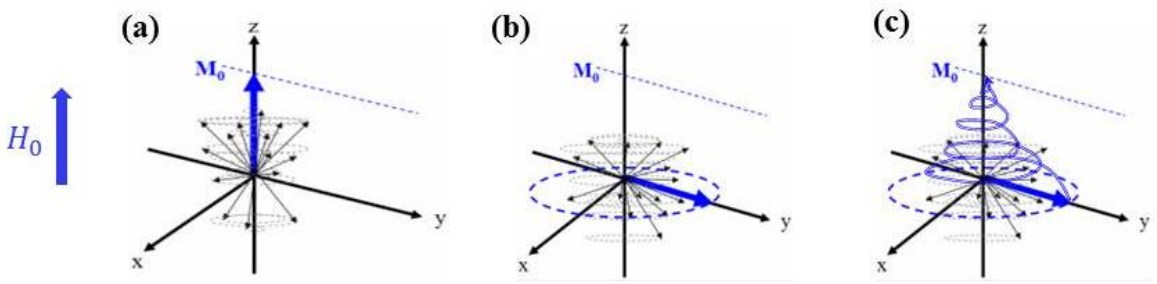

Figure 2.2 (a) The net magnetization along the external magnetic field as a vectorial sum of all the individual magnetic moments before applying the rf pulse (b) Rotation of the magnetization into xy plane by applying the rf pulse, $H_1 \neq 0$ (c) relaxation of the magnetization towards the equilibrium condition, after setting $H_1 = 0$.

Bloch equations can simply be written by recalling Equations (2.7) and (2.9) [1]:

$$\frac{dM_z}{dt} = \gamma(\boldsymbol{M} \times \boldsymbol{H})_z + \frac{M_0 - M_z}{T_1} \tag{2.10}$$

$$\frac{dM_x}{dt} = \gamma(\boldsymbol{M} \times \boldsymbol{H})_x - \frac{M_x}{T_2} \tag{2.11}$$

$$\frac{dM_y}{dt} = \gamma(\boldsymbol{M} \times \boldsymbol{H})_y - \frac{M_y}{T_2} \tag{2.12}$$

where $\boldsymbol{H}$ is the static external longitudinal field $\boldsymbol{H} = \boldsymbol{H_0} = H_0\hat{z}$ and the transverse rf field is $\boldsymbol{H_1} = H_1 \cos(\omega_n t)\,\hat{x} + H_1 \sin(\omega_n t)\hat{y}$. M_0 is the equilibrium value of the magnetization directed along H_0. From Equation (2.10) one can see that the spin-lattice relaxation time T_1 is the characteristic time that the magnetization needs to recover the equilibrium value M_0 along the z axis, exchanging energy with the lattice. The transverse (T_2) relaxation arises from the spread in precession rates produced by the "inhomogeneities" of the static magnetic fields due to different internal fields. Therefore T_2 is called spin-spin relaxation rate. The relaxation times T_1 and T_2 introduced in the Bloch equations are purely phenomenological parameters. In a material these parameters can be related to the microscopic structure and to the various degrees of freedom of the "lattice". In the following, we thus discuss the expression of T_1 and T_2 within the framework of a microscopic model.

2.3 Microscopic model of nuclear relaxation

As we have remarked in section 2.2, the Bloch equations are just phenomenological equations. Experimentally, it was found that the Bloch equations are solely able to explain spin relaxation in liquids but not in solids. Redfield solved this problem by the introduction of the spin temperature concept [4].

From a microscopic point of view the relaxation corresponds to the transition of nuclear spins between Zeeman levels starting from a non-equilibrium population distribution. Since the population of each level is determined by the Boltzmann distribution, we can think that the spin system at equilibrium condition is characterized by a common temperature, the so-called spin temperature T_S.

The spin system is also in thermal contact with the lattice, where can be considered as a heat reservoir at temperature T_L. The spin temperature approach makes the assumption that the strong coupling between nuclear spins simply establishes a common temperature for the spin system and that the lattice coupling causes this temperature to change. There is a close analogy with the process of heat transfer between a gas and the walls of its container, in which the role of the collision within the gas is to maintain a thermal equilibrium among the gas molecules. As we shall see, the perturbation within the spin system (for example a rf pulse in a NMR experiment) leads to a non-equilibrium condition where $T_S > T_L$. Removing the perturbation, the nuclear spins interact with the lattice degrees of freedom and tend to reach the lattice temperature ($T_S = T_L$ at equilibrium) with a characteristic spin-lattice relaxation time T_1. In general, internal equilibrium means that the whole nuclear spin system is at the same spin temperature T_s, while external equilibrium means that the spin temperature T_s is the same as the lattice temperature T_L. To perturb the spin system means to change of its spin temperature. Consequently, we can think the spin-spin relaxation time T_2 as the characteristic time that the spins need to reach an internal thermal equilibrium within the spin system, and T_1 as the characteristic time the spins need to reach external equilibrium with the lattice.

The so-called density matrix approach is used to complement the spin temperature approach [5]. Density matrix method is ideally suited to treat problems in which the resonance is narrowed by the physical motion of the nuclei; however, it is also applicable to the nuclei presenting broad line spectra. This method makes use of the conventional time-dependent perturbation theory.

Here below, we first present the spin Hamiltonian (Equation (1.1)) based on the time-dependent perturbation theory. Then, by using the first order perturbation term, we derive an expression for the relaxation transition probabilities between the Zeeman's levels. Finally, the expression of T_1 and T_2 are analytically derived for three different temperature regions.

The nuclear spin Hamiltonian can be generally written as

$$\mathcal{H} = \mathcal{H}_e + \mathcal{H}_n + \mathcal{H}_{ne} \tag{2.13}$$

where $\mathcal{H}_e$ is the electron spin Hamiltonian and mainly consists of the exchange energy, Zeeman term, and magnetic anisotropy terms. The second term, $\mathcal{H}_n$, is the nuclear Hamiltonian and consist only of the Zeeman term and the nucleus-nucleus dipolar interaction. The last term $\mathcal{H}_{ne}$ represents the hyperfine coupling between nuclear and electron spins. To isolate the time-dependent hyperfine perturbation term (thus allowing to use the perturbation theory), Equation (2.13) can be re-written as

$$\mathcal{H} = \mathcal{H}_0 + \mathcal{H}_1(t) \tag{2.14}$$

with a time independent part ($\mathcal{H}_0 = \mathcal{H}_e + \mathcal{H}_n$) and a time dependent one ($\mathcal{H}_1 = \mathcal{H}_{ne}$).

At this point two different approaches should be adopted depending on the ratio between the intensity of $\mathcal{H}_0$ and $\mathcal{H}_1(t)$: if $\mathcal{H}_1 \ll \mathcal{H}_0$ the nuclear system and its relaxation has to be treated within the so-called “weak collision” approximation. In the “weak collision” approach the time dependent

Hamiltonian terms can be treated as a small perturbation which induces a transition probability between the stationary energy levels of the spin system, with the assumption that the correlation time τ of the electronic spin fluctuation is much shorter than the nuclear relaxation time ($\tau \ll T_1$) [6]. When the assumption $\mathcal{H}_1 \ll \mathcal{H}_0$ breaks down (i.e. $\mathcal{H}_1 \sim \mathcal{H}_0$ or $\mathcal{H}_1 > \mathcal{H}_0$), the "strong collision" theory must be employed and $\mathcal{H}_1$ represents no longer a perturbation. Different physical phenomena could be responsible for the weak collision break down. For example molecular rotations and the consequent change of the quantization axis of the electric field gradient tensor were found to strongly affect the spin relaxation [7]. Other processes yielding the strong collision regime are the change of the local dipolar field due to diffusion of nuclei [8].

In Molecular Nano Magnets, the breakdown of the "weak collision" approximation can occur at very low temperature when a tunneling transition between degenerate states reverses the orientation of the molecular magnetization. This phenomenon was indeed observed in Fe_8, in the case of ^{57}Fe NMR in zero external magnetic field [9]. Since this type of magnetic effect is not present in the AFM rings investigated here, the weak collision approximation is adopted in the present work.

In the weak collision approach, the perturbation term (electron-nucleus hyperfine interaction; $\mathcal{H}_{ne} = \mathcal{H}_D + \mathcal{H}_c$) consists of two different contributions, i.e. the electron-nuclear dipolar interaction $\mathcal{H}_D$

$$\mathcal{H}_D = \frac{g^2 \mu_e \mu_n}{2} \sum_{ij} \left[\frac{\boldsymbol{I}_i \cdot \boldsymbol{s}_j}{r_{ij}^3} - 3 \frac{(\boldsymbol{I}_i \cdot \boldsymbol{r}_{ij})(\boldsymbol{s}_j \cdot \boldsymbol{r}_{ij})}{r_{ij}^5} \right] \tag{2.15}$$

and the contact-Fermi interaction $\mathcal{H}_c$ given by:

$$\mathcal{H}_c = \sum_{ij} \boldsymbol{I}_i \cdot \widetilde{\boldsymbol{A}}_{ij} \cdot \boldsymbol{s}_j \tag{2.16}$$

where $\widetilde{\boldsymbol{A}}_{ij}$ is a symmetric tensor of order two. It is possible to combine the two interactions by introducing a new tensor $\widetilde{\boldsymbol{T}}_j$ which represents the interaction of the nuclear spin $\boldsymbol{I}_i$ with the electronic spin $\boldsymbol{s}_j$. So the perturbation Hamiltonian becomes

$$\mathcal{H}_{en} = \sum_{ij} \boldsymbol{I}_i \cdot \widetilde{\boldsymbol{T}}_j \cdot \boldsymbol{s}_j \tag{2.17}$$

with a tensor component given by

$$T_j^{\alpha\beta} = A_j^{\alpha\beta} + \gamma_e \gamma_n \hbar^2 \left(\frac{\delta_{\alpha\beta}}{r_j^3} - 3 \frac{x_j^\alpha x_j^\beta}{r_j^5} \right),$$

where x_j^α are the various components of $\boldsymbol{r}_j$. We can now introduce an expression for the local hyperfine field at the nuclear site due to the surrounding electron spins as

$$\boldsymbol{H}(t) = \sum_j \boldsymbol{H}_j(t) = \sum_j \widetilde{\boldsymbol{T}}_j \cdot \boldsymbol{s}_j \tag{2.18}$$

The time dependence of $\boldsymbol{H}(t)$ can be easily understood by considering that nuclear and electronic spins experience both thermal agitation and diffusion processes, and thus fluctuate in time. Finally by replacing Equation (2.18) into Equation (2.17) we obtain

$$\mathcal{H}_{ne} = \sum_{ij} \boldsymbol{I}_i \cdot \boldsymbol{H}_j = \sum_{ij} [I_i^z H_j^z + \frac{1}{2}(I_i^+ H_j^- + I_i^- H_j^+)] \tag{2.19}$$

where $H^+ = H_x + iH_y$ and $H^- = H_x - iH_y$ are respectively the raising and lowering operators of the local hyperfine field, While, $I^+ = I_x + iI_y$ and $I^- = I_x - iI_y$ are the raising and lowering nuclear spin operators. We are now able to calculate the transition probability by using the perturbation Hamiltonian $\mathcal{H}_1(t) = \mathcal{H}_{ne}(t)$.

The transition probability per unit time between two Zeeman levels i (initial state) and f (final state after transition) in the first-order time-dependent perturbation theory is given by [1]

$$W_{i,f} = W_{f,i} = \frac{1}{\hbar^2}\int_0^t [(f|\mathcal{H}_1(t')|i)(i|\mathcal{H}_1(t)|f)e^{i\frac{E_f - E_i}{\hbar}(t'-t)} + (f|\mathcal{H}_1(t)|i)(i|\mathcal{H}_1(t')|f)e^{i\frac{E_f - E_i}{\hbar}(t-t')}]dt' \tag{2.20}$$

The Equation (2.20) can be considered as a general one, due to the not specified nature of the perturbation $\mathcal{H}_1(t)$ that, for example, could vary randomly in time. By calculating the average over a statistical ensemble, one obtains:

$$W_{i,f} = W_{f,i} = \frac{1}{\hbar^2}\int_0^t [\overline{(f|\mathcal{H}_1(t')|i)(i|\mathcal{H}_1(t)|f)}e^{i\frac{E_f - E_i}{\hbar}(t'-t)} + \overline{(f|\mathcal{H}_1(t)|i)(i|\mathcal{H}_1(t')|f)}e^{i\frac{E_f - E_i}{\hbar}(t-t')}]dt' \tag{2.21}$$

The ensemble average such as

$$\overline{(f|\mathcal{H}_1(t')|i)(i|\mathcal{H}_1(t)|f)} \tag{2.22}$$

depends on t and t' only through their difference τ ($\tau = t - t'$). Thus, by replacing τ into Equation (2.22) the ensemble average is given by

$$\overline{(f|\mathcal{H}_1(t-\tau)|i)(i|\mathcal{H}_1(t)|f)} \tag{2.23}$$

that is independent of t, but is a function both τ and of the pair of levels, i and f. The dependence on τ, f, and i leads us to define a quantity $G_{fi}(\tau)$ by the equation

$$G_{fi}(\tau) = \overline{(f|\mathcal{H}_1(t-\tau)|i)(i|\mathcal{H}_1(t)|f)} \tag{2.24}$$

Equation (2.24) becomes independent of t if the perturbation $\mathcal{H}_1(t)$, is a stationary perturbation. In this case, one has

$$G_{fi}(\tau) = \overline{(f|\mathcal{H}_1(t)|i)(i|\mathcal{H}_1(t+\tau)|f)} = \overline{(i|\mathcal{H}_1(t+\tau)|f)(f|\mathcal{H}_1(t)|i)} = G_{fi}(-\tau) \tag{2.25}$$

The function $G_{fi}(\tau)$ is called the "correlation function" of the perturbation Hamiltonian $\mathcal{H}_1(t)$, because it tells us how $\mathcal{H}_1$ at one time is correlated to its value at a later time. The correlation function $G_{fi}(\tau)$ goes to zero when $\mathcal{H}_1(t+\tau)$ and $\mathcal{H}_1(t)$ are fully uncorrelated; for τ = 0 it takes the form: $G_{fi}(0) = \overline{(i|\mathcal{H}_1(t)|f)}^2 \geq 0$. More generally, the perturbation $\mathcal{H}_1(t)$ varies in time, owing to some physical movement. Thus one can determine a critical time τ_c, called the "correlation time". For time less than the correlation time ($\tau < \tau_c$), the motion may be considered negligible, so that $\mathcal{H}_1(t) \cong \mathcal{H}_1(t+\tau)$. For $\tau > \tau_c$, the values of $\mathcal{H}_1(t+\tau)$become progressively less and less correlated to $\mathcal{H}_1(t)$ so that G_{fi} goes to zero. Thus $G_{fi}(\tau)$ has a maximum at τ = 0 and falls off for $|\tau| > \tau_c$ as shown in Figure 2.3(a).

We now rewrite the transition probability in terms of the correlation function:

$$W_{i,f} = W_{f,i} = \frac{1}{\hbar^2}\int_0^t [G_{fi}(\tau)e^{-i\frac{E_f-E_i}{\hbar}(\tau)} + G_{fi}(-\tau)e^{i\frac{E_f-E_i}{\hbar}(\tau)}]d\tau = \frac{1}{\hbar^2}\int_{-t}^t G_{fi}(\tau)e^{-i\frac{E_f-E_i}{\hbar}(\tau)}d\tau \tag{2.26}$$

We confine our attention to times longer than correlation the time $t \gg \tau_c$, where the limit of the integration may be taken as $\pm\infty$ so that the transition probability becomes time independent.

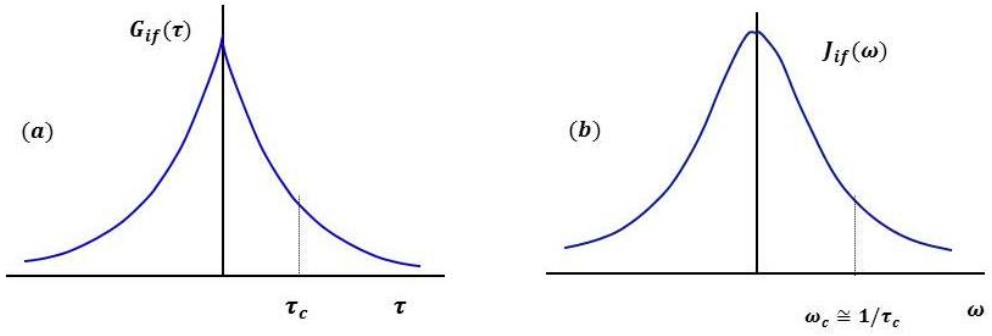

Figure 2.3 (a) Correlation function for a typical experimentally decay (b) Corresponding spectral density plot

Since from an experimental point of view one is often interested in spin correlations as a function of frequency, it is useful to define the Fourier Transform of the correlation function $G_{fi}(\tau)$ as a spectral density function given by:

$$J_{fi}(\omega) = \int_{-\infty}^{+\infty} G_{fi}(\tau) e^{-i\omega\tau} d\tau \tag{2.27}$$

It should be noted that $J(\omega)$ is significantly different from zero for frequencies up to the order of $1/\tau_c$. Moreover, since τ_c is related to the dynamics of the coupled ions, it depends on temperature. It can be also shown that a long τ_c, corresponding generally to low temperature, leads to a slow decaying correlation function and to a spectral density that is significantly different from zero only in a narrow (low) frequency interval. On the other hand, a temperature increase leads to shorter correlation times and hence to a larger spread of the spectral density. The behavior of a typical correlation function and of the corresponding spectral density are shown in Figure 2.3.

By replacing the perturbation Hamiltonian[1] into the correlation function, Equation (2.25), we can obtain

$$G_{fi}(\tau) = \overline{(f|\mathcal{H}_1(t)|i)(i|\mathcal{H}_1(t+\tau)|f)}$$
$$= \gamma_n^2 \hbar^2 \sum_{p,p'} (f|I_p|i)(i|I_{p'}|f)\overline{H_p(t)H_{p'}(t+\tau)} \tag{2.28}$$

The spectral density function can be obtained by assuming $p = p'$, which means that the different components of the magnetic field fluctuate independently:

$$J_{fi}^{p}(\omega) = \gamma_n^2 \hbar^2 \left|(f|I_p|i)\right|^2 \int_{-\infty}^{+\infty} \overline{H_p(t)H_p(t+\tau)} e^{-i\omega\tau} d\tau \tag{2.29}$$

Having the expression of the relaxation transition rate probability $W_{i,f}$, we are now able to evaluate T_1 and T_2. We confine the problem to a spin ½ system.

By recalling the Master equation (see section 2.1) the spin lattice relaxation rate is given by

$$T_1^{-1} = 2W_{+1/2\to-1/2} \tag{2.30}$$

According to Equation (2.30), the problem of studying $1/T_1$ is strictly related to the transition probability $W_{i,f} \approx W_{1/2\to-1/2}$ between the two Zeeman's levels ±1/2. By using Equations (2.26), (2.27) and (2.29) one can simply obtain:

$$W_{fi} = \frac{1}{\hbar^2}\gamma_n^2 \hbar^2 \left|(+\frac{1}{2}|I_p| - \frac{1}{2})\right|^2 \int_{-\infty}^{+\infty} \overline{H_p(t)H_p(t+\tau)} e^{-i\omega\tau} d\tau \tag{2.31}$$

Equation (2.31) shows that the shape of J (ω) requires information on the physical basis of the field fluctuations.

---

[1] Starting from Equation (2.27), we specialize a particular form for the hyperfine interaction as $\mathcal{H}_1(t) = -\gamma_n \hbar \sum_{p=x,y,z} H_p(t) I_p$ which consist of a fluctuating magnetic field with x-, y-, and z-components that couple to the components of the nuclear moment.

However, since the operators H_p only contain electronic spin operators, the correlation function $\overline{H_p(t)H_p(t+\tau)}$ can be expressed as a linear combination of spin-spin correlation functions given by $G^{\alpha\gamma}(\boldsymbol{r}_{ij},t) = \langle s_i^{\alpha}(0)s_j^{\gamma}(\tau)\rangle$ [10]. The time evolution of $s_j^{\gamma}(t)$ is governed by the spin Hamiltonian introduced in chapter 1 and is given by

$$s_j^{\gamma}(t) = e^{i\mathcal{H}t/\hbar}s_j^{\gamma}(0)e^{-i\mathcal{H}t/\hbar} \tag{2.32}$$

By using the quantum mechanics principle (for writing a quantum observable), the statistical average of the Correlation Function (CF) is written as

$$G^{\alpha\gamma}(\boldsymbol{r}_{ij},t) = \frac{Tr\left\{e^{-\beta\mathcal{H}}s_i^{\alpha}(0)e^{\frac{i\mathcal{H}t}{\hbar}}s_j^{\gamma}(0)e^{-\frac{i\mathcal{H}t}{\hbar}}\right\}}{Tr\{e^{-\beta\mathcal{H}}\}} \tag{2.33}$$

where Tr{…} represents the trace of the operator and $\beta = 1/k_BT$. It is worth noticing that Equation (2.33) gives the probability that at the generic time t the γ component of the spin located in the j-th site has a given value knowing the value of the α component for the i-th spin at time t = 0.[1]

Another simplification in Equation (2.31) can be introduced taking into account the symmetry of the Hamiltonian. Furthermore, in particular, if we assume that the dominant mechanism for inducing nuclear relaxation is the time dependent dipolar interaction between the nuclear magnetic moments and the electronic ones, the following expression can be obtained for $1/T_1$ [1, 6][2].

$$\frac{1}{T_1} = 2\gamma_n^2\gamma_e^2\hbar^2 s(s+1)\sum_{ij}\left\{\alpha_{ij}\int_{-\infty}^{+\infty}\langle s'^{+}_i(\tau)s'^{-}_j(0)\rangle e^{i(\omega_n\pm\omega_e)\tau}d\tau + \beta_{ij}\int_{-\infty}^{+\infty}\langle s_i^z(\tau)s_j^z(0)\rangle e^{i\omega_n\tau}d\tau\right\} \tag{2.34}$$

where ω_e and ω_n are the nuclear and electron Larmor frequency, respectively. The geometrical coefficients α_{ij} and β_{ij} depend on the polar angles θ_{ij}, ϕ_{ij} and the relative distance r_i or r_j. One should take into account here that expressing the correlation function for the transverse components ($s^{\pm}$) of the spin, we have separated the time-dependence rotation term due to the coherent Larmor precession around the magnetic field, from the random time-dependence. This hypothesis is acceptable as long as the system is in the paramagnetic state and magnetically isotropic. Equation (2.34) is the starting point for all theoretical interpretations in the case of T_1 in a perfect Heisenberg system.

For what concerns the spin-spin relaxation time T_2, i.e. the characteristic time of the irreversible decay of the transverse magnetization, it should be observed that T_2 processes are associated with the spread in the local fields (thus a spread of the Larmor frequency) produce for example by the other nuclear spins through dipolar interactions.

---

[1] more details about the Correlation Function (CF) and its formalism in terms of collective q-variables is presented in Appendix 1.

[2] Since detailed theoretical calculations are beyond the scope of the present work, the interested reader should follow more details in a review by Moriya [1, 12]

In a rigid lattice we can visualize the spin-spin relaxation process as a process of dephasing of the spins during their Larmor precession around the applied magnetic field. Therefore in this case we can define the spin-spin relaxation rate as the inverse of dephasing time of the free-precession signal. It should be noted that in the presence of static quadrupole effects which produce splitting and/or shifts of the resonance line, a definition of the spin-spin relaxation rate is not always possible. A solution for the spin-spin relaxation rate can be obtained in the fast motion approximation as below [1, 10, 11]:

$$\frac{1}{T_2} = \frac{1}{2T_1} + 2\gamma_n^2\gamma_e^2\hbar^2 s(s+1)\sum_{ij}\left\{\epsilon_{ij}\int_{-\infty}^{+\infty}\langle s_i^z(\tau)s_j^z(0)\rangle d\tau + \beta_{ij}\int_{-\infty}^{+\infty}\langle s_i^+(\tau)s_j^-(0)\rangle d\tau\right\} \qquad (2.35)$$

where ϵ_{ij} and β_{ij} are geometrical functions similar to the ones of $1/T_1$. The first term is due to life-time effects and the second term is proportional to the spectral density function at zero frequency because there is no energy exchange between lattice and spins.

As it is discussed in Appendix 1, by introducing the Fourier representation of the spin components in reciprocal space in a manner analogous to that employed in describing the normal modes of a harmonic crystal, we can also obtain an expression for the spin-spin correlation functions in terms of the collective variable **q** (see Appendix 1). One could also extend such formalism to $1/T_1$ and $1/T_2$. Recalling Equations (A_1.3) and (A_1.4), the spectral density of spin fluctuations in reciprocal space, we can rewrite Equation (2.34) and (2.35) as linear combinations of the dynamical structure factors $S^{\alpha\gamma}(\boldsymbol{q},\omega)$ as below:

$$\frac{1}{T_1} = \frac{2\gamma_n^2\gamma_e^2\hbar^2 s(s+1)}{N}\sum_{\boldsymbol{q}}(a_q S^+(\boldsymbol{q},|\omega_n \pm \omega_e|) + b_q S^z(\boldsymbol{q},\omega_n)) \qquad (2.36)$$

and

$$\frac{1}{T_2} = \frac{1}{2T_1} + \frac{2\gamma_n^2\gamma_e^2\hbar^2 s(s+1)}{N}\sum_{\boldsymbol{q}}(e_q S^z(\boldsymbol{q},0) + b_q S^+(\boldsymbol{q},0)) \qquad (2.37)$$

where a_q, b_q and e_q are simply the Fourier expansions in reciprocal space of the geometrical factors given in equations (2.34) and (2.35) as below

$$a_q = \sum_{ij}\alpha_{ij}e^{\boldsymbol{q}\cdot\boldsymbol{r}_{ij}}, \qquad b_q = \sum_{ij}\beta_{ij}e^{\boldsymbol{q}\cdot\boldsymbol{r}_{ij}}, \qquad e_q = \sum_{ij}\epsilon_{ij}e^{\boldsymbol{q}\cdot\boldsymbol{r}_{ij}} \qquad (2.38)$$

So far we have established that the nuclear spin lattice relaxation rate temperature and field dependence is governed by the temperature and field behavior of the electronic spin-spin correlation function. In the following we go a step further making a link between the theoretical models and the relevant phenomenological observations in three different temperature regions namely high, intermediate, and low temperatures.

2.3.1 NMR at high temperature ($k_BT \gg J$)

In the high temperature regime ($k_BT \gg J$)[1], there is a weak correlation among spins, and we can consider the magnetic response of the system to be isotropic:

$$G_{ij}^{+}(\boldsymbol{r}_{ij},t) = G_{ij}^{-}(\boldsymbol{r}_{ij},t) = G_{ij}^{z}(\boldsymbol{r}_{ij},t) \tag{2.39}$$

It was also found that the spin correlation in this region is strongly affected by the dimensions of the spin lattice. Consequently, it is convenient to follow the problem of the correlation function according to the dimension (D) of the spin lattice.

(i) 3D-systems

In the case of 3-dimensional lattice, it has been often assumed [6, 12] that one can truncate the short-time expansion of a correlation function at the second term and approximate it with a Gaussian form over the entire time scale

$$\langle s_i^{\alpha}(t) s_j^{\alpha}(0)\rangle = \frac{1}{3} s(s+1) e^{-\frac{1}{2}t^2\omega_{ex}^2} \tag{2.40}$$

with the exchange frequency ω_{ex} given by

$$\omega_{ex}^2 = \frac{8}{3}\frac{J^2}{\hbar^2} z s(s+1) \tag{2.41}$$

where z is the number of nearest-neighbors magnetic ions of a given ion; the exchange frequency is a typical frequency for the decay of the correlation function. The above discussion is adopted solely in 3D because the information can disperse in three different isotropic directions, so that the correlation function goes to zero rapidly. However, this approximation is not valid for lower dimensional lattices. In those systems, the spin interactions take place within a plane (2D) or a chain (1D), and therefore the correlation between spins can survive at long time due to the spin topology restrictions.

(ii) Lower dimensional systems and spin diffusion approach

In the case of lower dimension, experimental results and theoretical predictions suggest that, in the case of an isotropic Heisenberg exchange interaction, the spin dynamics is dominated by a diffusive behavior of the spin excitations [13].

Therefore, by assuming a diffusive behavior of the spin excitations, one can predict the time dependent behavior of the correlation function. In particular, it has been shown that in the case of 1D linear chains of spins the autocorrelation function is given by $G^{\alpha\gamma}(t) \propto t^{-1/2}$, and in the case of 2D planar arrangements is: $G^{\alpha\gamma}(t) \propto t^{-1}$ [13 ,14]. The corresponding spectral densities obtained through Fourier transform are given by:

[1]High temperature regime is achievable if $e^{-\beta\mathcal{H}} \sim 1$, i.e. $k_BT \gg Js(s+1)$. This condition can be achieved at room temperature.

$$J_{ii}^{\alpha}(\omega) = \begin{cases} \omega^{-1/2} & 1D \\ -ln(\omega) & 2D \\ const & 3D \end{cases} \tag{2.42}$$

In the low dimensional system, 1D and 2D, Equations (2.42) predict a divergent behavior as $\omega \rightarrow 0$ which was observed experimentally. However, it must be noted that there are limitations to the applicability of the spin diffusion model in describing the dynamics in real spin systems. These limitations occur because the diffusion model requires certain conditions which are not always fulfilled in real systems, namely:

(1) The spin Hamiltonian that determines the time evolution of the spin system may contain anisotropic terms that are not negligible. The effect of these terms is to destroy the conservation of the total spin S_T (i.e. the commutation relation $[S_T, \mathcal{H}] \simeq 0$ is no longer verified). Therefore the diffusive model is no longer applicable.

(2) Chains and/or planar spin systems are isolated from one another only in principle. In fact there is always a small inter-chain and inter-plane dipolar interaction which, after a sufficiently long time ($t \gg t_{ex}$), affects the spin dynamics.

To take into account these effects, which are observed experimentally, one usually define a "cut off" time. For $t > t_{cutoff}$ the decay of the correlation functions is much faster and the corresponding spectral density can be replaced by a constant value for $\omega < \omega_{cutoff}$, where ω_{cutoff} is the "cut off" frequency. In the following we discuss in particular the case of 1D systems and closed chains corresponding to "open" and "closed" ring, respectively.

(ii-a) 1D spin systems

It has been already indicated that the correlation function in presence of a diffusive behavior in 1D spin system can be modeled as [15]

$$G_{ii}(t) = (4\pi D t)^{-1/2} e^{-\omega_c t} \tag{2.43}$$

where the first term represents the long time diffusive behavior while the exponential decay simulates the effect of the anisotropic intra-chain interactions and/or inter-chain interactions as explained above. The parameter D is the spin diffusion constant and ω_c is the cut-off frequency. By using the Fourier Transform of the correlation function, Equation (2.43), into the NSLR rate, $1/T_1$, and considering equation (2.39) one finally obtains [15, 16]

$$\frac{1}{T_1} = P\left\{\frac{(H_c^2 + H^2)^{1/2} + H_c}{[H_c^2 + H^2]}\right\}^{1/2} + Q \tag{2.44}$$

The constant Q represents the contribution to the spectral density of the fast decaying CF at short times, similar to 3D systems. This contribution becomes frequency independent at frequencies smaller than the exchange frequency defined by Equation (2.41). The first term in Equation (2.44) arises from the spectral density defined by the diffusive behavior and it contains the desired information about spin diffusion and cut-off effects. The cut-off field H_c has been introduced in place of the cut-off

frequency $\omega_c = \gamma_e H_c$, where γ_e is the electron gyromagnetic ratio. The constant P contains the information about the spin diffusion constant D in rad Hz, i.e. $P = C/2\pi(2D\gamma_e)^{1/2}$ where C is the average square of the hyperfine interaction between nuclei and electrons in unit of (rad Hz)^2. It is worth noticing that one can set $H_c = 0$ in $1/T_1$, when the cut-off effects are negligible in the field (frequency) range of investigation.

(ii-b) Magnetic closed rings

Here, we focus on systems composed of a finite number of spins which form a closed loop, as in the case of AFM rings. The autocorrelation function of these systems can be obtained by using a similar model used for an infinite Heisenberg chain where the discretized diffusion equation is applied to satisfy the cyclic boundary conditions of a closed ring. The same results for the CF can also be obtained by using the one-dimensional hopping model (hoping is referred to the change of orientation of a spin) on a closed loop where the cyclic condition is considered, so that all sites around the closed loop are completely equivalent, and therefore the CF is independent from the initial site [12, 17]. Consequently the CF decays rapidly at short times until it reaches a constant value that depends on the number of spins in the closed chain, given by 1/N with N the number of spins in the loop. The leveling-off of the time dependence of the CF at a value approximately given by 1/N is the result of the conservation of the total spin component for an isotropic spin-spin interaction. In practice the anisotropic terms in the spin Hamiltonian produce a secondary decay in the CF via energy exchange with the "Lattice" at long times. This decay can be explained by the cut-off concept similar to the one used for spin diffusion in 1D systems in the previous section. A sketch of the time decay of the CF and of the corresponding spectral density is shown in Figure 2.4. In the following we will discuss magnetic field dependence of $1/T_1$ at high temperature in terms of a simplified model.

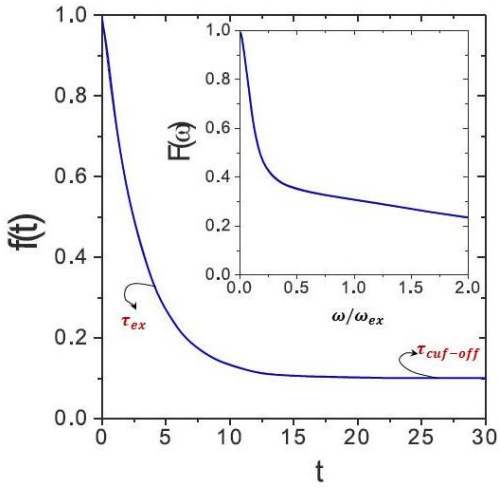

Figure 2.4 Sketch of the decay in time of the autocorrelation function of the electronic spins in a spatially restricted magnetic system (e.g. 1D or AFM rings or segment). The initial fast decay is characterized by the constant $1/\omega_{ex}$ while the decay at long times (not shown) is characterized by the constant $1/\omega_c$. In the inset behavior of the Fourier transform, i.e. the spectral density, is shown [16]

According to the sketch of the CF in Figure 2.4, one can model the CF as $G(t) \propto e^{t/\tau_{ex}} + e^{-t/\tau_{cut-off}}$ by assuming $\tau_{cut-off} \gg \tau_{ex}$. For simplicity we use "c" instead of "cut-off" in the following. The Fourier transform of the CF leads to the spectral density of fluctuations:

$$J^{\pm}_{e,n}(\omega) = J^{z}_{e,n}(\omega) = \frac{\omega_{ex}}{\omega_{ex}^2 + \omega^2} + \frac{\omega_c}{\omega^2 + \omega_c^2} \tag{2.45}$$

where ω denotes both ω_n (nuclear Larmor frequency) and ω_e (electron Larmor frequency). The first term in Equation (2.45) represents the Fourier Transform of the initial fast decay due to the exchange interaction while the second term determines the Fourier Transform of the second decay at long times due to anisotropic terms in the Spin Hamiltonian. Furthermore the same correlation function is assumed for the decay of the longitudinal (z) and transverse (±) components. Since the exchange frequency ω_{ex} is of the order of 10^{13}Hz for typical values of J/k_B (10÷20 K) and spin S (1/2÷5/2), one can assume that both ω_n and ω_e are much smaller than $\omega_{ex}/10$ (the plateau in the CF is reached after a time of the order of $10\omega_{ex}^{-1}$). As a result, the first term in Equation (2.45) for both longitudinal and transverse components is proportional to $1/\omega_{ex}$. Finally by assuming $\omega_e \ll \omega_c$ in Equation (2.34) and using Equation (2.34), one can obtain

$$\frac{1}{T_1} = K\left[\frac{1}{2}A^{\pm}\frac{\omega_c}{\omega_c^2 + \omega_e^2} + \frac{1}{2}\frac{A^{\pm}}{\omega_c} + A^{z}\left(\frac{1}{\omega_{ex}} + \frac{1}{\omega_c}\right)\right] \tag{2.46}$$

where the constant $A^{\pm}$ and A^{z} are averaged over all nuclei, and the constant K, which has been factored out from the dipolar tensor coefficients, is given by $K = \frac{(\hbar\gamma_n\gamma_e)^2}{4\pi g^2\mu_B^2} k_B T\chi(q=0)$.

It should be noted that Equations (2.44) and (2.46) point toward a very similar behavior regarding the magnetic field dependence of $1/T_1$. In fact the only difference in the time dependence of the CF for 1D systems and closed rings is in a short time interval between ω_{ex}^{-1} and ω_c^{-1} where the CF in 1D chains has a slow $t^{-1/2}$ dependence while in a ring is practically constant. This point will be illustrated when we discuss the possibility of detecting spin diffusion effects in closed and open magnetic rings (see section 3.2.1).

2.3.2 NMR at intermediate temperature ($k_BT \approx J$)

As the temperature is lowered and it becomes comparable to the magnetic exchange interaction J ($k_BT \approx J$), strong correlations among the magnetic moments start building up. Consequently, in this temperature range two interesting mechanisms occur, namely:

(1) The spin correlation functions change their behaviors when the system crosses over from an uncorrelated finite size paramagnet to a total spin S quantum state.

(2) The local electronic spins fluctuate close to its ground state.

To study the behavior of $1/T_1$ at intermediate temperature, and far from the level crossing condition we can start from the general Equation (2.36) in terms of collective variable q. Using the fluctuation dissipation theorem[1] in high temperature limit, the dynamical structure factor is expressed as

$$S(\boldsymbol{q},\omega) \simeq \frac{k_B T}{\pi g^2 \mu_B^2 \omega} \chi''(\boldsymbol{q},\omega) \tag{2.47}$$

where $\chi''(q,\omega)$ is the dissipative part of the generalized susceptibility. It is also convenient to separate the correlation function for collective variable into a static and a time-dependent part as below

$$S(\boldsymbol{q},\omega) = S(\boldsymbol{q}) J_q(\omega) \tag{2.48}$$

Where $J_q(\omega) = \int_{-\infty}^{+\infty} J_q(t)dt$ (see CF), and the $S(\boldsymbol{q})$ is the static structure factor[2] related to the static wave-vector dependent susceptibility $\chi''(\boldsymbol{q},0)$, given by

$$S(\boldsymbol{q}) = \frac{k_B T}{\pi g^2 \mu_B^2} \chi''(\boldsymbol{q},0) \tag{2.49}$$

By replacing Equation (2.49) into (2.48) and recalling the main equation for $1/T_1$, one can obtain

$$\frac{1}{T_1} = \left(\frac{h\gamma_n\gamma_e}{\sqrt{4\pi} g \mu_B}\right)^2 k_B T \sum_q \left[\frac{1}{4} A^{\pm}(\boldsymbol{q}) \chi^{\pm}(\boldsymbol{q}) J_{\boldsymbol{q}}^{\pm}(\omega_n \pm \omega_e) + A^z(\boldsymbol{q}) \chi^z(\boldsymbol{q}) J_{\boldsymbol{q}}^z(\omega_n)\right] \tag{2.50}$$

where $\omega_n = \gamma_n H_0$ and $\omega_e = \gamma_e H_0$ are the nuclear and electron Larmor frequency, respectively, g is the Landè factor, μ_B is the Bohr magneton, k_B is the Boltzmann constant, $\chi(\mathbf{q})$ is the generalized q-dependent spin susceptibility and $J_q(\omega)$ is the spectral density of the collective spin fluctuations. The coefficient $A^{\pm}(\mathbf{q})$ and $A^z(\mathbf{q})$ are the Fourier Transforms of the spherical components of the product of two dipole interaction tensors describing the hyperfine coupling of a given nuclear spin (i.e. spin in ^{1}H NMR measurements) with the electron magnetic moments.

For the specific case of AFM rings and also ^{1}H NMR, we can consider some additional simplifications. More specifically since, in the present work, we are measuring the nuclear spin-lattice relaxation rate of a large number of protons distributed in different locations within the molecule we can reasonably assume that the geometrical factors ($A^{\pm}(\mathbf{q})$ and $A^z(\mathbf{q})$ corresponding to α_{ij} and β_{ij}, respectively) are averaged over all positions and orientations.

Thus the geometrical factors expressed the **q** space do not depend significantly on different values of q. As a result one can set $A^{\pm}(\mathbf{q}) = A^{\pm}$ and $A^z(\mathbf{q}) = A^z$. Furthermore since we are in the high temperature limit, a perfect isotropic response function can be supposed so that $1/2\chi^{\pm}(q) = \chi^z(q) = \chi(q=0)$. According to above approximations, Equation (2.50) reduces to

---

[1]The spectrum of the fluctuations is related to the response to a dynamic perturbation by the fluctuation dissipation theorem [8].

[2]The static structure factor can be found by integrating over the whole frequency spectrum and using the Kramers-Kronig relations; $S(\boldsymbol{q}) = 1/2\pi \int S(\boldsymbol{q},\omega)d\omega$

$$\frac{1}{T_1} = \left(\frac{h\gamma_n\gamma_e}{\sqrt{4\pi}g\mu_B}\right)^2 k_B T\chi(0)\left[\frac{1}{2}A^{\pm}J^{\pm}(\omega_n \pm \omega_e) + A^z J^z(\omega_n)\right] \quad (2.51)$$

Assuming a correlation function that decays exponentially as a function of time with a characteristic frequency ω_c(T,H) and that $\omega_e \gg \omega_n$ (those conditions are satisfied in semi-integer AFM rings at intermediate temperature and far from the level crossing) one can obtain [6]

$$\frac{1}{T_1} = A\chi T \frac{\omega_c(T,H)}{\omega_c^2(T,H) + \omega_n^2} \quad (2.52)$$

where AχT is the average square of the transverse fluctuating hyperfine field in frequency units. Generally Equation (2.52) is called BPP-like formula (from the original paper, ref. [11], by Bloembergen, Purcell and Pound), and it is used to describe the $1/T_1$ experimental results in liquid and molecular solids.

From (2.52) one can note that, interestingly, the measurements of the nuclear spin-lattice relaxation rate give access to information regarding the electron spin system via ω_c(T,H). In a finite size system, the correlation frequency ω_c(T,H) can be interpreted as the "lifetime" of the discrete magnetic energy levels. The "lifetime" of the electronic energy levels is given by the relaxation time of the magnetization of the molecular nanomagnet which is driven by the spin-phonon interaction. In the following we will briefly summarize the temperature and field dependence of ω_c(T,H) expected as a result of spin-phonon interaction which will be useful in the next chapter.

(i) Spin-phonon interaction

In general , the relaxation process of the molecular magnetization which is responsible for the correlation frequency ω_c(T,H) defined above involves the emission or absorption of a quantum of energy by the electronic spin system, and we are now going to consider how this quantum can be absorbed or emitted by the lattice vibration (the phonon). It should be taken into account that a transition between two levels of the spin system can only be induced by an oscillatory electromagnetic field of the right frequency, and it could happen that the mechanical vibrations of the lattice can produce such an oscillatory field. This mechanism results in the so-called spin-phonon interaction. Although different processes can be invoked to explain the different T-dependence and H-dependence of the spin-phonon interaction, we will here report some of those processes that can explain the relaxation of the magnetization in molecular nanomagnets, namely (a) direct process, (b) Orbach process and (c) Raman process [18].

(a) Direct process. In this process one phonon is emitted or absorbed in a given electronic transition (characterized then by a "relaxation" time). Analyzing this process, the temperature and field dependent of the correlation frequency is given by

$$\omega_c(T,H) \propto H^3 \coth\left(\frac{\hbar\gamma_e H}{2k_B T}\right) \quad (2.53)$$

$$or \qquad \omega_c(T,H) \propto H^2 T \; when \;\; \hbar\gamma_e H \ll k_B T$$

(b) Orbach process. This process involves two low-lying states for example $|a\rangle$, $|b\rangle$ and an excited state $|c\rangle$ at energy Δ higher than the low-lying states. It is possible for an electron spin in state $|b\rangle$ to absorb a quantum of energy (phonon) and jump to the state $|c\rangle$, and then to relax to the state $|a\rangle$ by emitting a quantum of slightly different energy (e.g. to the phonon bath). This occurrence corresponds to an indirect transfer between state $|b\rangle$ and state $|c\rangle$, with a typical frequency given by

$$\omega_c(T,H) \propto \frac{\Delta^3}{e^{\Delta/k_B T} - 1} \tag{2.54}$$

(c) Raman Process. This process is rather similar to the Orbach process but involve a "virtual" state at higher energy instead of $|c\rangle$. As in the previous case, the electron spin makes a transition from state $|b\rangle$ to, this time, a "virtual" state $|c\rangle$ accompanied by the absorption of a phonon of angular frequency ω_1, and subsequently return down to a state $|a\rangle$ (at different energy with respect to $|b\rangle$) with the emission of a phonon of frequency ω_2. The condition for conservation of energy is $\omega_1 - \omega_2 = \pm\omega$ and this condition makes the process much probable because is fulfilled almost over the whole phonon energy density spectrum. When the relaxation is driven by a Raman process, for the typical correlation frequency one obtains

$$\omega_c(T,H) \propto T^{\alpha} \qquad 7 \leq \alpha \leq 9 \tag{2.55}$$

As it will be explained in details further on, the spin-lattice relaxation rate as a function of temperature for many antiferromagnetic rings has been explained on a wide temperature range by assuming a temperature dependence of ω_c given by $\omega_c = CT^{\alpha}$ with α ~ 3.5 [9, 19]. This power law reminds Eq.(2.55) and the connection to Raman processes appears rather natural. It should be noticed however that cautions has to be taken, because in the T-region of the NMR nuclear spin-lattice relaxation rate anomalies, the assumption of a power law or an exponential dependence for ω_c give similar results.

2.3.3 NMR at low temperature ($k_B T \ll J$)

The low temperature approximation is satisfied when the temperature is much lower than the exchange interaction among moments ($k_B T \ll J$). In this situation, the system is mostly in its collective quantum ground state characterized by a total spin S. Therefore, generally a collective variables approach or a spin wave picture is essential to describe the excitations of the spin system in its lowest ground state. In brief, a spin wave consists of a single spin flip delocalized throughout the lattice by following a sinusoidal law. Since the spins are quantized, the corresponding excitations (magnons) are also quantized [20]. In the limit T→0 one can consider an expression for the dynamical structure factor in the form

$$S^{\alpha\gamma}(\boldsymbol{q},\omega) = S^{\alpha\gamma}(\boldsymbol{q})\delta\left(\omega - \omega_q\right) \tag{2.56}$$

where **q** is the frequency corresponding to an excitation mode of the fluctuations at a specific reciprocal wave vector **q**. The spin wave approximation allows one to treat the system as a set of modes that behaves like a system of independent harmonic oscillators and thus allows the calculation of the correlation function if an explicit form of spin Hamiltonian, and (in case) its symmetries, are known. In order to obtain an expression which can be used, one must also take into account that small interactions among the different excitations will eventually destroy the independence of the set of harmonic oscillators. Therefore the $\delta\left(\omega - \omega_q\right)$function in Equation (2.56) must be replaced by a proper function, for example a Lorentzian one, which accounts for the fact that the excitations will eventually decay in time. Since we are dealing with systems with a small finite number of spins the concept of spin wave is not directly applicable except when the molecular nanomagnets develop long range order as the result of weak intermolecular interactions [21].

Nevertheless it is useful to use the analogy with spin waves provided one replaces the spin wave concept with a collective excitation of the finite spin system were the single spin flip is delocalized over the finite AFM ring. This approach has been formulated in the case of magnetic rings by Cornia et al [22] and will be used in the discussion of our experimental results in the present work. A summary of the theoretical results is given in the following section.

(i) Low temperature theory of ^{1}H NMR in AFM rings

The nuclear relaxation rate, specifically proton spin-lattice relaxation rate $1/T_1$, at low temperature and near level crossing fields can be calculated starting from the fundamental theory and by using a quantum approach[1]. Thus, one only needs to calculate the spin correlation function as matrix elements using the eigenstates of the total spin Hamiltonian, characterized by the quantum numbers S and M_s, whereby S is the total spin of the ring and M_s is the projection of S along the quantization axis. Since we are in the low temperature approximation, a few quantum states are occupied and the correlation function can be calculated by using Equation (2.33). By replacing it into Equation (2.34), the spin-lattice relaxation rate is given by [6, 23]

$$\frac{1}{T_1} = \frac{1}{2}(\gamma_e\gamma_n\hbar)^2 \sum_{ij}^{N} \frac{1}{(r_i r_j)^3} \frac{1}{\sum_f e^{-\beta E_f}} \sum_{f,i} e^{-\beta E_f} \pi\left[\delta\left(\omega_n + \omega_{fi}\right) + \delta\left(\omega_n - \omega_{fi}\right)\right]$$
$$\cdot \left[\alpha_{ij}\langle f|s_i^z|i\rangle\langle i|s_j^z|f\rangle + \frac{1}{4}\beta_{ij}(\langle f|s_i^-|i\rangle\langle i|s_j^+|f\rangle + \langle f|s_i^+|i\rangle\langle i|s_j^-|f\rangle)\right] \tag{2.57}$$

[1]The magnetic field dependence of 1/T1 is theoretically determined by means of the linear response theory [12, 24], starting from the unperturbed eigenvalues and eigenvectors of the magnetic ring as obtained from the spin Hamiltonian and introducing superhyperfine interactions as a perturbation [see section 2.3 in this chapter].

where α_{ij} and β_{ij} are the geometrical coefficients of the dipolar interaction (see Equation 2.34)) and depend on the position vectors $\mathbf{r}_i$ and $\mathbf{r}_j$, joining the nuclei (i.e. proton) with the i-th and j-th electron spin, respectively. Since the nuclear Larmor frequency ω_n is negligible for all the magnetic field values used in the experiments, the Dirac δ-functions are satisfied only near the level crossing between E_f and E_i, i.e. $\omega_{fi} = E_f - E_i = 0$. Since this theory is limited to the low temperature case[1] (i.e. T much less than the gap among the ground state and the first excited state), only the ground state $|g\rangle$ and the first excited state $|e\rangle$ are involved in the f-summation. For the i-summation, the Dirac δ-functions $\delta(\omega_{gi} \pm \omega_n)$ and $\delta(\omega_{ei} \pm \omega_n)$ are approximately satisfied for $|i\rangle = |g\rangle$ and $|i\rangle = |e\rangle$, respectively, in any field regime.

Considering the above discussion, one can analytically calculate the matrix elements using the Irreducible Tensor Operator (ITO) formalism and the Wigner-Eckart theorem [24] to obtain the NSLR rate as [21]:

$$\frac{1}{T_1} = \frac{1}{2N^2}(\gamma_e\gamma_n\hbar)^2\left[2\pi\delta(\omega_n)\frac{1}{1+e^{-\beta\hbar\omega_{eg}}}\left[S^2 + e^{-\beta\hbar\omega_{eg}}(S+1)^2\right]G_\alpha + \pi\left[\delta(\omega_n + \omega_{eg}) + \delta(\omega_n - \omega_{eg})\right]\frac{(S+1)[(Ns+1)^2 - (S+1)^2]}{2(2S+3)}G_\beta\right] \quad (2.58)$$

where the ground state $|g\rangle$ and the first excited state $|e\rangle$ are described by $|S, -S\rangle$ and $|S+1, -(S+1)\rangle$, respectively. The coefficients $G_\alpha = \sum_{ij}\alpha_{ij}(r_i r_j)^{-3}$ and $G_\beta = \sum_{ij}(-1)^{i+j}\beta_{ij}(r_i r_j)^{-3}$ involve the geometrical properties of the magnetic ring. The first contribution in Equation (2.58) is the quasi-elastic term centered at zero frequency $\delta(\omega_n)$, and arises from the fluctuations of the magnetization of the magnetic ring in the first magnetic excited state. These fluctuations, due to spin-phonon interactions, can be modeled with a Lorenzian broadening Γ_1 of the magnetic state. Consequently, the quasi-elastic part of the NSLR is driven by a Lorenzian spectral density function at the Larmor frequency ω_n, $2\pi\delta(\omega_n) = 2\Gamma_1/(\Gamma_1^2 + \omega_n^2)$. The second term, the "inelastic" one, is centered at the frequency ω_{eg} which implies that the δ-function is different from zero only for $\omega_n = \omega_{eg}$. As a result, the inelastic term becomes significance only around the crossing field and arises from direct transitions between nuclear Zeeman states accompanied by a transition among the magnetic state of the molecule. In essence, in this situation an energy transfer between the electron and nuclear spin system occurs. However, even in this case a broadening Γ_2 of the magnetic state of the molecule has to be introduced in order to allow the energy conservation. The inelastic contribution becomes very big when the energy gap between the ground state and the first excited state Δ_{ge} becomes of the order of the broadening Γ_2. More details on this theory will be discussed in the next chapter where we present our experimental data in the case of Cr_8Zn in the low temperature limit.

[1]Assumin the low temperature approximation is referred to a condition that such a two level-scheme is totally justified.

3. NMR experiments and analysis in Molecular Antiferromagnetic (AFM) rings

In this chapter we report ^{1}H NMR experimental data including Nuclear Spin-Lattice relaxation rate (NSLR) $1/T_1$, spin-spin relaxation rate $1/T_2$, and NMR spectra, which have been collected in three different temperature ranges according to the classification indicated in section 2.3 . This chapter is organized as follows. In the first section 3.1 we briefly explain how ^{1}H NMR data were experimentally collected. The high temperature NSLR data are discussed in section 3.2, divided in two subsections regarding semi-integer and integer spin systems respectively. We then report the ^{1}H NMR intermediate temperature data in section 3.3. The first part of section 3.3 (Sec 3.3.1) contains a comparison of spin dynamics in semi-integer spin antiferromagnetic closed and open molecular Cr-based rings, i.e. Cr_8 and Cr_8Zn, while the second part is devoted to integer-spin systems, i.e. V_7Ni and V_7Zn. Finally, the low temperature ^{1}H NMR data including the low temperature level crossing investigation will be discussed in section 3.4.

3.1 Experimental techniques

^{1}H NMR measurements were performed as a function of temperature ($1.6 < T < 300$ K) at different magnetic fields and as a function of magnetic field ($0.3 < \mu_0 H < 9$ T) at different temperatures.
To control the temperature, we used two different cryostats: a dynamic/static continuous flow cryostat for the temperature range from room temperature down to 4.5 K and a bath cryostat from 4.5 to 1.6 K. In the case of flow cryostat, the cooling down of the system takes place by means of thermal exchange with cryogenic fluid, namely liquid Nitrogen for $T > 77$ K, and liquid Helium for $T < 77$K. The bath cryostat does not require a constant supply of the cryogenic fluid, as it is based on a reservoir of liquid that needs to be filled only at the beginning of the measurements. Since the liquid Helium temperature at atmospheric pressure is 4.2 K, lower temperatures can be obtained by pumping the Helium vapors away from the liquid surface of the Helium bath. The lowest temperature achieved by this technique is approximately 1.5 K.

To set the value of magnetic field that was needed in NMR measurements, two different set-ups were used: an electromagnet for the lower magnetic field range ($0.3 < H < 1.7$ T), and a superconducting-magnet for the higher range ($2 < H < 9$ T).

^{1}H NMR measurements, including $1/T_1$, $1/T_2$ and NMR spectra have been performed by using a standard TecMag Fourier transform pulse NMR spectrometer.

The value of the NSLR, $1/T_1$, was determined by monitoring the recovery of the longitudinal nuclear magnetization measured by a $\pi/2_x - \pi_y$ pulse sequence (a $\pi/2_y$ pulse instead of the π_y pulse was used at $T < 100$ K), following a saturation comb of radiofrequency (rf) pulses. The length of the rf comb was adjusted to ensure the best initial saturation condition at the different temperatures and resonance frequencies. Every recovery curve was then obtained by measuring the spin echoes at progressively longer delay times between the comb and the $\pi/2_x - \pi/2_y$ reading sequence ($\pi/2_y$ at $T > 100$ K). It is worth noting that the spin echo signal is the response of the whole set of protons of the irradiated line after a certain delay time and each $1/T_1$ data point at fixed temperature/field is extracted from one recovery curve.

Transverse relaxation measurements, $1/T_2$, were performed mainly by using a $\pi/2_x - \tau - \pi/2_y - \tau$ spin echo pulse sequence. The decay curves were acquired by measuring the echo signal at progressively longer delay times, i.e. τ. In essence, a curve of $M_{xy}(t)$ gives the irreversible decay of the transverse nuclear magnetization in the x-y plane.

In the case of ^{1}H NMR spectra different strategies were employed. For the high and intermediate temperature regions where the whole NMR line could be excited by a single rf pulse, the proton NMR spectra were simply obtained from the Fourier transform of half of the echo signal. On the other hand, in the low temperature region, the whole NMR line could not be irradiated by means of only a single rf pulse and thus a field-sweep method was adopted to collect the whole spectra. In this latter technique, the radio frequency is kept fixed while the applied magnetic field is swept over a selected range around the resonance Larmor field of the bare nucleus. Pulse sequences (solid-spin-echo) are repeated continuously during the sweep with a repetition time usually of the order of 100 ms. The experimental point of the spectrum is given, at any field value, by the integral of the acquired spin-echo signal [1]. In order to resolve the fine structure in the spectrum, it is required that the magnetic field variation during one point acquisition is small compared to the width of the spectral structures of interest. In our experimental measurements, we also employed the frequency-sweep technique in addition to the magnetic field-sweep. In this method, the magnetic field is kept fixed while the frequency is manually swept over a selected range around the Larmor frequency. The echo signal is then acquired after tuning and matching at the desired frequency. Finally, by plotting all the NMR data points obtained from each echo signal (corresponding to different frequencies) in the same figure one can obtain the complete spectrum. The main drawback of this second method lies in the long time of the acquisition.

One should take into account that the experimental results are undoubtedly affected by several different errors mainly due to electronic noise, signal integration, and the evaluation of the signal intensity at infinite delay time in T_1 measurements. Since the statistical study of the experimental error

is not practical we have used an average estimated experimental uncertainty for all data points of +/- 5% .

3.2 High temperature regime

As we discussed in the previous chapters, finite spin systems are good model systems for spin dynamics investigation, where one can obtain semi-classical or numerical theoretical results to be compared with the experiments, particularly in the paramagnetic phase at high temperature. Early numerical calculations on these systems indicated a persistence at long time of the decay of the pair correlation function (CF) [2]. This result was later confirmed by analytical solutions of a 1D Heisenberg chain which showed a diffusive behavior at long times of the spin CF due to the conservation of the total spin value S [3-5].

The most direct experimental verification for this theory comes from the NSLR measurements. In fact, the nuclei couple to the magnetic electrons by means of the hyperfine interaction and are thus sensitive to the fluctuations of the electron spins. Since NSLR is proportional to the spectral density at the Larmor frequency, by performing NSLR measurements as a function of applied magnetic field (i.e. resonance frequency ω), one can probe directly the low frequency behavior of the spectral density (see section 2.3.1(ii)). The aim of the present high-temperature work is to study the spectral density of the electronic spin CF in two different groups of AFM rings: (1) semi-integer Cr-based AFM rings e.g. Cr_9, Cr_8, Cr_8Zn, and Cr_7Cd; (2) integer V-based AFM rings e.g. V_7Ni and V_7Zn.

Nuclear spin-lattice relaxation rates (NSLR), $1/T_1$, were measured as a function of magnetic field ($0.2 < \mu_0 H < 9$ Tesla) at room temperature on powder or single crystal as explained in section 3.1. In the case of semi-integer AFM rings, recovery curves show bi-exponential behavior at room temperature. Since the initial fast component contains more than 85 percent of the whole recovery curve, an effective T_1 value can be defined as the time for which the magnetization has recovered to 1/e of the equilibrium value $M(\infty)$. On the other hand, the magnetization recovery curves for integer spin systems showed a single exponential behavior at room temperature and therefore T_1 values were simply extracted by fitting the recovery with a single exponential function as

$$1 - \frac{M_z(t)}{M_z(\infty)} = \exp\left(-\frac{t}{T_1}\right) \tag{3.1}$$

In the following, we first report our experimental data for semi-integer AFM rings, along with a theoretical discussion in section 3.2.1. Then, in section 3.2.2 the first experimental observation of the NSLR data at high temperature for integer-spin AFM rings will be presented.

3.2.1 Semi Integer-spin AFM rings: Cr_9, Cr_8, Cr_8Zn, and Cr_7Cd

The experimental NSLR data as a function of magnetic field for closed homometallic (i.e. Cr_8 and Cr_9) and open heterometallic (i.e. Cr_8Zn and Cr_7Cd) AFM rings are shown in Figure 3.1(a) and 3.1(b), respectively. The comparison of these experimental data with theoretical predictions will be done by considering two different aspects: on one hand, we study the spin dynamics of semi-integer homometalic systems by using the closed chain theory (see section 2.3.1(ii-b)); on the other hand we extend the investigation of spin diffusion behavior observed in 1D Heisenberg chains (see section 2.3.1(ii-a)) to semi-integer closed and open rings, i.e. segments. In fact, the aim of this comparison is to understand if the long time diffusive behavior of the CF observed in 1D Heisenberg chains can be also observed in open rings, which should correspond to 1D finite spin segments.

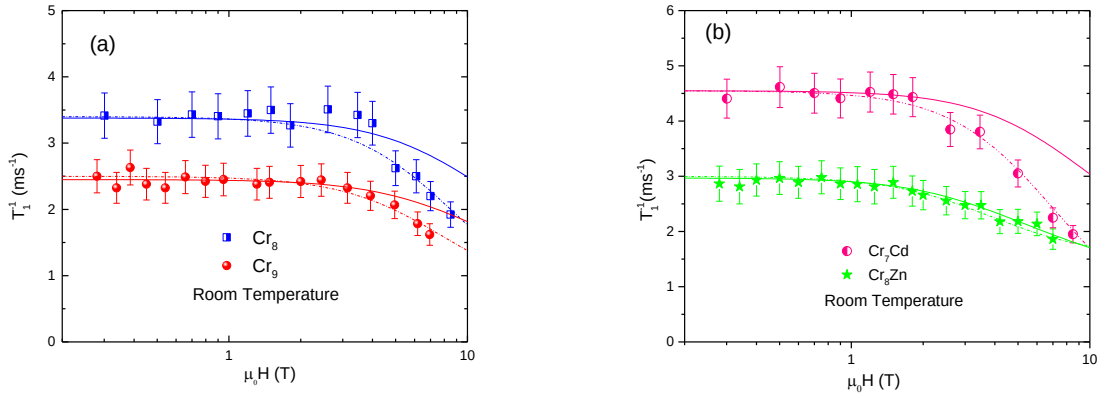

Figure 3.1: Proton NSLR, $1/T_1$, as a function of the external magnetic field at room temperature in (a) homometallic Cr_8 and Cr_9 closed rings (b) open rings i.e. Cr_7Cd and Cr_8Zn. The dashed lines are the best fits according to Equation (3.2), i.e. closed chain theory, with the set of fitting parameters listed in Table 3.1. The solid lines are the best fits according to the 1D spin diffusion model, i.e. Equation (3.3), with the set of fitting parameters listed in Table 3.2.

The theoretical problem of the high temperature ($T \gg J/k_B$) spin dynamics in 1D periodic structures like closed rings made up of Heisenberg coupled spins was discussed in chapter two. Starting from Equation (2.46), and by assuming $\tau_{ex} > \tau_c$ one can obtain

$$\frac{1}{T_1} = \frac{A}{1+(H/H_c)^2} + C \qquad (msec)^{-1} \qquad (3.2)$$

where the magnetic field H is expressed in Tesla with the cut-off field $H_c = \omega_c/\gamma_e$ (Tesla). Equation (3.2) is the function used to fit the experimental data. The most significant parameter in this equation is H_c which estimates the cut-off frequency ω_c of the electronic spin-spin correlation function. It is worth to recall that the cut-off effect is provided by any magnetic interaction which does not conserve the total spin components. In practice, these interactions stem from a variety of mechanisms including intra-cluster dipolar and anisotropic exchange interaction, single ion anisotropies, inter-ring dipolar or exchange interactions [6]. The constant C represents the contribution due to the spectral density of the

fast decaying CF at short times. This contribution becomes frequency independent at frequency smaller than the exchange frequency ω_{ex}.

The experimental data shown in Figure 3.1 were fitted successfully by using the closed chain theory i.e. Equation (3.2) and the parameters obtained from the fit are summarized in Table 3.1.

Table 3.1: The fitting parameters of Equation (3.2) for different semi-integer spin systems, see Figures 3.1.

AFM rings	Type / Ground State (S_T)	A (ms^{-1})	H_C (T)	C (ms^{-1})
Cr_8	Closed // $S_T = 0$	2.9 (0.3)	8.8 (0.8)	0.5 (0.1)
Cr_9	Closed // $S_T = 3/2$	1.84 (0.3)	8 (0.7)	0.66 (0.1)
Cr_7Cd	Open // $S_T = 3/2$	4.25 (0.8)	7 (0.5)	0.3 (0.1)
Cr_8Zn	Open // $S_T = 0$	1.45 (0.2)	3.8 (0.4)	1.55 (0.2)

We are now going to analyze our data by using 1D spin diffusive model. According to the theory, the $1/T_1$ behavior in a 1D Heisenberg chain is given by (see section 2.3.1(ii-a))

$$\frac{1}{T_1} = P\left\{\frac{(H_c^2 + H^2)^{1/2} + H_c}{[H_c^2 + H^2]}\right\}^{1/2} + Q \qquad (3.3)$$

where H_c determines the cut-off field (frequency $\omega_c = \gamma_e H_c$), as in Equation (3.2), the constant Q represents the contribution due to the spectral density of the fast decaying CF at short times, as the C parameter in Equation (3.2), and the constant P contains the information about the spin diffusion, i.e. $P = B/2\pi(2D\gamma_e)^{1/2}$ where D is the spin diffusion constant in rad·Hz and B is the average square of the hyperfine interactions between nuclei and electrons in unit of $(\text{rad}\cdot\text{Hz})^2$. The solid lines in Figure 3.1 are the best fits according to Equation 3.3, with the set of fitting parameters listed in Table 3.2.

From a theoretical standpoint both expressions, i.e. Equations 3.2 and 3.3 give generally a similar description of the spin-lattice relaxation rate as a function of magnetic field at high temperature. In essence, they represent a relaxation due to the spectral density of a CF which has a fast decay at short times (high frequency) and a cut-off at long times (low frequency), and the main difference is at the intermediate times. Actually, in Equation (3.2) the CF should remain constant before the cut-off time because of the periodic boundary conditions of a closed ring. On the other hand in Equation (3.3), the decay of the CF before the cut-off time is described by an inverse square root time dependence ($1/t^{0.5}$) of the CF followed by a cut-off[1].

[1] In fact, the inverse square root time dependence is due to spin diffusion and is responsible for the inverse square root field dependence of $1/T_1$ in Equation 3.2.

A comparison between the experimental data and fitting curves (see Figures 3.1(a) and (b)) indicates that within the experimental errors both formula can fit well the experimental data at low fields (where one probes the spectral density at low frequencies corresponding to the correlation function at long time) as indicated by the cut-off field values extracted from both fits which are the same within experimental uncertainty (see Tables 3.1 and 3.2). On the other hand, the high field data points in the case of closed rings, Cr_9 and Cr_8, and Cr_7Cd are fitted by the closed ring theory (Equation 3.2) but not by 1D spin diffusive model (Equation 3.3).

In order to observe clearly if there is a spin-diffusion region one should investigate a spin system in magnetic fields H larger than the cut-off field H_c ($H_c < H$). As it appears from the data in Table 3.1 and 3.2 the cut-off field is very high in all AFM rings except the open ring Cr_8Zn which is thus the only system where one can hope to see spin diffusion effects .

Table 3.2: The fitting parameters of Equation (3.3) for different semi-integer spin systems, see Figures 3.2.

AFM rings	Type / Ground State (S_T)	P ($T^{1/2}$ ms^{-1})	H_C (T)	Q (ms^{-1})
Cr_8	Closed // $S_T = 0$	6.79 (0.5)	8.5 (0.7)	0.08 (0.05)
Cr_9	Closed // $S_T = 3/2$	4.4 (0.4)	8 (0.3)	0.25 (0.1)
Cr_7Cd	Open // $S_T = 3/2$	8.43 (0.8)	6.9 (0.7)	0.01 (0.01)
Cr_8Zn	Open // $S_T = 0$	3.05 (0.3)	3.5 (0.3)	0.7 (0.1)

In order to explore further this point we compare now the experimental data with the behavior expected in the region of magnetic fields higher than the cut-off field. In fact, if we assume the cut-off field negligible in the field range investigated, i.e. $H_c = 0$, then Equation (3.3) is reduced to

$$\frac{1}{T_1} = PH^{-1/2} + Q \tag{3.4}$$

This equation is the limit of Equation (3.3) where the cut-off effects are not visible and it was previously demonstrated by experiments in other magnetic systems [7]. To study the behavior of NSLR data by Equation (3.4), $1/T_1$ is plotted as a function of the inverse square root of the applied magnetic field in Figure 3.2(a) and 3.2(b) for closed and open rings, respectively.

The straight dashed lines, corresponding to the spin diffusion results given by Equation (3.4), have negative intercepts (negative Q constant) for Cr_8, Cr_9, and Cr_7Cd. This is an unphysical result which confirms that no spin diffusion can be detected in these systems as expected since the cut-off field is too high. On the other hand, in Cr_8Zn it appears that there is a limited range at high magnetic fields where the spin diffusion is present. The fitting parameters for Cr_8Zn are given by Q = 1ms^{-1}, and P = 2.5 $T^{1/2}ms^{-1}$ close to the values obtained from the full expression (3.3) and reported in Table 3.2. It is worth noticing that the deviation from the straight line at lower fields is due to the cut-off effects.

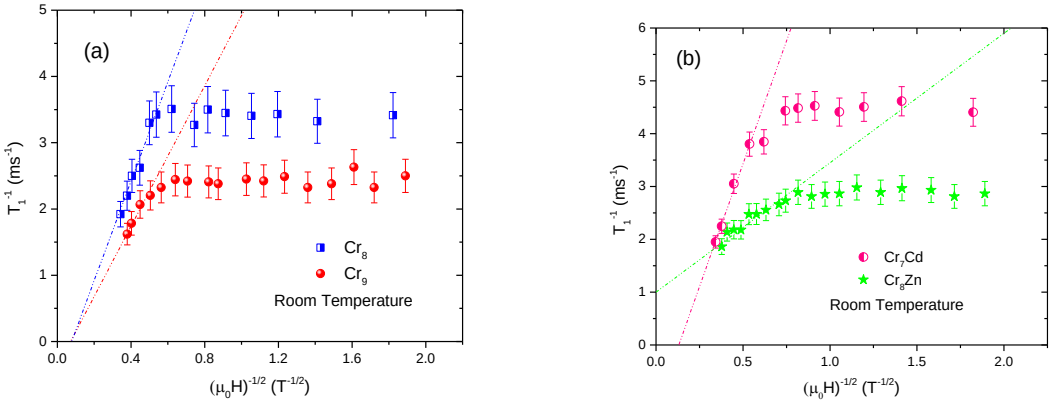

Figure 3.2: Proton NSLR, $1/T_1$, as a function of the inverse square root of the applied magnetic field at room temperature in (a) homometallic Cr_8 and Cr_9 closed rings (b) open rings i.e. Cr_7Cd and Cr_8Zn. The dashed straight lines are the limiting behavior of Equation (3.3) for $H_c = 0$, i.e. Equation (3.4).

One can conclude that only the Cr_8Zn which has a low cut-off field shows a limited region where there may be the spin diffusion [8]. In the closed rings Cr_8 and Cr_9 and the open ring Cr_7Zn, one cannot observe spin diffusion because the cut-off field is too high. Thus in order to investigate further spin diffusion effects in closed vs. open rings one should be able to perform experiments in systems with very low anisotropy effects which translates in low cut-off field.

3.2.2 Integer-spin AFM rings: V_7Zn and V_7Ni

In this section, we report preliminary unpublished experimental data of $1/T_1$ at room temperature vs. frequency in integer-spin AFM rings, namely V_7Zn and V_7Ni. Unfortunately, since it is not possible to have a stable V_8 ring due to undesired oxidization, we were not able to do a direct comparison between closed homometallic and open heterometallic integer-spin rings. The investigated systems V_7Zn and V_7Ni, in the ground state are characterized by a total spin $S_T = 1$ and $S_T = 0$, respectively, resulting from AFM interactions between nearest-neighbor V^{3+} (s = 1) ions and, only in the case of V_7Ni, between V^{3+} and the substituting ion Ni^{2+} (s = 1). In the case of V_7Zn as the substituting ion is Zn^{2+} (s=0), no magnetic interaction occurs between V^{3+} and Zn^{2+}, resulting in an uncompensated total S = 1 ground state. Consequently, V_7Ni is a heterometallic "closed" ring and V_7Zn can be considered a "broken" ring.

The problem of the spin dynamics at high temperature in spin-1 one dimensional (1D) "infinite" Heisenberg antiferromagnetic chains is particularly interesting, due to the existence of a spin excitation gap measurable also at high temperature. This phenomenon was first predicted by Haldane in 1983 [9] and is now well established from numerical calculations [10] and experiments [11, 12]. The s =1 chains have the advantage that (i) the large gap (about 300 K or more) allows to measure $1/T_1$ over a wide range of magnetic field without changing appreciably the thermal population of the excited level [13], and (ii) the single ion anisotropy is much smaller than the gap [14]. The AFM molecular rings studied

in the present thesis are composed of s = 1 magnetic centers and the finite number of such centers allows in principle to compare the behavior of an infinite "Haldane" chain to the one of a finite "Haldane" chain where the gap is affected by the finite size effect.

NSLR experimental data were measured as a function of magnetic field at high temperature where the system behaves like a paramagnet. We present our data as a function of magnetic field and as a function of square root of magnetic field in Figure 3.3(a) and 3.3(b), respectively, similarly to the analysis done in the semi-integer Cr-based AFM rings in the previous section. The experimental data in Figure 3.3(a) are well reproduced by using both Equation (3.2) and (3.3), and the fitting parameters are listed in Table 3.3 and 3.4 respectively.

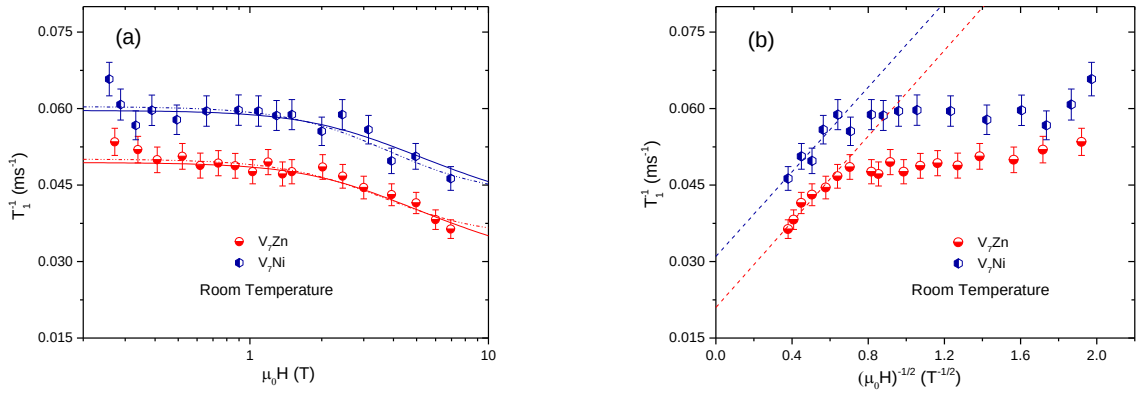

Figure 3.3: Proton NSLR, $1/T_1$ at room temperature for V_7Zn and V_7Ni. (a) the data are plotted as a function of the external magnetic field. The dashed lines are the best fits according to Equation (3.2) with the set of parameters listed in Table 3.3. The solid lines are the best fits according to the 1D spin diffusion model, i.e. Equation (3.3) with the set of fitting parameters listed in Table 3.4; (b) the data are plotted as a function of the inverse square root of the applied magnetic field. The dashed straight lines are the limiting behavior of Equation (3.3) for $H_c = 0$, i.e. Equation (3.4).

Table 3.3: The fitting parameters of Equation (3.2) for different integer spin systems, see Figures 3.3(a).

AFM rings	Type / Ground State (S_T)	A (ms^{-1})	H_C (T)	C (ms^{-1})
V_7Zn	Open // $S_T = 1$	0.015 (5E-3)	3.65 (0.4)	0.035 (0.01)
V_7Ni	Closed heterometallic// $S_T = 0$	0.017 (5E-3)	3.8 (0.4)	0.043 (0.01)

Table 3.4: The fitting parameters of Equation (3.3) for different integer spin systems, see Figures 3.3(b).

AFM rings	Type / Ground State (S_T)	P ($T^{1/2}ms^{-1}$)	H_C (T)	Q (ms^{-1})
V_7Zn	Open // $S_T = 1$	0.032(5E-3)	3.2 (0.4)	0.024 (0.01)
V_7Ni	Closed heterometallic// $S_T = 0$	0.032 (5E-3)	3.3 (0.4)	0.034 (0.01)

As one can see from the inspection of the fitting parameters and the experimental data, the results are similar in the two systems, with a small difference in the C and Q values. The main result is that the cut-off field is "low" (and lower than Cr-based rings) and this allows to observe that spin diffusion occurs in a small field range, as shown by the straight line fitting high fields data in Figure 3.3(b). The lower cut-off field in V rings could be due to the different local anisotropy of V^{3+} ions with respect to Cr^{2+} ions, and/or the difference between the spin values, i.e. s = 1 for V^{3+} ions and s = 3/2 for Cr^{2+} ions, and/or a different intermolecular interaction. To get more information about the physical origin of the cut-off frequency a theoretical investigation is essential. It is important to remark that the spin diffusion seems to be present both in closed and open heterometallic rings. For future work, it remains to be established if spin diffusion can be observed also in the closed homometallic ring which, as anticipated, at present is not available.

3.3 Intermediate temperature regime

In this section, we deal with the interpretation of the ^{1}H NMR experimental data including $1/T_1$, $1/T_2$ and proton NMR spectra in selected AFM rings at intermediate temperature regime, i.e. $T \approx J/k_B$. In the temperature range of the order of the magnetic exchange interaction J/k_B a correlation among the magnetic moments of the ions starts to develop [6]. It was previously found that around this temperature, $1/T_1$ displays a universal behavior in semi-integer AFM rings characterized by a magnetic field dependent peak which can be reproduced by a BPP type of expression [15].

In this work, to gain a much deeper understanding of the spin dynamics in this temperature range we first present a comparison of the spin dynamics in semi-integer AFM closed and open molecular Cr-based rings, i.e. Cr_8 and Cr_8Zn. Then, the preliminary observation of the ^{1}H NMR experimental data in integer spin systems V_7M (M = Zn and Ni) will be reported.

3.3.1 Semi Integer-spin AFM rings: Cr_8 and Cr_8Zn

Both Cr_8 and Cr_8Zn are composed of eight Cr^{3+}, s = 3/2, magnetic ions with the only difference in the boundary conditions, whereby the non-magnetic ion Zn^{2+}, s = 0, disconnects the AF interaction between nearest-neighbor Cr^{3+} spins in the case of Cr_8Zn. The magnetic properties and crystalline structure of two systems were discussed in chapter 1 (see section 1.2.1). The ^{1}H NMR experimental data for Cr_8Zn were collected in single crystal with H in the plane of the ring as a function of temperature ($1.6 < T < 300$ K) at two different external magnetic fields $\mu_0H = 0.5$ and 1.5 Tesla [16], while the data for Cr_8 were taken in polycrystalline powder sample from the previous work [17].

In the case of Cr_8Zn, the nuclear magnetization recovery curves showed temperature dependent two-exponential behavior below 4 K due to the presence of nonequivalent groups of ^{1}H sites in the molecule. Since all the recovery curves above 4 K showed a single exponential behavior and the first component below 4 K contains more than 60 percent of the whole recovery, we monitored the relaxation rate of the first component in whole temperature range at both magnetic fields. For Cr_8 rings,

the recovery of the nuclear magnetization was found to follow a multi-exponential law, and thus the T_1 "effective" values were extracted by taking the value of the time at 0.6 of the normalized recovery curves [17]. This section is organized as follows: In subsection *(i)* a comparison of the ^{1}H NMR line width between open and closed rings is reported. The NSLR experimental data including a theoretical discussion is presented in subsection *(ii)*. Finally, the wipe-out effect on ^{1}H NMR data is shown in the last part *(iii)*.

(i) ^{1}H NMR spectra

The proton NMR spectra were determined by the Fourier transform of half of the echo signal in both Cr_8Zn and Cr_8. This is because in this temperature range from 300 K down to 1.6 K for applied magnetic fields well below the level crossing fields, i.e. $\mu_0 H_{c1}$ = 2.15 T for Cr_8Zn and $\mu_0 H_{c1}$ = 7.34 T for Cr_8, the whole NMR line could be irradiated by a single rf pulse.

The full width half maximum (FWHM) of the NMR spectra in MNMs shows a temperature dependent behavior. The shape and width of the ^{1}H NMR are governed by the nuclear-nuclear dipolar interaction and the hyperfine interaction of the protons with Cr^{3+} magnetic ions. The first interaction depends on the hydrogen distribution in the molecule and yields a magnetic field and temperature independent contribution to the proton NMR line width. The second contribution, i.e. hyperfine field interaction, to the line-width is associated with the average static component of the magnetic moment. It is noted that the hyperfine field resulting from the interaction of protons with local magnetic moments of Cr^{3+} magnetic ions may contain contributions from both the classical dipolar interaction and from a direct contact term due to the hybridization of proton s-wave function with the d-wave function of magnetic ions. The contact interaction has scalar form and it can generate a shift of the line for certain groups, each one constituted by equivalent protons in the molecule. Since we have not observed any sizeable shift of the proton NMR line from the Larmor frequency in our measurements, we can conclude that the dominant hyperfine interaction is of dipolar origin because the latter is anisotropic and it generates a broadening of the line with no average shift.

In the simple Gaussian approximation, the NMR line-width is related to the sum of the second moments due to interactions described above as follows [18]:

$$FWHM \propto \sqrt{\langle \Delta\nu^2 \rangle_d + \langle \Delta\nu^2 \rangle_m} \tag{3.5}$$

where $\langle \Delta\nu^2 \rangle_d$ is the intrinsic second moment due to nuclear-nuclear dipolar interactions and $\langle \Delta\nu^2 \rangle_m$ is the second moment of the local frequency-shift distribution (due to the nearby electronic moments) at the different proton sites of all molecules. The proportionality constant in Equation (3.5) is on the order of one, depending on the exact shape of the spectrum. The relation between $\langle \Delta\nu^2 \rangle_m$and the local Cr^{3+} electronic moment for a simple dipolar interaction is given by [18, 19]

$$\langle \Delta\nu^2 \rangle_m = \frac{1}{N} \sum_R \sum_{i \in R} \left(\langle \nu_{R,i} - \nu_L \rangle_{\Delta t} \right)^2 \cong \frac{\gamma^2}{N} \sum_R \sum_{i \epsilon R} \sum_{j \epsilon R} \left[\frac{A(\theta_{i,j})}{r_{i,j}^3} \langle m_{z,j} \rangle_{\Delta t} \right]^2 \quad (3.6)$$

where R labels different molecules, i and j refer to different protons and Cr^{3+} magnetic ions respectively within each molecule, and N is the total number of protons. $\nu_{R,i}$ represents the resonance frequency of the nucleus i in molecule R, and thus the difference $\nu_{R,i} - \nu_L$ represents the shift in frequency for the nucleus i due to the local field generated by the nearby moments j in one molecule. $A(\theta_{i,j})$ is the angular coupling constant between the proton i and the moment j, and r_{ij} is the corresponding distance between them. Finally, $\langle m_{z,j} \rangle$ is the component of the magnetic moment j (Cr^{3+}) in the direction of the applied field averaged over the NMR data acquisition time scale.

Equation (3.6) can be further simplified by assuming that the sample behaves as a simple paramagnet. It must be taken into account that this assumption can be justified only in the high temperature limit, above 50 K. In this case one expects $\langle m_{z,j} \rangle = (\chi/N_A)H$, where χ is the electronic magnetic susceptibility, N_A is Avogadro's number, and H is the applied magnetic field. Therefore, Equation (3.6) can be reduced to:

$$\sqrt{\langle \Delta\vartheta^2 \rangle_m} = A'_z \chi H = A'_z \chi \nu_L / \gamma_n = A_z \chi \nu_L / N_A \quad (3.7)$$

where A'_z and A_z are the dipolar coupling constants averaged over all protons and orientations.

In order to compare the predictions from Equation (3.7) with the experimental data one should plot the FWHM (shown in Figure 3.4 as a function of temperature), as a function of the magnetic susceptibility measured by means of SQUID [17, 19]. However, we found that the analysis of the experimental data in the temperature range where the system behaves like a paramagnet is complicated by two factors: on one hand the $1/T_1$ experimental data in both rings display a wide bump in the temperature range 80 ÷ 200 K which is due to the rotation of the CH_3 groups, see Figure 3.5 [20]; on the other hand a considerable signal loss is observed in the temperature range (50 ÷ 120 K), see Figure 3.5. As a result, a quantitative analysis of the results appears difficult and we thus confine our discussion to a qualitative comparison between the open and closed rings.

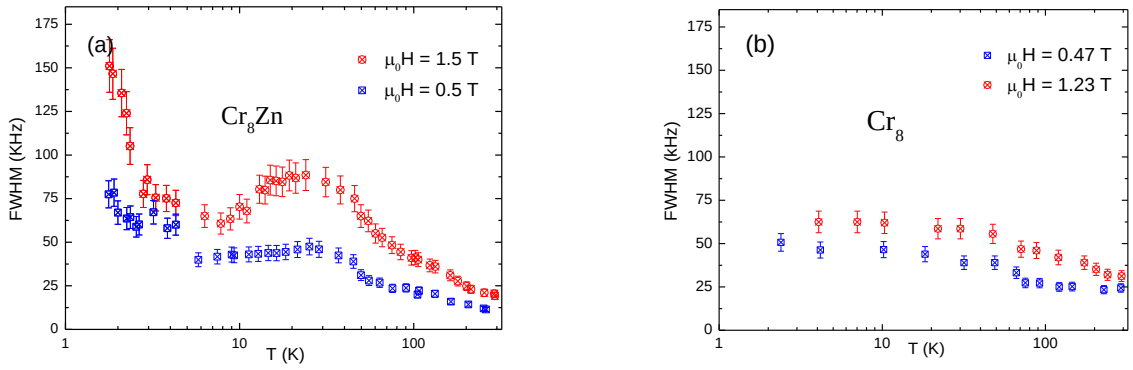

Figure 3.4: Proton NMR linewidth as a function of temperature at two different external magnetic fields for (a) Cr_8Zn and (b) Cr_8.

As it is shown in Figure 3.4, the NMR line width for both open and closed ring has the same temperature behavior as the magnetic susceptibility shown in Figure 1.2. This is consistent with a dominant contribution to the FWHM coming from the nuclear-electron dipolar interaction given by Equation (3.7).

In the case of Cr_8Zn there is a pronounced increase in the line width at low temperature (see Figure 3.4(a)) compared with Cr_8 (see Figure 3.4(b)) and this is due to the different magnetic energy level structure between the two rings. In fact, at μ_0H = 0.5 T and 1.5 T we are relatively close to the first level crossing field (μ_0H_c = 2.15 T), which means some molecular rings start to populate the first level excited state, S_T = 1 at low temperature. Consequently the local magnetic field at the nuclear site increases owing to the distribution of magnetic moments of the Cr ions and therefore the proton NMR line-width increases for Cr_8Zn (see Equation 3.7). This is not the case in Cr_8 because the first level crossing for Cr_8 occurs at μ_0H_c = 7.34 T which is far from both magnetic fields μ_0H = 0.47 T and μ_0H = 1.23 T and thus the Cr magnetic moment at low temperature is close to zero being the molecule in the non-magnetic ground state S_T = 0. The broad maximum observed particularly in Cr_8Zn at the higher magnetic field is an artifact due to the wipe-out effect which is described in section 3.3.1 (iii).

(ii) ^{1}H NMR relaxation rates: $1/T_1$ and $1/T_2$

In early measurements in Cr_8 AFM ring [21] it was found that the proton (^{1}H) NMR spin-lattice relaxation rate (NSLR), $1/T_1(T)$, displays a universal behavior common in semi-integer antiferromagnetic (AFM) rings characterized by a magnetic field dependent peak centered at a temperature $T \sim J/k_B$. The peak can be fitted with a simple BPP-like formula [15, 22] used to describe the NSLR in liquids and molecular solids which can also be derived from Moriya theory [23] of nuclear relaxation in paramagnets in the high temperature limit. It is given by Equation (2.57):

$$\frac{1}{T_1} = A\chi T \frac{\omega_c(T)}{\omega_c^2(T) + \omega_L^2} \tag{3.8}$$

where ω_L is the nuclear Larmor frequency, $A\chi T$ is the average square of the transverse fluctuating hyperfine field in frequency units and χT corresponds to the Curie constant in the expression of the paramagnetic susceptibility χ. The physical mechanism underlying Equation (3.8) is a nuclear relaxation process driven by an exponential decay of the correlation function of the hyperfine field at the nuclear site, with a single correlation frequency $\omega_c(T) = 1/\tau_c(T)$ being associated with the relaxation (i.e. fluctuations) of the ring magnetization.

A detailed first principle calculation of the NSLR in magnetic molecules has justified the validity of the phenomenological Equation 3.8 [24]. In fact, one should first consider that $1/T_1(H,T)$ (where H is the external applied magnetic field) is in its general form related to the spectral density expressed as a weighted sum of components containing different correlation times τ_{ci}, each one related to different spin-phonon interaction terms (see section 2.3.2). However, in most cases one single characteristic time $\tau_c(H,T)$ can be dominant over a wide range of temperature and applied field, with temperature dependence given by an Arrhenius law [24]. In a slightly different theoretical approach [25], the nuclear spin lattice relaxation rate has been related to the fluctuations of the magnetization of the ring which includes one-phonon, two-phonon, as well as Raman processes, thus yielding a dominant correlation frequency $\omega_c(H,T)$ with a universal power law temperature dependence [25]. Both Arrhenius-law and power-law dependence $\omega_c(H,T)$ in the vicinity of the NSLR peak are in agreement with the experiments [6,24,25], with just some slight differences in the simulated peak shape.

Here with the aim of getting further insights about the spin dynamics and related dominant correlation frequencies in different temperature and magnetic field ranges in half-integer spin AFM rings we present the NSLR experimental data for both open and closed semi-integer rings: Cr_8Zn and Cr_8, respectively, along with a theoretical discussion based on the above cited theories.

The temperature dependence of $1/T_1$, for both open and closed rings at $\mu_0H = 0.5$ and $\mu_0H = 0.47$ Tesla respectively, is shown in Figure 3.5. The local maximum observed at the intermediate temperature of about 15 K is similar to the one observed in most molecular magnets, rings and clusters [6] and it appears to have a similar width and height in both closed and open rings. On the other hand the open ring Cr_8Zn displays a well resolved secondary peak around 2.5 K, which may be present in the form of a shoulder in the closed ring Cr_8. The experimental results for Cr_8 have been reported previously [17] but the low temperature shoulder was not analyzed. The inset of Figure 3.5 shows the enhancement of the spin-spin relaxation rate $1/T_2$, on lowering the temperature, which is related to the slowing down of the fluctuations and is responsible for the wipe-out effect of the NMR signal discussed in section 3.3.1(iii).

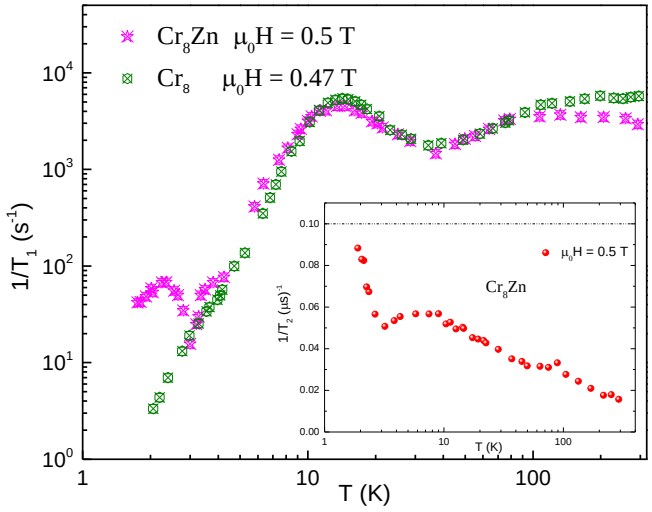

Figure 3. 5: Temperature dependence of the spin-lattice relaxation rate, $1/T_1$, for both Cr_8Zn and Cr_8 rings at approximately the same magnetic field. **Inset:** temperature dependence of spin-spin relaxation rate, $1/T_2$, for Cr_8Zn at 0.5 T. The dashed line is the limit of the NMR spectrometer.

In order to analyze the experimental data, one should plot $1/T_1$ divided by χT so that the experimental behavior reflects only the spin dynamics contained in the correlation frequency $\omega_c(T)$ (see Equation (3.8)). The plots are shown in Figure 3.6. It is noted that by dividing the data of NSLR by χT the shoulder in the data of Cr_8 is more distinguishable. This shoulder could be tentatively related to the well resolved secondary, low-temperature peak observed in Cr_8Zn (see Figure 3.5). It should be noted also that at $T \sim 4 \div 5K$, i.e. in a temperature region near to the one where an anomalous broad shoulder is observed in Cr_8, the Cr_8Zn sample exhibits a small hump that, however, is quite narrow in temperature (with respect to the Cr_8 shoulder) and appears to fall within the experimental error. For this reason we believe that, to attribute with certainty this hump to another relaxation process and to analyze it quantitatively, a refined theoretical model including calculations of dominating relaxation times (possibly even more than one) in this low temperature range is needed.

The main peak in the NSLR can be fitted with Equation (3.8) for both the open ring (Figure 3.6(a)) and the closed ring (Figure 3.6(b)), whereby the results in Cr_8 are in agreement with the data reported and analyzed earlier [7, 21]. The correlation frequency in Equation (3.8) is assumed to have a power law dependence i.e. $\omega_c(T) = CT^{\alpha}$. The fitting parameters for both systems are summarized in Table 3.5.

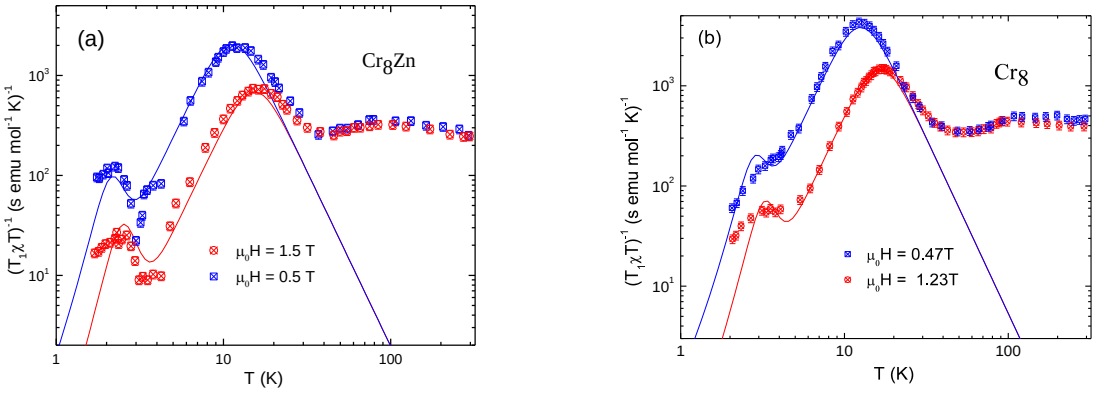

Figure 3.6: Temperature dependence of the spin-lattice relation rate divided by χT with fitting curve (solid lines) obtained by using equation (3.9) as discussed in the text for (a) Cr_8Zn and (b) Cr_8**.**

The factor A, which represents the average square nuclear-electron dipolar interaction, is different for the two types of ring. The difference is easily explained by the fact that for a dipolar interaction "A" is proportional to $1/r^6$ with r being the proton – magnetic ion separation averaged over all protons in the molecule. This average distance is bigger in Cr_8Zn as a result of the bigger radius of the ring (9.5 Å against 8.7Å for Cr_8) and also because several groups of protons are located at the edge of the open ring, where a magnetic ion is missing. The difference in the value of the correlation frequency between the closed and open ring, which is just outside the experimental uncertainty, is probably related to the small difference of the exchange constant J (see section 1.2.2), which differs by only about 20% for the closed and open ring.

Table 3.5: The values of the parameters obtained from the best fit for $1/T_1\chi T$ data using equation (1) for the Cr_8Zn "open" and Cr_8 "closed" rings.

Molecule	**A** rad^2 mol/s^2 emu K	**C** rad/s	**α**
Cr_8Zn	0.57×10^{12}	$2.8(0.3)\times10^{4}$	3.5 (0.1)
Cr_8	1×10^{12}	$1.8(0.3)\times10^{4}$	3.5 (0.1)

If one uses equation (3.8) one can fit only the main peak in Figure 3.6. In order to reproduce also the low temperature peak in C_8Zn (Figure 3.6(a)) and the shoulder in Cr_8 (Figure 3.6(b)) we added to Equation (3.8) a second correlation frequency ω_{c2}. The corresponding new equation is

$$\frac{1}{T_1\chi T} = A\left\{\frac{\lambda_1\omega_{c1}(T)}{\omega_{c1}^2(T)+\omega_L^2} + \frac{\lambda_2\omega_{c2}(T)}{\omega_{c2}^2(T)+\omega_L^2}\right\} \qquad (3.9)$$

where ω_L is proton Larmor frequency and A is the fitting constant, proportional to the average square of the dipolar interaction between protons and magnetic transition metal ions, that is assumed to be temperature and magnetic field independent. λ_1 and λ_2 are the relative weight of the two correlation frequencies in the spectral weight of the relaxation of the magnetization of the molecule [24, 26]. For A

and ω_{c1} we utilize the values shown in Table 3.5 which refer to the fit of the main peak while λ_1, λ_2 and ω_{c2} are chosen to fit the low temperature secondary peak. For ω_{c2} a power-law temperature dependence $\omega_{c2} = C_2T^{\alpha 2}$ was assumed. The results of the complete fit with Equation (3.9) are reported in Figure 3.6. The parameters used in the fit of Figure 3.6 are: $\lambda_1 = 0.96(0.06)$, $\lambda_2 = 0.04(0.003)$ and $\alpha_2 = 7$ the same for both Cr_8Zn and Cr_8 while for Cr_8Zn, $C_2 = 60\times10^4$ rad/s and for Cr_8, $C_2 = 8\times10^4$ rad/s with an estimated uncertainty of the order of 10%. The much larger value of the temperature exponent ($\alpha_2 = 7$) for the secondary correlation frequency indicates a different relaxation mechanism of the magnetization possibly related to Raman spin-phonon processes discussed in section 2.3.2 [25, 27]. The relevant result here is that the second correlation frequency $\omega_{c2} = C_2T^7$ is almost one order of magnitude larger for the open ring Cr_8Zn than for the closed ring Cr_8. The difference should be related to the much smaller gap among the non-magnetic ground state and the first excited magnetic state observed in Cr_8Zn with respect to Cr_8 (see section I). We also tried to improve our fit using an exponential dependence in 1/T for ω_{c1} and ω_{c2} (i.e. $\omega_c = C\cdot\exp(\Delta/k_BT)$), which could be explained as the result of indirect Orbach relaxation processes, discussed in section 2.3.2, as hypothesized in literature [26, 27], but the quality of the fit appears to be worse. We would finally remark that the T^7 dependence of ω_{c2} has to be taken as a qualitative result, as well as the suggestion of associated Raman processes. In fact, the calculation of the behaviour of $1/T_1$ over the whole temperature range for both systems requires a complete theoretical model, outside the (experimental) aims of the present paper. This required theoretical model could be useful also for the investigation of the low temperature ($T < 5K$) spin dynamics at fields higher than 1.5 Tesla where, for Cr_8Zn, Equation (3.9) fails due to different physical mechanisms influencing the nuclear relaxation at a field close to the first level crossing conditions ($\mu_0H = \mu_0H_{c1} \approx 2.15$ Tesla) .

(iii) Wipe-out effect

The wipe-out effect consists in a loss of measurable NMR signal intensity by lowering the temperature. The effect has been previously observed in most of MNMs and magnetic clusters [6, 28] and attributed to a combination of a strong hyperfine coupling of nuclei to the electronic spin and a slowing down of the fluctuations of the magnetic moment of the ions. In fact the slowing down of the fluctuations of the magnetization of the molecule produces a T_2 shortening (and a corresponding shortening of T_1), whereby the decay of the transverse nuclear magnetization occurs in a time shorter than the detection time, τ_d, of the spectrometer. The minimum value for τ_d is about 10 μs, below which the true observation of the NMR echo signal is not possible due to the instrumental limits. An approximate simple model has been already proposed [28] to fit the experimental results and it will be used here. We start considering the expression of T_2 in the weak collision, fast motion approximation where the relaxation rate can be expressed in terms of the spectral density of the fluctuating hyperfine fields at zero frequency [18, 19]:

$$\frac{1}{T_2} = \gamma_N^2 \langle \delta H_z^2 \rangle \, \tau(T) = \gamma_N^2 \frac{\langle \delta \mu_e^2 \rangle}{r^6} \tau(T) \tag{3.10}$$

where δH_z is the local longitudinal fluctuation field originating from a magnetic moment at a distance r from the proton spin, and τ is the correlation time, $\tau = 1/\omega_c$, which is determined by the dynamics of the exchanged coupled magnetic ions. When the correlation time in Equation (3.10) becomes gradually longer with decreasing temperature, then the relaxation rate $1/T_2$ becomes larger and eventually T_2 crosses the limiting value of τ_d as shown in inset of Figure 3.5. As a result, one should expect that the critical value, τ_d, is gradually reached by all the proton sites, with the ones closer to magnetic ions being wiped out first, generating a loss of the NMR signal intensity.

One can approximately assume a central ion surrounded by the total number of protons homogenously distributed at distances up to a maximum value R^*, with a number density ρ ($\rho = n_0/[(4\pi/3)R^*]$). On the other hand, a number of protons close to the magnetic ion with a T_2 value shorter than the critical value, τ_d, form a notional sphere of critical radius $r_c(T)$, [$r_c(T) < R^*$], and do not contribute to the measured NMR signal intensity. The protons located outside this sphere can be detected and their number can be determined as $n(T) = n_0 [1-(r_s/R^*)^3]$. The value of r_c can be obtained from Equation (3.10) by setting $T_2^{-1} = \tau^{-1}_d$. Then one can express n(T) in terms of the correlation time as

$$\frac{n(T,H)}{n_0} = 1 - \frac{\gamma_N \sqrt{\langle \delta \mu_e^2 \rangle}}{R^{*3}} \sqrt{\tau(T) \cdot \tau_d} \tag{3.11}$$

This model was previously used to explain the wipe-out behavior in Cr_8 [17], by using the temperature dependence of the correlation time extracted from the spin-lattice relaxation rate, $\tau_c = 1/\omega_c = C^{-1}T^{-3.5}$ (see Equation (3.8) and table 3.5). We used the same model to reproduce the experimental data in Cr_8Zn as shown in Figure 3.7.

The fitting parameters for the open and closed ring are compared in Table 3.6. For the correlation time τ_c we used the values of C in Table 3.5. The theoretical curves reproduce reasonably well the wipe-out effect at high temperature, which occurs at the same temperature in both Cr_8 and Cr_8Zn.

Table 3.6. The values of the parameters used to fit the wipe-out data using equation (3.11).

Molecule	**τ_c (s/Rad)**	**$\sqrt{\langle \delta\mu^2_e \rangle}/(R^*)^3$ (G)**
Cr_8Zn	$0.4(0.1)\times10^{-4}\ T^{-3.5}$	650(60)
Cr_8	$0.6(0.1)\times10^{-4}\ T^{-3.5}$	650(60)

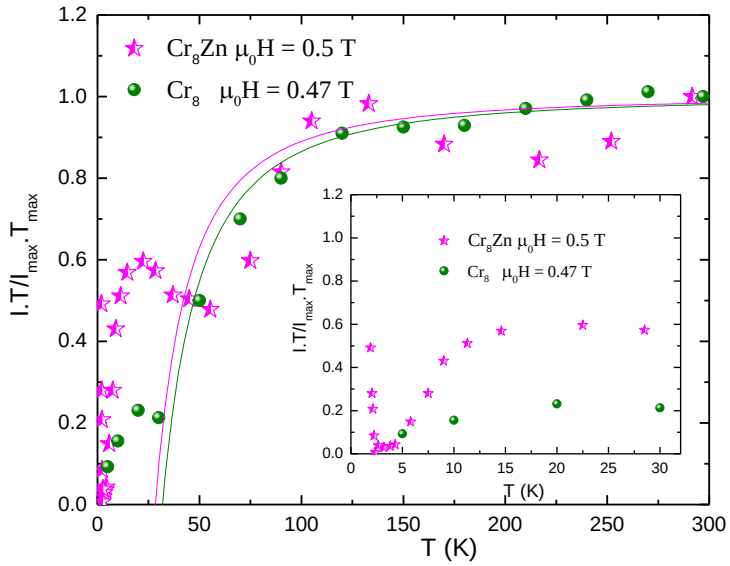

Figure 3.7: ^{1}H NMR signal intensity times the temperature normalized to the maximum value as a function of temperature for Cr_8Zn at H = 0.5 T and Cr_8 at H = 0.47 T. The solid lines obtained by using Equation (3.11) as explained in the text. The inset is a zoom of the wipe-out behavior in low temperature region.

At low temperature one can observe a second step in the wipe-out which occurs at different temperature for the open and closed ring respectively. This suggests that the second wipe-out is due to the second correlation frequency discussed in relation to the NSLR results (see section 3.2.1(ii)), found to be different for the two types of ring.

3.3.2 Integer-spin AFM rings: V_7Zn and V_7Ni

In this section, we are going to present the ^{1}H NMR experimental data for integer-spin AFM rings vs. temperature (1.6 < T < 300 K) at different external magnetic fields. It should be noted that while the NMR study of Cr based AFM rings presented in this thesis is based mostly on published results, the NMR results in Vanadium based rings are presented in the thesis for the first time and are largely unpublished. This justifies the fact that the data are often incomplete and the analysis is only qualitative, since a quantitative analysis would require an extensive collaborative theoretical effort.

The data were collected on a single crystal with H parallel to the molecular rings' plane at different applied magnetic fields (μ_0H ~ 0.5, 1.5, 3, and 6 T). The magnetic properties and the crystalline structure of these two systems have been previously discussed in section 1.3. The aim of this part of the study is to understand the behavior of the NSLR rate, $1/T_1$, in spin-1 AFM rings as the system, by decreasing temperature, crosses over from a paramagnetic state where the spins are essentially weakly correlated, to a collective quantum ground state with a total spin S_T (S_T = 0 for V_7Ni and S_T = 1 for

V_7Zn). A comparison of the spin dynamics at intermediate temperature, between semi-integer and integer AFM rings is another focus of this investigation.

The longitudinal magnetization recovery curves in both V_7Ni and V_7Zn showed a single exponential behavior from high temperature down to 50 K for all magnetic fields. For lower temperatures, the recovery curves revealed a bi-exponential behavior composed of a fast and a slow relaxation component, due to the presence of nonequivalent groups of ^1H nuclei. This behavior is due to the different hyperfine field experienced by ^1H nuclei in nonequivalent crystallographic sites that give rise to different "average" values of the relaxation rates. However, it is worth noticing that the first exponential component of the nuclear magnetization longitudinal recovery curves, the so-called fast component, has a higher weight from more than 95% at room temperature to about 60% at the lowest temperature T < 2 K (see Figure 3.8), for all applied fields. This is an important remark, since it means that the T_1 values extracted from the fast component are an average of the relaxation times of the majority of protons. It should be noticed that the variation of the percent weight of the different relaxation components is related to the wipe-out effect. For the data analysis, we made use of just the fast T_1 data.

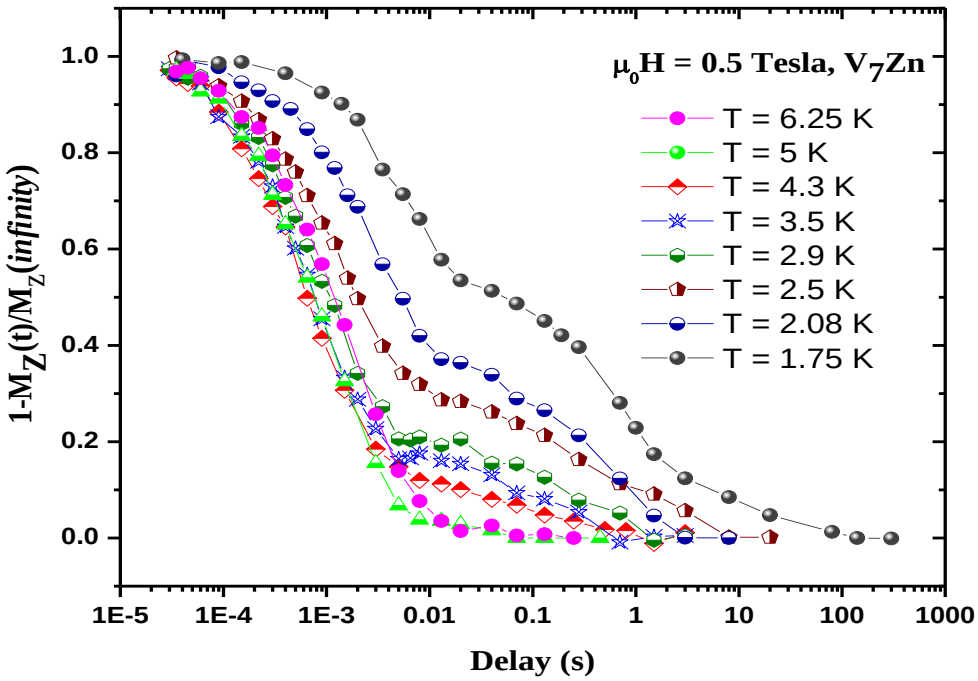

Figure 3.8: Selected spin-lattice relaxation recovery curves of V_7Zn single crystal at different temperature at μ_0H = 0.5 T.

The transverse nuclear magnetization decay curve, i.e. $M_{xy}(t)$ follows a single exponential relaxation function at all temperatures and magnetic fields. Although different T_2's pertaining to non-

equivalent hydrogen nuclei could be expected, it has to be taken into account that their very short values force the proton nuclear system to "thermalize" before the beginning of the NMR signal detection, thus giving rise to a single exponential decay. Proton NMR spectra in the intermediate temperature regime, were obtained from the Fourier transform of half of the echo signal. In V_7Zn at low temperature ($T < 4.2$ K) due to the condensation of the system in the magnetic ground state and the consequent line broadening, the spectra have been collected by frequency-sweep technique at $\mu_0 H$ = 1.5, 3 and 6 Tesla.

(i) ^{1}H NMR spectra

The magnetic field dependence of the proton NMR spectra at room temperature was determined by Fourier transforming half of the echo spin signal, since the whole NMR line could be irradiated with one rf-pulse. The acquired experimental data, shown in Figure 3.9, indicate that the FWHM in both systems stay almost constant at low magnetic fields and slightly increase for $\mu_0 H > 2$ Tesla. At this temperature the discrete structure of the energy levels does not influence the magnetic behavior of the systems, because they are still essentially paramagnetic.

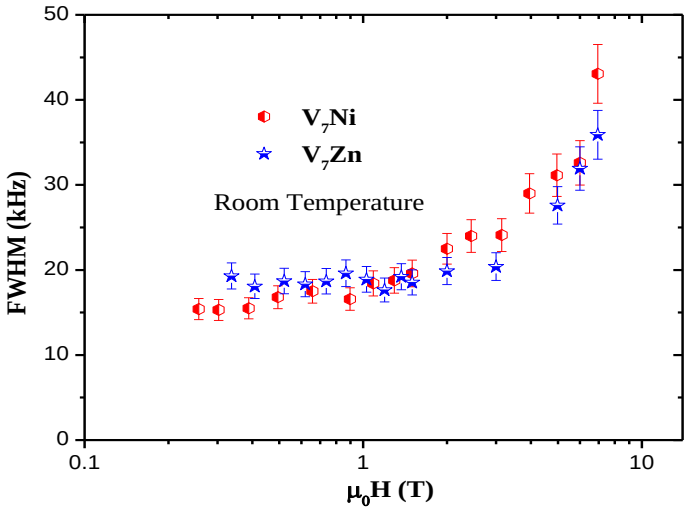

Figure 3.9: Proton NMR line width as a function of magnetic field at room temperature for V_7Zn and V_7Ni.

The observed FWHM at high temperature is mainly due to the nuclear-nuclear dipolar interaction which is magnetic field and temperature independent, and it was previously measured to be around 20 kHz for semi-integer AFM rings, for instance 20 kHz for Cr_7Ni at $\mu_0 H$ = 0.47 T and 15 kHz for Cr_7Cd at $\mu_0 H$ = 0.63 T [17]. For $\mu_0 H > 2$ Tesla the molecular magnetization increases (the system is a paramagnet) and consequently one can observe a NMR line broadening proportional to the magnetic field as described by Equation (3.7) and shown in Figure 3.9. The effect of the inhomogeneous broadening due to the hyperfine interaction of the nuclei with the local moments of the Cr^{3+} ions

becomes more relevant as the temperature is decreased, as shown by the proton NMR line width plotted as a function of temperature at different magnetic fields for both V_7Zn and V_7Ni in Figures 3.10(a) and (b), respectively.

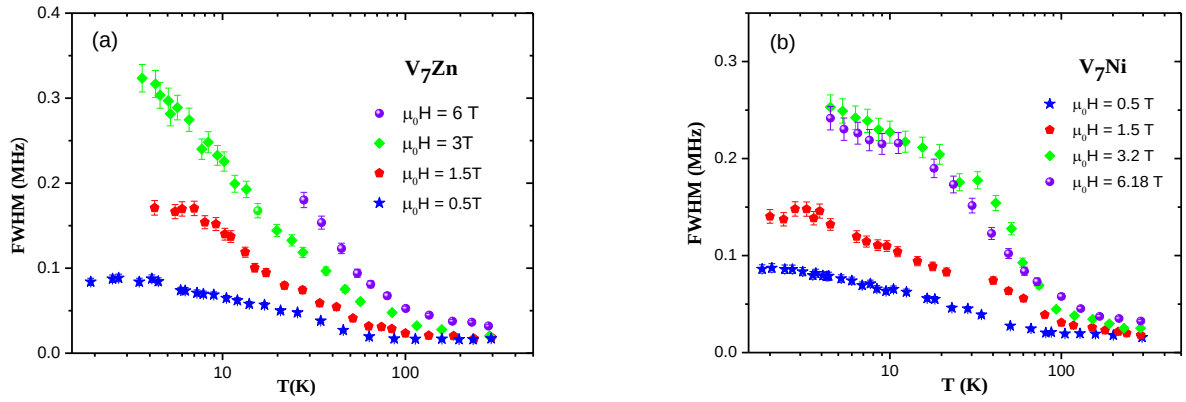

Figure 3.10: Proton NMR line width as a function of temperature at four different external magnetic fields for (a) V_7Zn and (b) V_7Ni.

As shown in Figure 3.10 the NMR line width increases as the temperature is lowered down to about 20 K and in this temperature range it tracks the magnetic susceptibility reported in Figure 1.8 as expected from Equation (3.7). At lower temperatures the system is no longer a simple paramagnet as shown by the deviation from the Curie-Weiss plot in Figure 1.11. In fact at low temperature the magnetization of the rings is due to the molecular population of the low lying discrete magnetic energy states governed by the Boltzmann law, and the NMR line width is no longer proportional to the magnetic susceptibility as can be seen by comparing the data in Figure 3.10 with the susceptibility data of Figure 1.8. Moreover it has to be remarked that, when the external field is increased, the NMR line width as well as the magnetization at low temperature are determined by the progressive change of the magnetic energy levels spacing and the consequent change in the thermal population. This leads also to level crossings effects at the critical fields H_{c1}, H_{c2}, etc. (see section 1.3.3) [29].

Due to the large FWHM observed in V_7Zn at 3 and 6 Tesla (see Figure 3.10(a)), at very low temperature frequency-sweep technique is used to truly measure the broadening of the ^1H NMR line width. Figure 3.11 displays the spectra collected at T = 4.2 K and T = 1.7 K for V_7Zn at μ_0H = 1.5, 3 and 6 Tesla. As one can see from Figure 3.11, a single rf pulse with the Larmor frequency can irradiate the whole NMR line at μ_0H = 1.5, 3 Tesla within a reasonable error, while at higher field, i.e. 6 Tesla, the FWHM is of the order of 1 MHz which means that the line cannot be fully irradiated by only one rf pulse; thus, for this field the magnetic field sweep or frequency-sweep technique becomes essential to estimate the FWHM at temperatures T < 20 K (actually some points are missing, see Figure 3.10(a)). A quantitative investigation of the origin of this broadening requires a better knowledge of the ground state of the system, which can be acquired by means of refined theoretical calculations and other thermodynamic measurements namely susceptibility, specific heat, and torque measurements.

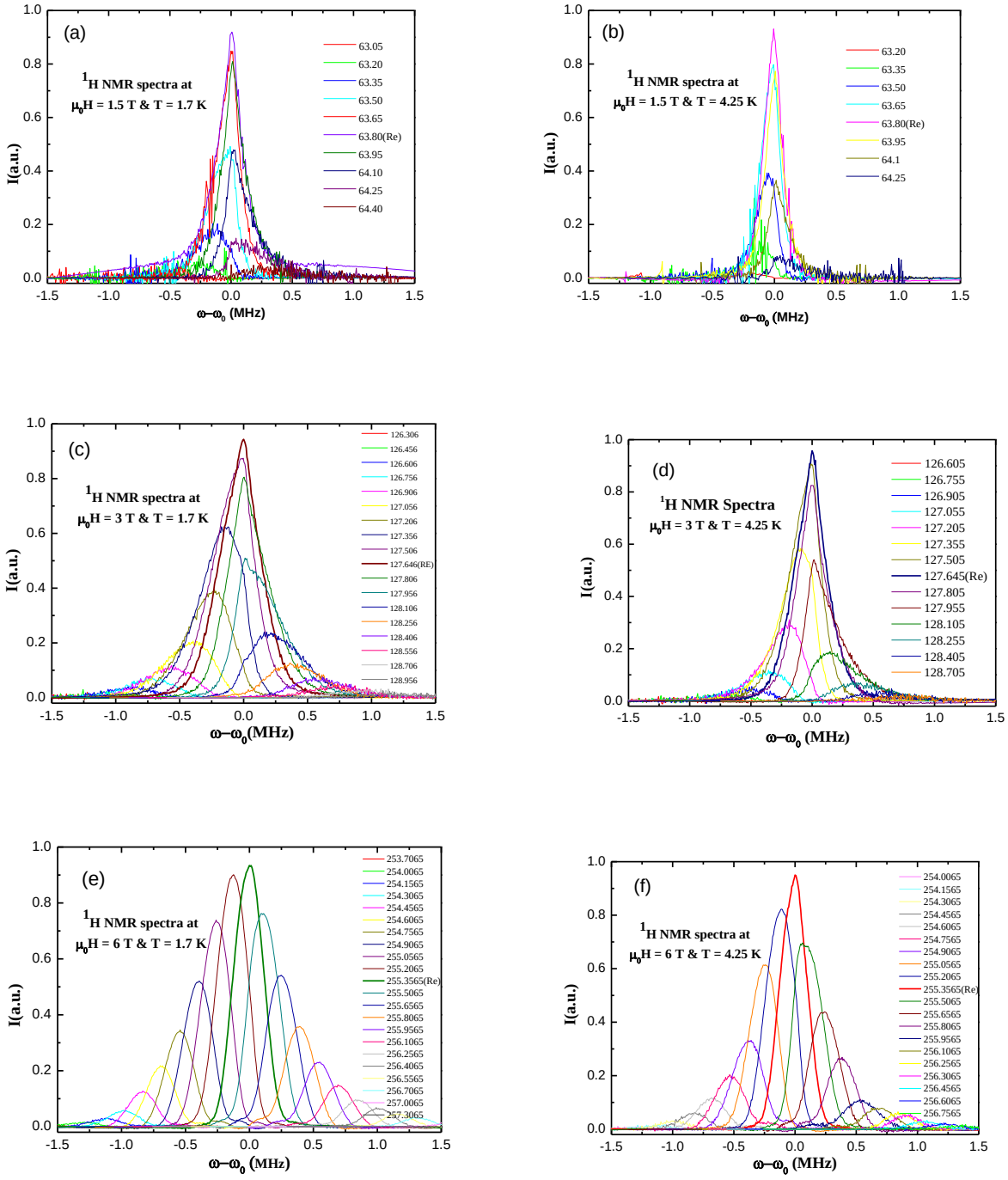

Figure 3.11: Proton NMR spectra collected by frequency-sweep technique in V_7Zn at: (a) μ_0H = 1.5 T and T = 1.7 K; (b) μ_0H = 1.5 T and T = 4.25 K; (c) μ_0H = 3 T and T = 1.7 K; (d) μ_0H = 3 T and T = 4.25 K; (e) μ_0H = 6 T and T = 1.7 K; (f) μ_0H = 6 T and T = 4.25 K.

(ii) ^{1}H NMR relaxation rates: $1/T_1$ and $1/T_2$

The ^{1}H NMR spin-lattice relaxation rate experimental data, $1/T_1$, as a function of temperature in a number of semi-integer AFM molecular rings has shown a large enhancement of the relaxation rate at low temperatures, resulting in a field dependent peak of $1/T_1$ vs. T curve centered at a temperature of the order of the magnetic exchange constant J/k_B [6]. The presence of the peak is due to the strong correlation between magnetic moments that arises as the temperature is lowered. As it was previously discussed, the BPP model with only one correlation time can reproduce the experimental data for semi-integer Cr-based AFM rings with some differences due to a different correlation time τ_c for different systems and/or to the presence of more τ_c (see discussion in section 3.2.1(ii)). In this section, we analyze the $1/T_1$ vs. T experimental data of spin-1 AFM rings, i.e. V_7Zn and V_7Ni, with the same model.

The experimental data are shown in Figure 3.12(a) and (b) for V_7Zn and V_7Ni, respectively, at different fields. As one can see from Figure 3.12, the temperature dependence of the $1/T_1$ data for both rings is characterized by a peak centered at around 3÷6 K. The position and height of the peaks are reported in Table 3.7 (a) and (b) for V_7Zn and V_7Ni, respectively. The peak in $1/T_1$ decreases in height and shifts toward higher temperatures as the magnetic field is increased. It can be noticed that the peak appears at temperatures of the order of $T \sim J/k_B$ (see section 1.3.2). The solid lines in Figure 3.12 are the best fit by using the simple BPP model (with just one correlation time) discussed in section 3.2.1(ii), i.e. Equation (3.8). For these fits, ω_c was assumed to be in the power law form ($\omega_c = CT^{\alpha}$) according to what was found in the previous publications [16, 21, 25]. The parameters used in the fit of Figure 3.12 are: A = 1.9 (0.5) $\times 10^{11}$ rad^{2}mol/s^2 emu K, C = 3.1 (0.5) $\times 10^6$ rad/s, and α = 3 (0.5) for V_7Zn, and A = 2 (0.5) $\times 10^{11}$ rad^{2}mol/s^2 emu K, C = 3.5 (0.3) $\times 10^6$ rad/s, and α = 3 (0.5) for V_7Ni.

As seen in Figure 3.12 the lower field data are fitted well, while the higher field data are not well reproduced as regards the amplitude of the peak value. To better compare the behavior of $1/T_1(T)$ experimental data at different applied magnetic fields with the BPP model, in Figure 3.13 we report for V_7Ni and V_7Zn the height of the maximum of $1/(T_1\chi T)$ (see experimental data points in Table 3.7) vs. 1/B, and the BPP fit of the $\mu_0 H$ = 0.5 Tesla data for V_7Zn. As can be seen, the discrepancy is strong. To make sure that the problem does not arise from the choice of the T dependence of the correlation frequency we also tried to fit the data using an exponential dependence for ω_c i.e. $\omega_c = C \cdot \exp(\Delta/k_B T)$ [24], where Δ is the energy gap between two electronic levels, but the quality of the fits did not improve. In addition, we also tried [29(a)] to fit our experimental data using a more refined model [31, 32], where more than one correlation frequency determine the form of the spectral density of the electronic fluctuations (proportional to $1/T_1$), which thus results a sum of Lorentzian functions pertaining to different correlation frequencies $\omega_c^{(i)}$. To simulate the existence of many dominating correlation frequencies, we assumed that the spectral density is given by a continuous distribution of frequencies (see Appendix 2). The corresponding model for $1/T_1$ does not work (fitting curves not shown).

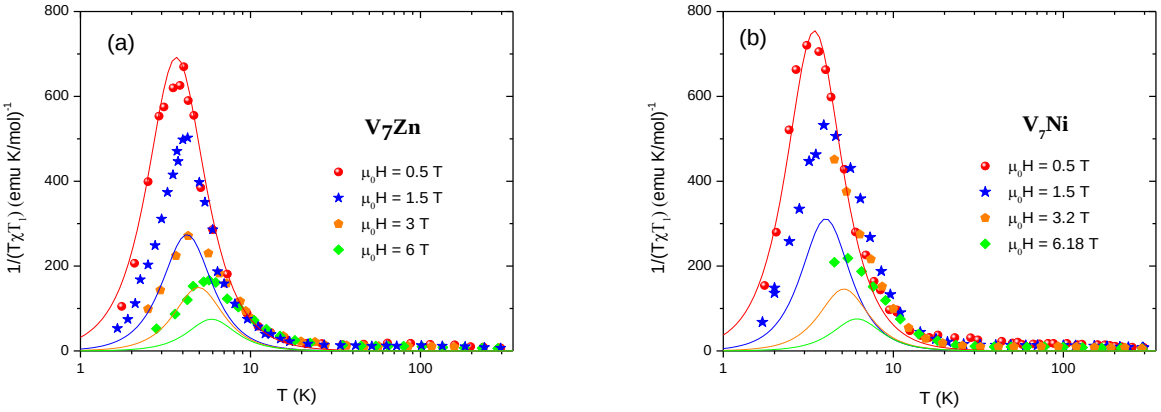

Figure 3.12: Temperature dependence of the spin-lattice relation rate divided by χT with fitting curve (solid lines) obtained by using Equation (3.8) as discussed in the text for (a) V_7Zn and (b) V_7Ni.

Let's now go back to the BPP model with the use of just one correlation time (solid lines in Figure 3.12). The observed discrepancy could signify that the spin correlation function G(t) is completely different from the simple exponential one assumed in Equation 3.8 as a result of the difference between the electronic spins of V^{3+} ion (s = 1) with respect to the Cr^{2+} spin (s = 3/2) . On the other hand, since the shape of the peak and the position of the maximum at different fields seem to be well reproduced by the usual model (Equation 3.8), one could propose an explanation of the fact that the height of the peak does not scale with 1/B as an experimental artifact due to the wipe-out effect. In fact the NSLR data around the peak were collected in the temperature range in which there is a loss of ^1H NMR signal (wipe-out effect, see Figure 3.15). It should remarked that in this temperature range we keep measuring the fast relaxing component and this fast component decreases in intensity with respect to the slow component (see Figure 3.8) signaling that we are losing the fast relaxing nuclei. Therefore is very likely that the measured NSLR is less than it would be if the fastest relaxing nuclei were detected. A theoretical analysis which takes into account the wipe-out effect is rather complex but it was shown to be possible for a different molecular ring [26] and should be used here to analyze our results.

Table 3.7: Position and height of the NSLR rate "$1/(T_1\chi T)$" for (a) V_7Zn and (b) V_7Ni spin-1 AFM rings.

(a) V_7Zn

Field (T)	T_{peak} (K)	Height $(eum \cdot S \cdot K \cdot mol^{-1})^{-1}$
μ_0H = 0.5 T	3.77	662.5
μ_0H = 1.5 T	4.2	499.9
μ_0H = 3 T	4.4	271.7
μ_0H = 6 T	5.6	165.2

(b) V_7Ni

Field (T)	T_{peak} (K)	Height $(eum \cdot S \cdot K \cdot mol^{-1})^{-1}$
μ_0H = 0.5 T	3.13	724.4
μ_0H = 1.5 T	3.89	532.5
μ_0H = 3.2 T	-	-
μ_0H = 6.18 T	5.28	214.66

An important experimental result which is independent of the theoretical analysis is contained in the fact that, as shown in Figure 3.13, the T and H dependence of NSLR in V_7Ni and V_7Zn are practically the same. Therefore, one could conclude that the spin dynamics in the intermediate temperature range ($T \approx J/k_B$) is not affected by the ground state spin value S_T and/or topological effects, since the V_7Zn and V_7Ni are "open, $S_T = 1$" and "closed, $S_T = 0$" spin-1 AFM ring, respectively.

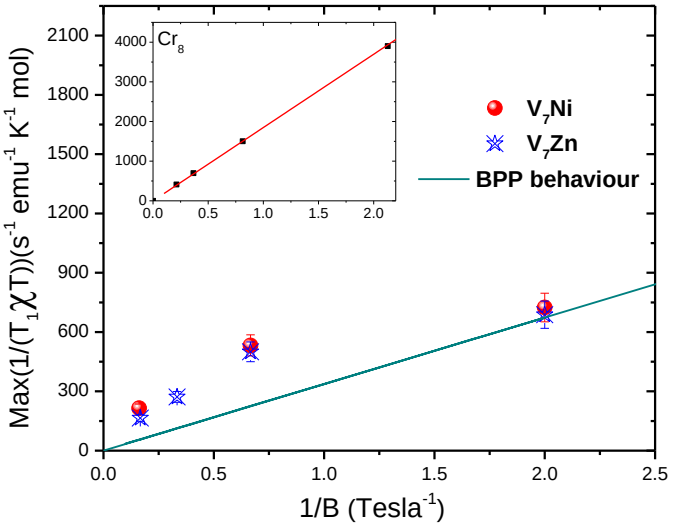

Figure 3.13: Experimental height of the peaks of $1/(T_1\chi T)$ of V_7Zn and V_7Ni for the different values of the inverse magnetic field (scattered points), compared with the BPP behavior (solid line), calculated for V_7Zn by fitting the experimental data at $\mu_0 H = 0.5$ T. **Inset:** Experimental height of the peaks of $1/(T_1\chi T)$ in Cr_8 for the different values of the inverse magnetic field (scattered points), compared with the BPP behavior (red solid line) [30].

In order to obtain additional information about the spin dynamics, we performed proton spin-spin relaxation measurement (T_2) as a function of temperature. Figures 3.14(a) and (b) show the behavior of $1/T_2$ as a function of temperature for V_7Zn and V_7Ni, respectively. As one can see, no specific anomaly can be found within the experimental error except a T_2 shortening by lowering temperature, which should be due to the progressive enhancement and slowing down of the electronic spin fluctuations (see Figure 3.12). This behavior was observed also in semi-integer AFM rings [6, 17] (see inset of Figure 3.5). As discussed in the next section the shortening of T_2 is responsible for the signal intensity loss (i.e. wipe-out effect).

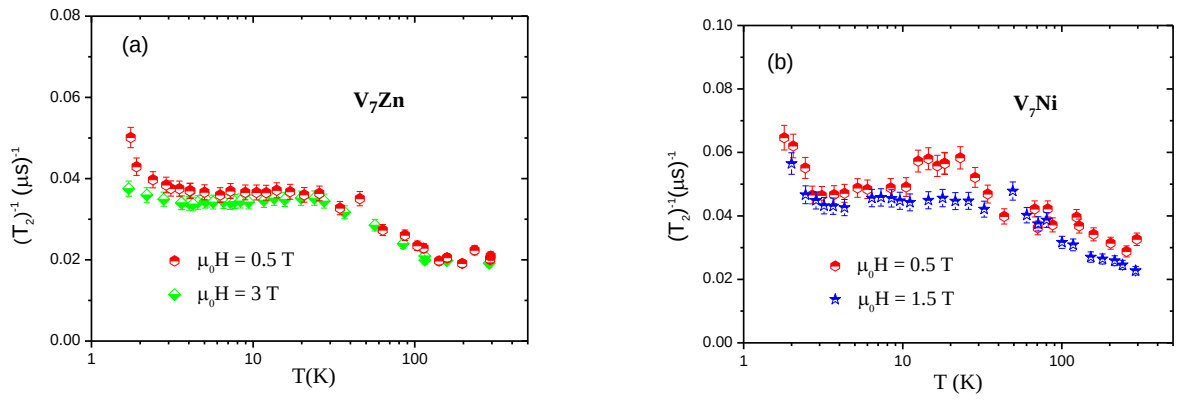

Figure 3.14: Temperature dependence of spin-spin relaxation rate, $1/T_2$, for (a) V_7Zn at $\mu_0H = 0.5$ T and $\mu_0H = 3$ T (b) V_7Ni at $\mu_0H = 0.5$ T and $\mu_0H = 1.5$ T.

(iii) Wipe-out effect

The phenomenon of the wipe-out was already discussed in section 3.2.1(iii) in the case of semi-integer AFM rings. The loss of the NMR signal intensity (wipe-out effect) is ascribed to a shortening of the spin-spin relaxation time T_2 (followed by a shortening of the spin-lattice relaxation time), which produces a decay of the transverse nuclear magnetization in a time shorter than the dead time of the spectrometer, τ_d. The origin of the wipe-out effect, in the case of molecular rings was attributed to a combination of a strong hyperfine coupling of the nuclei to the electrons and a slowing down of the fluctuations of the magnetic moments of the ions. The study of the wipe-out effect could thus yield information regarding both the hyperfine coupling and the electron spin dynamics. Here, we are going to show the behavior of the signal intensity $M_{xy}(0)\cdot T$ vs. T in spin-integer AFM rings, V_7Ni and V_7Zn.

Figure 3.15 shows ^1H NMR signal intensity times the temperature, $M_{xy}(0)\cdot T$, normalized to the room temperature value of $M_{xy}(0)\cdot T_{RT}$. The experimental curves show two major drops as the temperature is lowered. The first one occurs at T ~ 125 K, while the second one appears at around T ~ 25 K.

Since the wipe-out effect is more pronounced at lower magnetic fields, we confine our data analysis to the lowest magnetic field experimental data i.e. $\mu_0H = 0.5$ T, as shown in Figure 3.16. Moreover, we analyzed the wipeout in the most interesting temperature range T [1.7 ÷ 35 K], where the $1/T_1$ peak occurs. The signal intensity ($M_{xy}(0)\cdot T$) was hence corrected once again in order to have the data at 35 K renormalized to 1, as shown in Figure 3.16. It is worth noticing that the following data analysis has been done to get a general view of the wipe-out effect in comparison with semi-integer AFM rings.

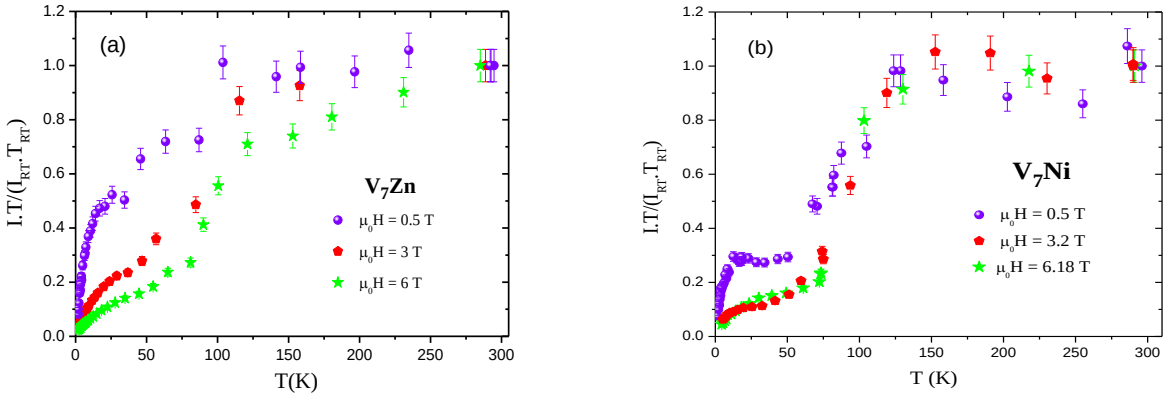

Figure 3.15: ^{1}H NMR signal intensity times the temperature, normalized to the room temperature value, as a function of temperature for (a) V_7Zn at μ_0H = 0.5, 3, and 6 T (b) V_7Ni at μ_0H = 0.5, 3.2, and 6.18 T.

The analysis was carried on by using the simple model that was already proved to be successful in Cr-based AFM rings [16, 18] (see section 3.3.1(iii)). As mentioned before, this model is based on the assumption that the dominant contribution to $1/T_2$ comes from the dephasing due to the hyperfine interactions with the exchange coupled magnetic ions (see Equation (3.11)).

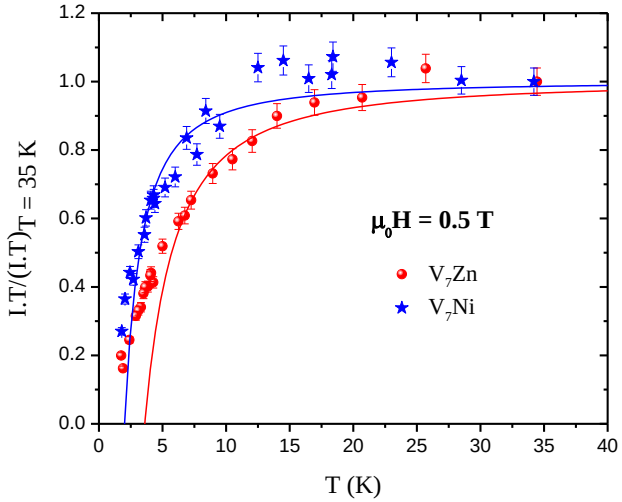

Figure 3.16: The second drop in the $M_{xy}(0)\cdot T$ normalized to the value at T = 35 K ($M_{xy}(0)\cdot T_{35\ K}$). The solid lines are the best fit by using Equation (3.11) as discussed in the text.

Although the fit of the NSLR vs. T ran into the problem of explaining the peak intensity as a function of the external field (see section 3.3.2(ii)) we believe that the information regarding the correlation frequency of the molecular magnetization should still be valid. Therefore we use a power law function for the correlation time ($\tau_c = 1/\omega_c$, i.e. $\tau_c = C'T^{-\alpha}$) to fit the wipeout experimental data,

similarly, to the Cr-based rings [16, 17]. We hence used in Equation 3.11 the results obtained from the $1/T_1$ fits (for the lowest field) for τ_c in the previous section and $\sqrt{\langle \delta\mu_e^2 \rangle}/R^{*3}$ was considered to be the only free parameter in the fitting procedure. The obtained fit parameter is $\sqrt{\langle \delta\mu_e^2 \rangle}/R^{*3} = 150$ (15) G, and $\sqrt{\langle \delta\mu_e^2 \rangle}/R^{*3} = 65$ (10) G for V_7Zn and V_7Ni, respectively. The values reported for the same parameters in the Cr rings are ~ 850 G for Cr_7Cd and ~ 500 G for Cr_7Ni [17]. The difference must be due to a larger hyperfine interaction for the case of Cr rings. It is important to remark that this difference is perfectly consistent with the values of the A parameter in Equation 3.8 which measures the average square of the fluctuating hyperfine interaction and are found to be one order of magnitude larger for Cr rings (see Table 3.5) with respect to the V rings (see section (ii) above) .

We can conclude that the spin dynamics in the intermediate temperature range appears to be the same for V rings and Cr rings with no clear evidence of an effect due to the different spin value (s = 1 vs. s = 3/2 respectively). Thus the problem of the Haldane gap has to be investigated by measurements of the size and of the field dependence of the gap in closed and open integer AFM rings to be compared with the results established for the semi-integer AFM rings.

3.4 Low temperature regime

We are now going to present the low temperature experimental data to mainly study the discrete energy structure of the finite spin systems. Our experimental investigation has been confined to the semi-integer AFM rings, namely Cr_8Zn in the present work. The Cr_8 system was previously studied by Micotti et al., [34] and its results will be used for comparison purpose between open and closed rings.

3.4.1 Semi Integer AFM rings: Cr_8Zn

The aim of the low temperature investigation of Cr_8Zn is to study the multiple level crossings (LCs) by means of ^1H NMR technique. The energy structure of Cr_8Zn shown in Figure 3.17 was previously presented according to the theoretical calculations in section 1.2.3. Here, we are going to present ^1H NMR experimental data, including nuclear spin-lattice relaxation rate, $1/T_1$, spin-spin relaxation rate, $1/T_2$, and ^1H NMR spectra. The experimental data have been collected on a Cr_8Zn single crystal as a function of magnetic field in a range where different level crossings occur, i.e.$1 \leq \mu_0 H \leq 8$ T at constant low temperature ~ 1.7 K. The measurements were performed with the external magnetic field approximately parallel to the ring's plane, i.e. perpendicular to the molecular axis ($\theta = 90°$). Finally, the comparison of the experimental data with theoretical prediction will be discussed.

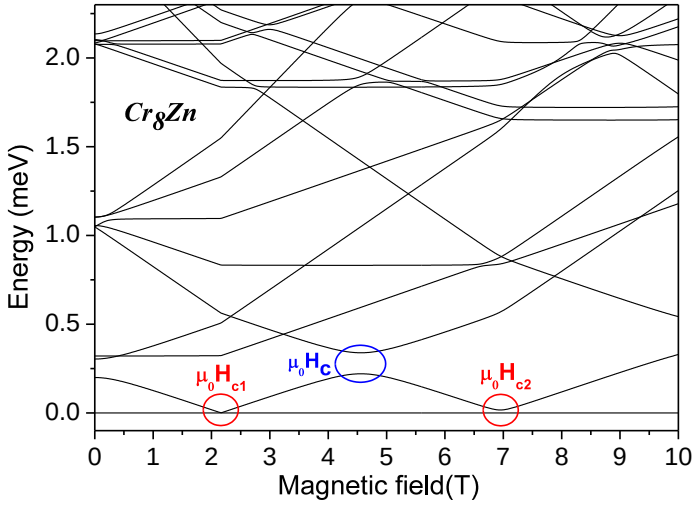

Figure 3.17: Magnetic field dependence of the low-lying energy levels of Cr8Zn calculated according to Equation (1.14). The field lies in the plane of the ring. The two ground state level crossings fields $\mu_0 H_{c1}$ and $\mu_0 H_{c2}$ are indicated in red, while the excited states level anti-crossing $\mu_0 H_c$ is indicated in blue.

(i) Spin-Lattice relaxation rate, $1/T_1$

(i-a) *Experimental results*

The value of $1/T_1$ was determined by monitoring the recovery of the longitudinal nuclear magnetization. Recovery curves show magnetic field dependent multi-exponential behaviors (see Figure 3.18) due to the presence of nonequivalent groups of ^{1}H sites in the molecule whereby each group possesses its own "average" relaxation rate.

Since the relative weight of the different experimental components significantly changes near the level crossings the T_1 values have been obtained by fitting the recovery with two exponential components, which labeled as fast and slow component:

$$1 - \frac{M_z(t)}{M_z(\infty)} = A_{fast} \exp\left(-\frac{t}{T_{1fast}}\right) + A_{slow} \exp\left(-\frac{t}{T_{1slow}}\right) \qquad (3.12)$$

where A_{fast} and A_{slow} are the relative weights and T_{1fast} and T_{1slow} are the spin-lattice relaxation times of the two components, respectively. The fast component is ascribed to the groups of ^{1}H closer to the transition metal ions Cr^{+3} since those nuclei sense a larger hyperfine field, while the slow decay corresponds to the ^{1}H nuclei which are farther away from the magnetic ions.The magnetic field dependence of the two components $1/T_{1fast}$ and $1/T_{1slow}$ are plotted separately in Figures 3.19(a) and 3.19(b). $1/T_{1fast}$ reveals a sharp peak at the first ground state level crossing (i.e. $|S = 0, M_s = 0>$ to $|S = 1, M_s = -1>$) for $\mu_0 H_{c1} \approx 2.15$ T as shown in Figure 3.17, while $1/T_{1slow}$ shows an anomaly at $\mu_0 H_{c1} \approx 2.15$ T and a broad maximum in correspondence to the excited level anti-crossing at $\mu_0 H_c = 4.4$ T.

A broad and small peak is also present for the fast component around the second ground state level crossing (|S = 1, M_s = -1 > to |S = 2, M_s = -2 >) at $H_{c2} \approx 7$ T, while the slow relaxing protons show a very small bump at the same field (see Figure 3.17). The physical mechanisms responsible for the different behavior of fast- and slow-relaxation protons are still under theoretical investigation, the difference in the hyperfine field felt by the two groups being just one of the possible one. For the data analysis we focused on $1/T_{1fast}$ curve.

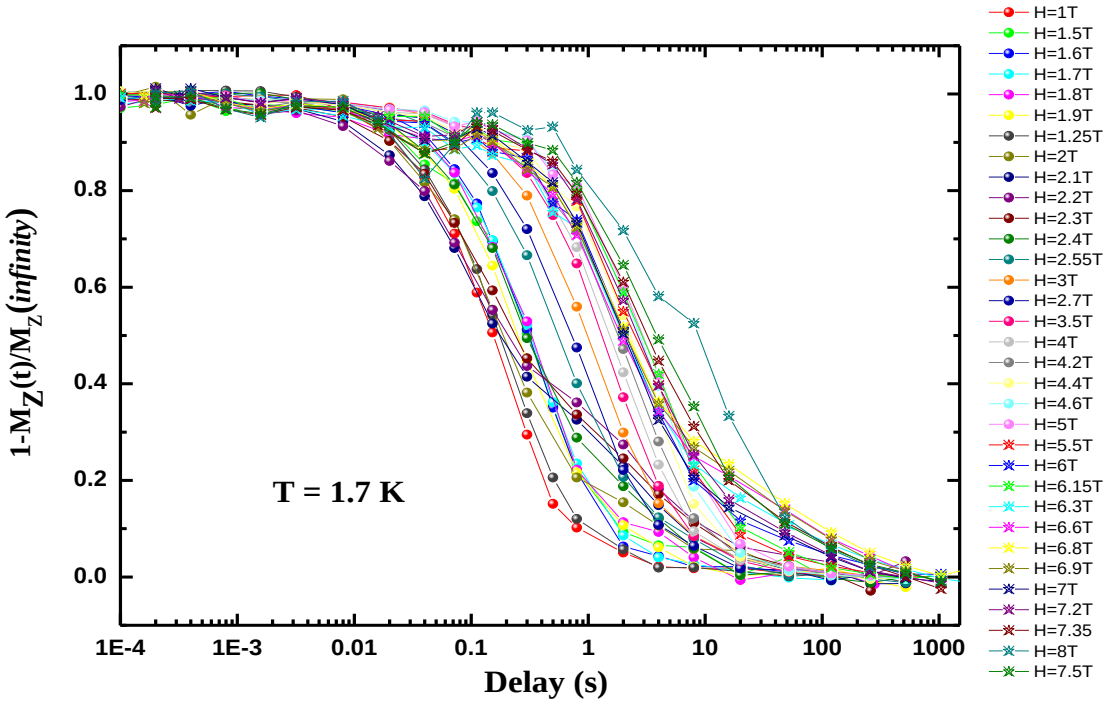

Figure 3.18: Low temperature spin-lattice relaxation recovery curves of Cr_8Zn single crystal at different magnetic fields.

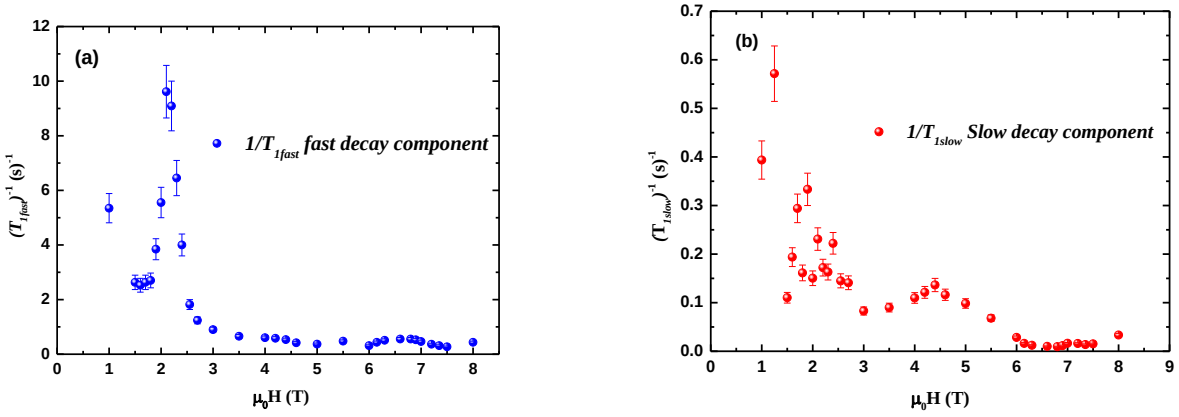

Figure 3.19: Proton spin-lattice relaxation rates as a function of magnetic field for (a) $1/T_{1fast}$, and (b) $1/T_{1slow}$ as a function of magnetic field, extracted by fitting the T_1 recoveries with two exponential components as explained in the text.

For the purpose of obtaining more information from the NSLR of the non-equivalent groups of ^{1}H sites in the molecule we plot their relative weights A_{fast} and A_{slow} as a function of magnetic field in Figure 3.20(a). The fact that at the first level crossing the relative weight of the fast component decreases while the one of the slow component increases, is due to the loss of signal intensity, i.e. wipe-out effect, coming mostly from the fast relaxing ^{1}H nuclei. The ^{1}H NMR signal intensity plotted as a function of magnetic field (see Figure 3.20(b)) indicates clearly a wipe-out effect in correspondence to the first level crossing, in agreement with the decrease of the weight of the fast component and the increase of the one of the slow component. This wipe-out effect of NMR signal is presented and discussed in section 3.4.1(ii).

It is worth noting that finding a proper interpretation for the experimental data collected at the highest magnetic field is more complicated due to the combination of T_2 shortening and the broadening effect of the NMR line.

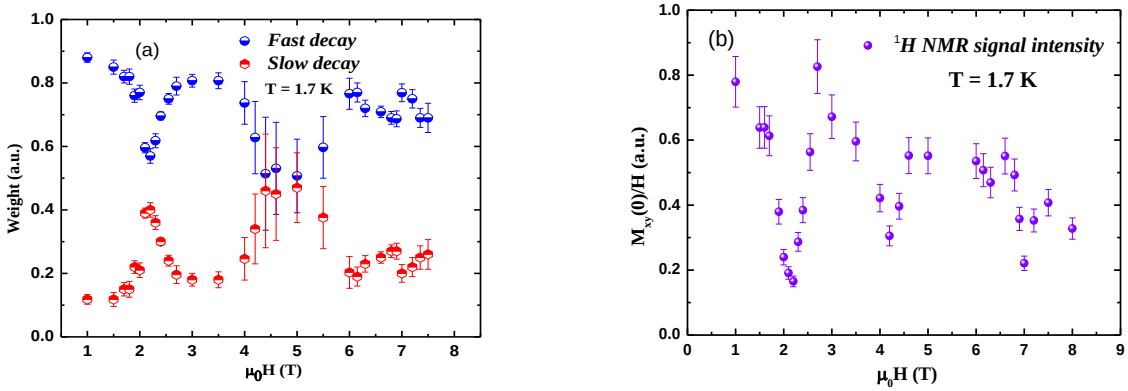

Figure 3.20: (a) The relative weights of the two components in spin-lattice relaxation recovery curves extracted as explained in the text. The error values are associated to the χ^2 minimization procedure in the fit progress. (b) ^{1}H NMR signal intensity divided by magnetic field as a function of magnetic field.

(i-b) Discussion of the experimental results at the level crossing

We are now going to analyze the results of proton spin-lattice relaxation rate, $1/T_1$, near the level crossings at low temperature in Cr_8Zn in order to gain information about the nature of the level crossing and the spin dynamics. The theory of NSLR in molecular magnets at low temperature was already developed in chapter 2. In the actual experimental conditions we can consider the system as two-level system[1] near to the level crossing. Thus NSLR can be analyzed using the model given in paragraph 2.3.3, where the relaxation rate is given by Equation (2.58). Assuming some simplification, Equation (2.58) is reduced to[2] [34, 35]:

[1]Two-level system means, a system with two energy states for instance ground state and first excited state.

[2]This expression was also utilized to analyze the first ground state level crossing in Cr_8 [34].

$$\frac{1}{T_1} = \frac{\exp(-\frac{\Delta_1}{kT})}{1+\exp(-\frac{\Delta_1}{kT})} A^2 \frac{\Gamma_1(T)}{\Gamma_1^2(T)+\omega_n^2} + B^2 \frac{\Gamma_2(T)}{\Gamma_2^2(T)+(\omega_n-\Delta_1)^2} \quad (3.13)$$

Let's now discuss the two contributions appearing in Equation (3.13). The first contribution is the quasi-elastic term which arises from the fluctuations of the magnetization of the molecule in the first magnetic excited state. These fluctuations due to spin-phonon interaction are modeled with a Lorenzian broadening Γ_1 of the magnetic state and the NSLR is simply proportional to the Lorenzian spectral density function at the Larmor frequency ω_L. Far from the level crossing the relaxation is mainly driven by this contribution, which means that the nuclear T_1 values are dominated by the quasi-elastic component of the longitudinal fluctuations [35, 36]. The $\exp\left(-\frac{\Delta_{01}}{kT}\right)/\left(1+\exp\left(-\frac{\Delta_{01}}{kT}\right)\right)$ term is actually an approximation of the magnetic susceptibility, $\chi = \partial M/\partial H$, which can simply be calculated from Equation (1.12) considering only the ground S = 0 and the first excited $S_T = 1$ state.

The second term is the inelastic term which arises from direct transitions between nuclear Zeeman states accompanied by a transition among the magnetic electronic state of the molecule. In fact, near the level crossing field, the energy separation between magnetic levels decreases and therefore the nuclear relaxation occurs through the inelastic scattering corresponding to an exchange of energy between electrons and nuclei. This term is important only close to a level crossing and becomes dominant when the gap Δ_1 is of the order of the broadening Γ_2 of the magnetic state of the molecule and/or the separation among the nucleus levels. The parameters A^2 and B^2 represent the average square local field fluctuation and are related to the average hyperfine interaction of the protons with the Cr^{3+} magnetic moments.

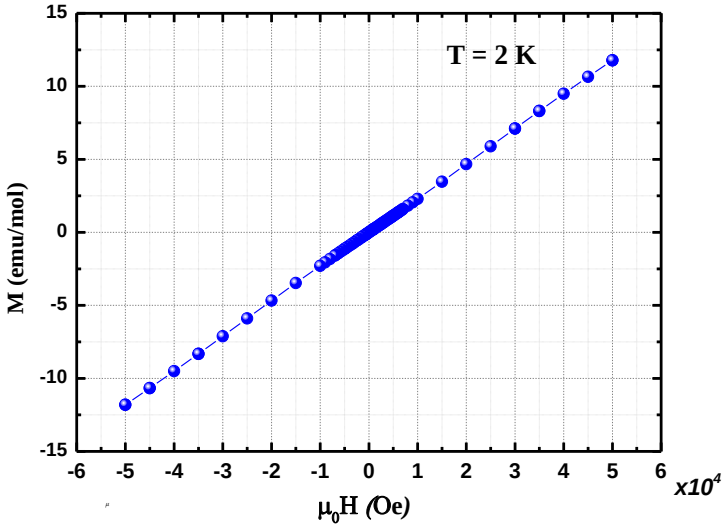

Figure 3.21: Magnetization curve as a function of magnetic field in a Cr_8Zn single crystal at T = 2 K.

In the case of Cr_8Zn, at T = 1.7 K and in the considered magnetic field range the χT term is constant since many magnetic excited states are populated. The magnetization curve as a function of magnetic field in Cr_8Zn at T = 2 K that is shown in Figure 3.21 is an indirect confirmation of the population of several levels, as the magnetization is linear in H like for a simple paramagnet. On the contrary, we would like to remind that, in the case of Cr_8 the gap between the non-magnetic ground state and the first excited magnetic state is larger than the measuring temperature and thus the term χT represents the effective moment of the excited state and is proportional to the Boltzmann population factor i.e. exp (-Δ/kT), with Δ being the gap between the nonmagnetic ground state and the magnetic exited state. It is interesting to note that since in Cr_8Zn the χT ($\frac{M}{H} \cdot T$) is field independent, a monotonic decrease is expected for the elastic term (see Equation (2.58)) while the peak of $1/T_1$ at the first LC in Cr_8Zn is entirely due to the inelastic term. This is not the case in Cr_8 where the peak at the first LC is due to both the elastic and inelastic contributions [34].

For simplicity, one can extract the magnetic susceptibility and the constant parameter which is the average square of the hyperfine interaction. Therefore Equation (3.13) can be given by

$$\frac{1}{T_1} = \chi T \mathrm{A}'^2 \left[\frac{\Gamma_1(T)}{\Gamma_1^2(T) + \omega_n^2} + \frac{\Gamma_2(T)}{\Gamma_2^2(T) + (\omega_n - \Delta_1)^2} \right] \tag{3.14}$$

where A'^2 is still the average square of the hyperfine interaction between protons and magnetic ions, and it is expected to be temperature and field independent. The fit of the NSLR for the first ground state LC ($\mu_0 H_{c1}$ = 2.15 T) as a function of the external magnetic field by using Equation (3.14), is shown in Figure 3.22. The gap between the ground state and the first excited state for the first ground state LC is given by

$$\Delta_1 = \sqrt{\Delta_{01} + [g\mu_0\mu_B(H_{c1} - H)]^2} \tag{3.15}$$

where we have taken into account a possible level anti-crossing gap Δ_{01}. The critical magnetic field is set to 2.15 T as deduced from the experimental data. Non zero value for $\Delta_{01}$is an important constraint which proves the presence of a small repulsion between the two levels at the first ground state LC. The second term in Equation (3.14), i.e. the inelastic one, becomes important in the neighborhood of the critical field $\mu_0 H_{c1}$ = 2.15T and is responsible for the peak in the NSLR data, while the $1/T_1$ data away from the critical field are dominated by the first term related to the quasi-elastic term. The parameters obtained from the fit in Figure 3.22 are: $\mathrm{A}'^2 = 5.7\times10^{11}$(rad^{2}mol)/(sec^2.emu.K) = 0.14×10^{12} rad^2/sec^2, Γ_1 = 1.4(0.14)$\times10^6$ rad/sec, Γ_2 = 2.4(0.14)$\times10^{10}$ rad/sec, and Δ_{01} = 1.1×10^{10} rad.Hz = 0.09(0.02) K while the χT (= 0.46 emu·K/mol) has been extracted from the experimental data M vs. T and M vs. H.

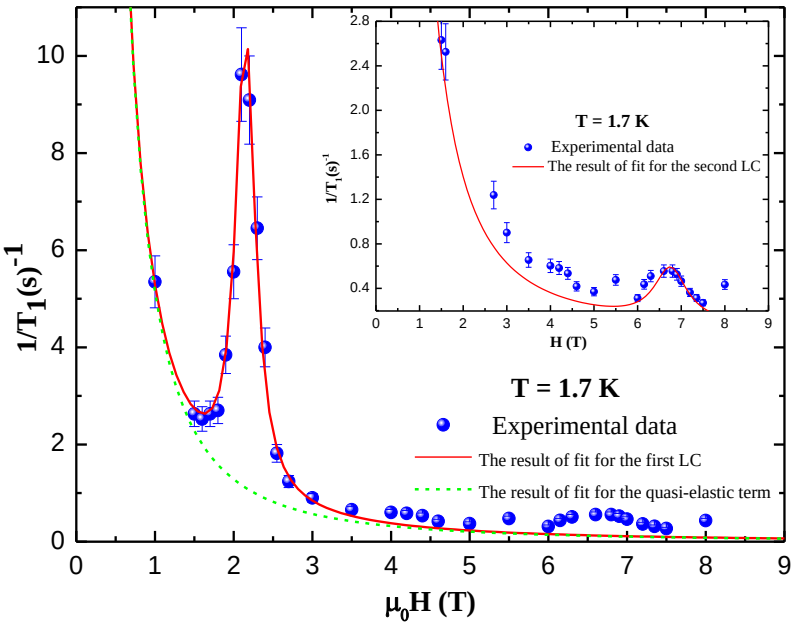

Figure 3.22: ^{1}H spin-lattice relaxation as a function of magnetic field in Cr_8Zn at T=1.7 K. The solid line is the fit for the first ground sate LC according to Equation (3.b) as explained in the text. The green dashed line is the fit obtained by using, only the quasi-elastic term in Equation (3.13). **Inset:** The zoom close to the second level crossing including the fit curve.

It is interesting to note that the order of magnitude of Γ_1 as determined above for the quasi-elastic contribution is close to the one obtained from the analysis of the NSLR results in Cr_8Zn at higher temperature (see section 3.3.1(ii)). This comparison indicates that far from level crossing the NSLR is determined at all temperatures by the broadening of the magnetic levels of the molecular magnet which is due to intrinsic lifetime and to the spin-phonon interaction.

The Equation (3.14) was also used to fit the experimental data near the second ground state level crossing where the NSLR data show a small peak. The inset of Figure 3.22 indicates that the experimental data are well reproduced by the fit function. The parameters obtain from the fit for the second ground state LC are: A'^2 = 5.7×10^{11}(rad^{2}mol)/(sec^2.emu.K) = 0.14×10^{12} rad^2/sec^2, Γ_1 = $1.5(0.15)\times10^6$ rad/sec, Γ_2 = $1.1(0.11)\times10^{10}$ rad/sec, and Δ_{12} = 0.8×10^{11} rad·Hz = 0.61 (0.08) K; χT (= 0.46 emu·K/mol) we still used the experimental values. The gap between S_T =1 and S_T = 2 states was assumed to follow the field dependent function given by $\Delta_2 = \sqrt{\Delta_{12} + [g\mu_0\mu_B(H_{c2} - H)]^2}$ where μ_0H_{c2} = 6.75 (0.2) T (from the experimental results) and Δ_{12} is the anti-crossing gap determined by the fit of the NSLR data.

Recently, thermodynamic measurements, mainly high field torque measurements, have been performed in Cr_8Zn in order to obtain more information about the LCs [37]. Those experimental data and the relevant theoretical calculations indicated different values for the level anti-crossing gaps: Δ_{01} = 0.01 k at μ_0H_{c1} and Δ_{12} = 0.19 k at μ_0H_{c2}. This inconsistency with the NMR data can be resolved by

adding the *J-strain* effect. This effect is present when different molecules in the crystal have slightly different values of Heisenberg exchange interaction constant, J, which leads to a J values distribution in the Heisenberg exchange term $\sum_i J_i S_i \cdot S_{i+1}$ [38]. In particular we observed that a distribution of values of J leads to a distribution of values of the crossing field $\mu_0 H(J)$ centered at the nominal $\mu_0 H_c$. Here, in the case of Cr_8Zn, it was found that the effect of *J-strain* is much more pronounced in the proximity of $\mu_0 H_{c2}$ than $\mu_0 H_{c1}$, as witnessed by the energy gap between the $S_T = 2$ and $S_T = 1$ multiplets (which cross at $\mu_0 H_{c2}$) that is about three times the exchange energy gap between the $S_T = 1$ and $S_T = 0$ multiplets involved in the crossing at $\mu_0 H_{c1}$. One can finally state that an agreement between ^{1}H NMR results and thermodynamic data has been found by adding the *J-strain* effect in the semi-phenomenological model for the level crossings, i.e. Equation (3.14) [37].

(ii) Spin-spin relaxation rate and wipe-out effect:

(ii-a) *Experimental results*

An interesting effect was observed at the level crossing, consisting in a loss of NMR measured signal intensity around the critical fields. This effect is called "Wipe-out effect" and it is shown in Figure 3.23(a), where we report the amplitude of the measured proton NMR signal, $M_{xy}(0)$, divided by the applied magnetic field (in order to eliminate the effect of the Boltzmann population of the nuclear Zeeman levels) vs. H. The absolute value of the proton NMR signal $M_{xy}(0)$ was determined by the echo amplitude of the decay curve extrapolated back at t = 0, considering that the decay of the echo signal follows an exponential law over the whole delay times range [28, 37].

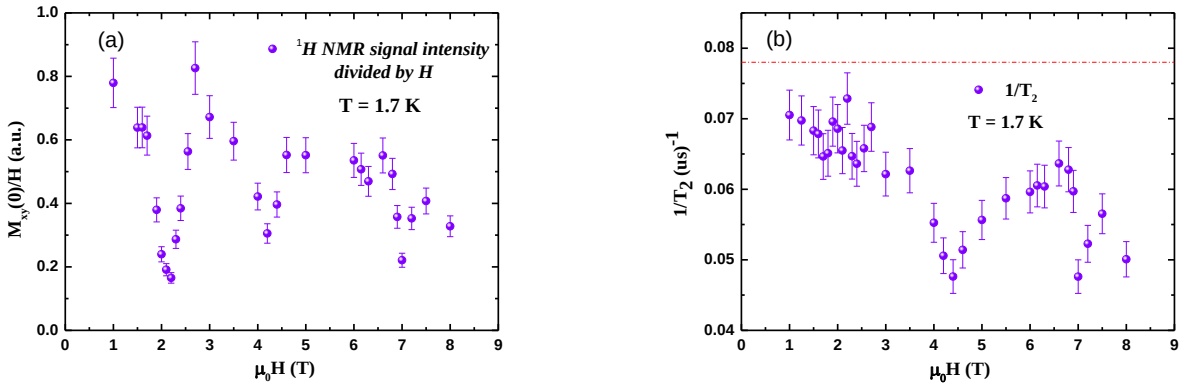

Figure 3.23: (a) ^{1}H NMR signal intensity divided by magnetic field as a function of magnetic field. (b) Proton spin-spin relaxation rate as a function of magnetic field. The dashed line is the estimated measurable upper limit due to the electronic "dead-time" of the instrument.

The wipe-out effect was observed previously in molecular magnets [28] but just in the temperature dependent measurements i.e. when $M_{xy}(0)*T$, is plotted as a function of temperature and has been widely discussed in our measurements presented in the previous sections. The one reported in Figure 3.23 (a) is the first observation of a wipe-out effect as a function of external magnetic field. In general,

the loss of measured NMR signal takes place when the proton spin-spin relaxation time, T_2, becomes so short that the echo signal decays within the "dead time" or "blind time" of the Fourier Transform pulse NMR spectrometer. The wipe-out effect is observed by lowering the temperature, when the electronic spins are slowing down thus causing the divergence of proton spin-spin relaxation rate, ^{1}H-$1/T_2$. In the present case we argue that the divergence of the relaxation rate, $1/T_2$, arises from the strong enhancement of the spin fluctuations at ω_L (due to the direct exchange of energy between electrons and nuclei) in the vicinity of the critical field for LCs. Thus the magnetic field dependence of the proton spin-spin relaxation rate was investigated. Since decay curves in T_2 measurement presented an exponential behavior of the echo amplitude as a function of delay times, the T_2 values were obtained by fitting the decay curves with an exponential function

$$M_{xy}(T) = M_{xy}(0)\exp\left(-\frac{t}{T_2}\right) \tag{3.16}$$

The T_2 results extracted from the Equation (3.20) are shown in Figure 3.23 (b). One should take into account that there is a minimum value of the delay τ_d (dashed red line) below which the observation of the NMR echo signal is not possible due to the instrumental dead time. As can be seen from the figure the value of T_2 around the first level crossing is very short, namely about 15 μs which is close to the limit of our instrument, estimated to be around 10 μs. Close to the LC the value of T_2 is likely become even shorter but the "peak" cannot be observed because of the limit of our measurements. The decrease of $1/T_2$ at the excited state LC and at the second ground state LC is most likely due to the broadening of the NMR line. In fact the broadening of the line is linked to stronger hyperfine interactions, that is shorter T_2 [39].

(ii-b) Discussion of the wipe-out effect

In order to analyze the wipe-out effect shown in Figure 3.23(a) we will adopt the approximate model introduced to explain the same effect observed in molecular nanomagnets as a function of temperature [28]. The starting point is the description of the mechanism for the irreversible decay of the nuclear magnetization which is described by the spin-spin relaxation rate parameter $1/T_2$. In a nonmagnetic molecular crystal where the protons are rigid in the lattice, the transverse relaxation is due to the dipolar interaction among the proton nuclei. This dipolar contribution is T and H independent and is of the order of the inverse line-width of the NMR line, i.e. about 20 kHz. It should be noticed that this value of the NMR line-width can be observed just at high temperature (T > 150K) as, when the temperature is decreased, the nuclei are subjected also to the hyperfine interaction with the magnetic ions, which broadens sensibly the spectrum. This interaction has a static component which determines an inhomogeneous broadening of the NMR line which generates a reversible decay of the transverse nuclear magnetization which does not contribute to T_2. On the other hand the time dependence of the hyperfine interaction generates spin-lattice and spin-spin nuclear relaxation. Based on weak collision

theory, in the fast motion approximation, $1/T_2$ can be expressed in terms of the spectral density of the fluctuating hyperfine field at zero frequency [39, 40] i.e.:

$$\frac{1}{T_2} \approx \frac{1}{T_2}\Big|_{f(\omega=0)} = \gamma_N^2 \langle \delta H_z^2 \rangle J(\omega = 0) = \gamma_N^2 \frac{\langle \delta \mu_e^2 \rangle}{r^6} f(\omega = 0) \tag{3.17}$$

where $\gamma_N^2 \langle \delta H_z^2 \rangle$ is the average square of the nuclear-electron dipolar interaction and δH_z is the local longitudinal fluctuating field originating from a magnetic moment sitting at a distance r apart from the proton spin. The spectral density function $f(\omega)$, is the Fourier Transform of the correlation function as

$$J(\omega) \propto \int \langle S_{j+}(t) S_{j-}(0) \rangle e^{-i\omega t} dt \tag{3.18}$$

By assuming for the time dependence of the two-spin correlation function in Equation (3.18) an exponential function with a time constant τ (correlation time), from Equations (3.17) and (3.18) one has

$$\frac{1}{T_2} = \gamma_N^2 \frac{\langle \delta \mu_e^2 \rangle}{r^6} \tau(H, T) \tag{3.19}$$

The correlation time can be temperature or magnetic field dependent and the validity of the Equation (3.19) ceases when one crosses the limit of the fast motion approximation, namely, when τ becomes of the order of the inverse of the interaction frequency $\omega = \gamma_N \delta H_z$ with γ_N the nuclear gyromagnetic factor. In the slow motion approximation, the nuclear-electron hyperfine interaction becomes static and it generates an inhomogeneous broadening of the NMR line. Normally the contribution to $1/T_2$ described by Equation (3.19) is negligible compared to the nuclear dipolar interaction and can be disregarded. However, in presence of slowing down of the spin fluctuations or, as in our case, in the vicinity of a LC, this contribution can become dominant and be responsible for the wipe-out effect. In fact the dependence of $1/T_2$ from the distance r of the non-equivalent protons with respect to the magnetic ions gives rise to a distribution of $1/T_2$ values. As a result, when the correlation time of the magnetic ions becomes gradually longer, T_2 becomes shorter and eventually crosses the limiting value of the instrument τ_d, below which the signal cannot be detected in the experimental setup (in Figure 3.23(b), this results in a dip of $1/T_2$ vs. H curve at LCs). In addition, if this increase of the correlation time is assumed to be monotonic, it is expected that the critical value of τ is progressively reached by all the proton sites, with the ones closer to magnetic ions being wiped out first, generating a gradual loss of the NMR signal intensity.

In order to obtain a quantitative model, one can assume the central magnetic ions surrounded by a large number of protons uniformly distributed at distance up to a maximum value R^*, the number density being $\rho = n_0/[\left(\frac{4\pi}{3}\right) R^*]$, where n_0 is the total number of protons in each molecule. Being in the regime of the wipe-out effect, and for a certain value of the correlation time, there is a certain number of protons having a T_2 value faster than the critical value. These protons are enclosed within a notional

sphere of radius r_c and do not contribute to the measured signal intensity. On the other hand, the protons located outside this sphere can be detected and their number $n(T,H)$ can be written as

$$n(T,H) = n_0[1 - \left(\frac{r_c}{R^*}\right)^3] \tag{3.20}$$

The value of the critical radius r_c in Equation (3.20) can be obtained from Equation (3.19) setting $T_2^{-1} = \tau_d^{-1}$. Then one can express $n(T,H)$ in term of τ as [28]:

$$\frac{n(T,H)}{n_0} = 1 - \frac{\gamma_N \sqrt{\tau_d}\sqrt{\langle \delta\mu_e^2 \rangle}}{R^{*3}}\sqrt{\tau(T,H)} \tag{3.21}$$

Equation (3.21) describes the wipe-out effect due to the slowing down of the fluctuations upon lowering the temperature and is identical to Equation (3.11) used to analyze the wipe out effect vs. T.

Here, we extend this model for the wipe-out effect at the level crossing. Thus we redefine the meaning of the correlation time τ in Equation (3.21). This can be done by observing that the inelastic term in Equation (3.14) contains the spectral density of the fluctuations at the Larmor frequency. Since according to Equation (3.17) the spin-spin relaxation rate depends on the spectral density of the fluctuations at zero frequency one has:

$$\frac{1}{T_2} \propto J(0) \sim \lim_{\omega_L \to 0}\left(\frac{\Gamma_2(T)}{\Gamma_2^2(T) + (\omega_L - \Delta_1)^2}\right) \approx \frac{\Gamma_2(T)}{\Gamma_2^2(T) + \Delta_1^2} \approx \tau^*(H) \tag{3.22}$$

We have made the tacit assumptions that the spectral density of the transverse hyperfine field fluctuations entering the $1/T_1$ theory is the same as the spectral density of the longitudinal (with respect to the external magnetic field) fluctuations entering the $1/T_2$ theory. The assumption should be valid for an isotropic Heisenberg magnetic system.

By replacing the effective correlation time $\tau^*(H)$ defined in Equation (3.22) into Equation (3.21) one finally obtains

$$\left(\frac{M_{xy}(0)}{H}\right) \propto \frac{n(T,H)}{n_0} = 1 - A\sqrt{\frac{\Gamma_2(T)}{\Gamma_2^2(T) + \Delta_1^2}} \tag{3.23}$$

where A, a constant parameter, includes the critical value for the detection time of the instrument and the size of the limiting hyperfine interaction, and Δ_1 is ascribed to the gap between the ground state and the first excited state given by Equation (3.15). The experimental results in Figure 3.23(a) are fitted well by Equation (3.23) (see Figure 3.24) in the case of the first level crossing with almost the same parameters Γ_2 and Δ_{01} extracted from the $1/T_1$ fitting, giving the fitting results: $A = 1.5 \times 10^5 (rad/sec)^{1/2} = 2.4(0.2) \times 10^{10} \frac{rad}{sec}$ and $\Delta_{01} = 1.1 \times 10^{10} rad\ Hz = 0.09(0.02)K$, where the assumption of a small anticrossing at the first critical field confirms the $1/T_1$ analysis of the previous

section. Although this model is very approximate, it appears to be able to interpret the wipe-out effect at LC and to confirm the importance of the inelastic mechanism for the NMR parameter.

The other two dips in the $M_{xy}(0)/H$ graph around $\mu_0 H_c$ = 4.4 T and $\mu_0 H_{c2}$ = 6.9 T correspond to the first excited states LC and the second ground state LC, respectively. However, unfortunately the analysis of the wipe-out results for these LCs is more complicate due to the combination of T_2 shortening and broadening effects of the NMR line and will not be attempted here. The broadening effect will be discussed in the following paragraph.

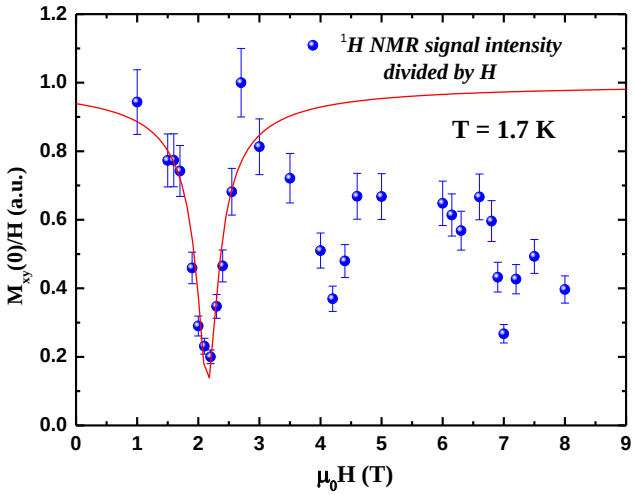

Figure 3.24: The magnetic field dependence of the normalized ^{1}H NMR signal intensity, i.e. $M_{xy}(0)/H$. The solid line is the theoretical curve discussed in the text.

(iii) ^{1}H NMR spectra:

The inhomogeneous broadening occurring at high magnetic field when the molecular ring goes in a magnetic ground state, is shown in Figure 3.25. ^{1}H NMR spectra were collected by using the magnetic field-sweep technique [1] at different fixed Larmor frequencies: before the first ground state level crossing at 51.1 MHz, between the 1st and 2nd ground state LCs at 234.16 MHz, and after the 2nd ground state level crossing at 340.608 MHz.

As shown in Figure 3.17, for fields lower than the first LC ($\mu_0 H < 2.2$ T), the system is in the $S_T = 0$ ground state and the local magnetic moment is very small (see M (H), Figure 3.21). In this field region, the spectral width is due to the nuclear-nuclear dipolar interaction plus an inhomogeneous contribution due to the distribution of local fields generated at the non-equivalent protons sites by the small average moment of the Cr spins resulting from the thermal molecular population of the excited states. The second spectrum (green one), was measured at 234.168 MHz ($\mu_0 H$ = 5.5 Tesla) where the system becomes magnetic ($S_T = 1$) as the result of the first level crossing. In the magnetic state the average moment of the Cr ions is larger and consequently the inhomogeneous broadening becomes also larger and dominant with respect to nuclear dipole-dipole contribution. For fields above the second level

crossing, the ground state becomes $S_T = 2$ and correspondingly the broadening increases. For fields up to 2 Tesla the proton NMR line width is approximately proportional to the external magnetic field as shown in the inset of Figure 3.25, indicating that the molecular ring remains in a paramagnetic state.

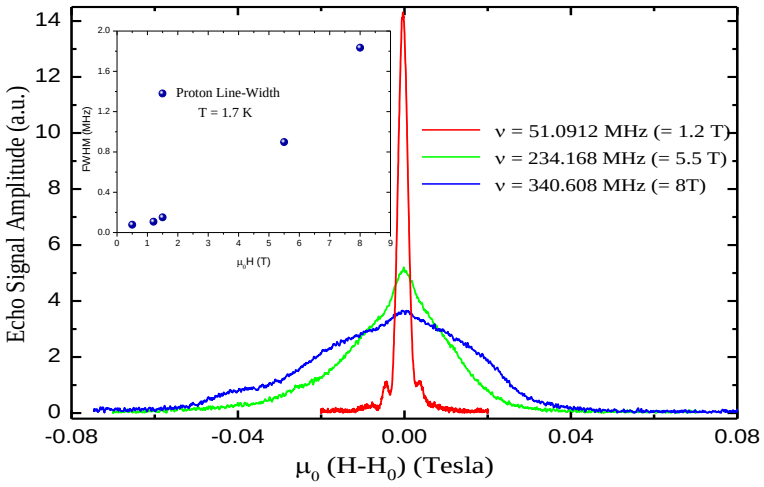

Figure 3.25: Low temperature ^{1}H NMR spectra at three different resonance frequencies, i.e. different magnetic fields. **Inset:** the proton line width as a function of magnetic field at T =1.7 K.

4. Summary and conclusions

The experimental investigation presented in this thesis falls into a broad experimental effort aimed at understanding the magnetic properties and spin dynamics of molecular nanomagnets. The novelty of these molecular systems is given by their nano size, which provides interesting features related to their being halfway between atoms and bulk. More specifically we have studied the properties of some molecular antiferromagnetic (AFM) rings: (a) Semi-integer Cr-based AFM rings, namely Cr_8 and Cr_8Zn, and (b) Integer V-based AFM rings, namely V_7Ni and V_7Zn. In these systems, the finite size produces a discreteness of the energy levels' distribution and every level can be labeled by the quantum number S (corresponding to the total spin of the molecules) and its projection M_S.

The experimental investigation was performed in three different temperature regions: (1) high temperature ($k_BT >> J$), where the magnetic moments in a spin system are weakly correlated and the system behaves like a paramagnet; (2) intermediate temperature ($k_BT \approx J$), where the evolution of the magnetic properties and the spin dynamics of the system reflect the progressively increasing interaction when temperature is lowered down to a very low value, where the system falls in a collective ground state; (3) low temperature ($k_BT << J$), where the system is in the collective ground state with total spin S_T and the quantum level crossings (between $S_T = 0$ and $S_T = 1$, $S_T = 1$ and $S_T = 2$, etc.) induced by a change of the magnetic energy levels spacings as a function of the applied magnetic field due to the Zeeman effect, can be studied.

To this aim we have employed nuclei as local probes of the spin dynamics. This is possible because the nuclear magnetic moments are coupled via hyperfine interaction to the electronic magnetic moments and thus, by measuring the nuclear magnetic parameters, it is possible to gather information about the local magnetic properties of the molecular magnets. Thus, Nuclear Magnetic Resonance (NMR) provides a powerful tool to get microscopic information about the spin dynamics from the analysis of the spin-lattice relaxation rate $1/T_1$, the spin-spin relaxation rate $1/T_2$, and the spectra.

Depending on the applied field and the temperature range of measurements, different novel experimental effects have been detected in the spin-lattice relaxation rate $1/T_1$ (T, H) and in the spectra:

(i) In the high temperature region, i.e. room temperature, the proton spin-lattice relaxation rate ($1/T_1$) as a function of magnetic field (frequency) in the range of $0.2 < H < 9$ Tesla reveals

generally a similar behavior in all selected semi-integer AFM rings, i.e. closed homometallic Cr_8 and Cr_9 rings, and open heterometallic Cr_8Zn and Cr_7Cd rings. In fact it is found that the spin dynamics is dominated by a persistence at long times of the electronic spin correlation due to the boundary conditions, and a large cut-off frequency which masks a possible spin diffusion behavior. Nevertheless the $1/T_1$ curve in Cr_8Zn, where the cut-off frequency is lower, seems to indicate that there may be a narrow field (frequency) range in which spin diffusion can be detected, in analogy with one dimensional (1D) Heisenberg magnetic chains. The same measurements performed in integer AFM rings (V_7M) indicate a similar behavior for both closed V_7Ni ring and open V_7Zn ring. However, it is found that the V based rings have in general a lower cut-off field (frequency) than the corresponding Cr based rings and thus they show a wider field range in which spin diffusion may be detected. The lower cut-off field in V rings could be due to the different local anisotropy of V^{3+} ions vs. Cr^{3+} ions, and/or the difference between the spin values, i.e. s = 1 for V^{3+} ions and s = 3/2 for Cr^{3+} ions, and/or a different intermolecular interaction. To learn more about spin diffusion effects, measurements in AFM rings of bigger size and/or lower anisotropy and at very high magnetic field would be desirable, as well as a theoretical investigation about the physical origin of the cut-off frequency.

(ii) At intermediate temperature, for different fields as a function of temperature in the range of $1.5 < T < 300$ K the proton spin-lattice relaxation rate, $1/T_1$, shows (for all the semi-integer and integer AFM rings investigated) a peak at a temperature close to $T_0(H) = J/k_B$. When the external applied magnetic field is increased the peak position shifts towards higher temperature and its intensity decreases. This fact suggests that the peak in the spin-lattice relaxation rate is related to a progressive slowing down of the electronic fluctuations till they match the nuclear Larmor frequency producing an enhancement in the transition probability between the nuclear states and consequently in the relaxation rate.

In the case of semi-integer AFM rings, both Cr_8 and Cr_8Zn display an additional small anomaly at low temperature (less than 4 K) which well resolves in a peak only in Cr_8Zn.

To explain the behavior of $1/T_1$ in the whole temperature range ($1.5 < T < 300$ K) a BPP-like formula with two different Lorentzian contributions (pertaining to two different correlation times, each one dominating in different temperature ranges), is used to reproduce the experimental data in semi-integer AFM rings. Every contribution is characterized by a correlation frequency which is interpreted as a life time broadening of the magnetic energy levels. The high T peak is fitted by using a correlation frequency $\omega_c \sim C \cdot T^{3.5}$ common to most AFM rings and interpreted as due to direct spin-phonon processes in the relaxation of the molecular magnetization. On the other hand the low T (less than 4 K) peak is fitted by a different correlation frequency $\omega_{c'} \sim C \cdot T^7$, whose temperature dependence could be qualitatively explained as the result of the Raman spin-phonon relaxation processes.

In the case of integer-spin AFM rings (i.e. V_7Zn and V_7Ni) we find a peak at a temperature of the order of the exchange interaction J as in all other AFM rings. A fit by using the usual BBP type expression with a single correlation frequency $\omega_c \sim C \cdot T^{3.5}$ reproduces the shape and the position of the peak but not the H dependence of the height. We propose that the disagreement can be due to either to an experimental artifact related to the signal loss as the temperature is lowered the broadening and/or shortening of the relaxation rates or a spin correlation function different from a simple exponential, thus resulting in a non-Lorentzian behavior of $1/T_1(T)$.

(iii) In the intermediate temperature region, the proton NMR spectral line width as a function of temperature in both integer and semi-integer AFM rings displays a magnetic field and temperature dependence which reflects the static magnetic properties of the molecular rings. In particular the full width at half maximum (FWHM) of the proton NMR spectra vs. temperature is approximately proportional to the magnetic susceptibility (except in the very low temperature region) indicating a dominant contribution coming from the hyperfine interaction of the nuclei with the electronic spins.

(iv) At low temperature (T~ 1.7 K), in the Cr_8Zn ring an enhancement of the $1/T_1(\mu_0 H)$ was found at the level crossing fields, i.e. $\mu_0 H_1 = 2.15$ T and $\mu_0 H_2 = 6.85$ T, corresponding to the first and second ground state level crossing respectively. The $1/T_1(H)$ peak at level crossings, has its origin in the exchange of energy among nuclear and electronic systems (inelastic term in $1/T_1$) occurring when the transition between states with different total spin value S, for gap values near to zero, is allowed. The $1/T_1$ at the first crossing between the non-magnetic ground state $S_T = 0$ and the magnetic state $S_T = 1$ shows a sharp and narrow peak, while at the second level crossing between magnetic states, i.e. $S_T = 1$ and $S_T = 2$ it presents a broad and small peak. Both anomalies can be reproduced by using a simple semi-phenomenological model that confirms the presence of both quasi-elastic and inelastic terms in the spin-lattice relaxation rate (this model has been also used to explain data at very low temperature in AFM rings like Cr_8 and Fe_{10}). From the data fitting, it is found that there is a small energy gap between the ground state $S_T = 0$ and the first excited state $S_T = 1$ ($\Delta_{01} = 0.09$ K) and a bigger energy gap between $S_T=1$ and $S_T = 2$ at the second ground state level crossing ($\Delta_{01} = 0.6$ K). The values of Δ_{01} and Δ_{02} calculated by using the $1/T_1(\mu_0 H)$ experimental data, are different from the ones estimated by means of other techniques like high field torque and specific heat measurements. By adding the J-strain effect into the theoretical analysis of the nuclear relaxation data, we found new values of Δ_{01} and Δ_{02} which are in agreement with the thermodynamic results.

(v) At low temperature, the measured proton NMR signal intensity $M_{xy}(0)$ divided by the applied magnetic field, plotted vs. field, indicates the loss of the NMR signal intensity around the level crossing fields, at both the ground state and the first excited state level crossing. This “wipe-out effect” was previously observed in molecular nanomagnet in the

temperature dependent measurements i.e. from $M_{xy}(0)*T$ vs. temperature (and we observe it as well in our systems). The low-temperature loss of signal reported here, represents the first observation of the wipe-out effect as a function of magnetic field due to the slowing down of the spin fluctuations by approaching the level crossing fields.

(vi) At low T, the experimentally measured ^1H NMR spectra show a progressive broadening due to the transition between different magnetic ground states caused by successive level crossings. When the molecule is mostly in the $S_T = 0$ ground state the spectrum is very sharp and its width is due to the contribution coming from the nuclear-nuclear dipolar interaction plus an inhomogeneous contribution due to the distribution of local fields, generated at the non-equivalent protons sites by the small average moment of the Cr spins. When the system becomes magnetic as the result of the level crossing ($S_T = 0 \rightarrow S_T = 1$, and $S_T = 1 \rightarrow S_T = 2$ crossings), the average magnetic moment becomes larger and consequently the inhomogeneous broadening becomes also larger and dominant with respect to nuclear dipole-dipole contribution.

By concluding, the present thesis has led to progresses in the understanding of the spin dynamics of open and closed AFM rings at high, intermediate and low temperature, in the case of magnetic ions with semi-integer or integer spins. It has also led to a better understanding of quantum effects at the level crossing fields for the situation of true crossing and anti-crossing.

Appendix 1:

Spin Correlation function in terms of collective **q**-variable

To describe the spin dynamics of strongly correlated spin systems usually a formalism in terms of collective q-variables is adopted [1]. Even though a description in q-space may not be entirely applicable in the case of finite number of interacting spins, in this appendix we give a brief description of this formalism. It is possible to introduce a Fourier representation of the spin components in the reciprocal space in a way similar to that adopted in studying the normal modes of a harmonic crystal as below [2]

$$s_q^\alpha = \frac{1}{\sqrt{N}} \sum_i s_i^\alpha \, e^{i\boldsymbol{q}\cdot\boldsymbol{r}_i} \qquad (A_1.1)$$

where N is the number of spins considered. If we assume a translational invariance of the lattice, the correlation function can be expressed as:

$$G^{\alpha\gamma}(\boldsymbol{r}_{ij}, t) = \langle s_i^\alpha(0) s_j^\gamma(t)\rangle = \sum_q \langle s_{-q}^\alpha(0) s_q^\gamma(t)\rangle \, e^{-i\boldsymbol{q}\cdot\boldsymbol{r}_{ij}} \qquad (A_1.2)$$

and in the reciprocal space:

$$F^{\alpha\gamma}(\boldsymbol{q}, t) = \langle s_{-q}^\alpha(0) s_q^\gamma(t)\rangle = \sum_{ij} \langle s_i^\alpha(0) s_j^\gamma(t)\rangle \, e^{i\boldsymbol{q}\cdot\boldsymbol{r}_{ij}} \qquad (A_1.3)$$

The space-time Fourier transform of the correlation function in Equation (2.19) gives the dynamical structure factor

$$S^{\alpha\gamma}(\boldsymbol{q}, \omega) = \int_{-\infty}^{+\infty} F^{\alpha\gamma}(\boldsymbol{q}, t) e^{-i\omega t} dt \qquad (A_1.4)$$

$$S^{\alpha\gamma}(\boldsymbol{q}, \omega) = \sum_{ij} \int_{-\infty}^{+\infty} \langle s_i^\alpha(0) s_j^\gamma(t)\rangle e^{-i(-\boldsymbol{q}\cdot\boldsymbol{r}+\omega t)} dt$$

that represents the spectral density of the spin fluctuations in reciprocal space.

Appendix 2:

A modified BPP-like formula with a distribution of correlation frequencies

As mentioned in chapter 3, in addition to the BPP model, we also tried [1] to fit the spin-lattice relaxation rate data for V-based ring at intermediate temperature (see section 3.3.2(ii)) using a more refined model [2, 3], based on the consideration that the spectral density of the correlation function is made of a sum of Lorentzian functions with different correlation frequencies $\omega_c^{(i)}$. This of course corresponds to assume that the correlation function is dominated by more than one correlation time. As the theoretical model for V-rings is still not setup, we simulated the presence of more than one correlation time with a distribution of correlation frequencies. In this case we can write:

$$\frac{1}{T_1\chi T} = A\int \frac{\omega_{cM}}{\omega_{cM}^2+\omega_L^2}\cdot P(\omega)d\omega \qquad (A_2.1)$$

where ω_{cM} is the mean value of the distribution, and $P(\omega)$ is the considered distribution. Two different distributions of the correlation times τ_c ($\tau_c = 1/\omega_c$) were chosen to fit the present experimental data:

The first attempt was made by assuming that the τ_cs present a rectangular distribution in the form of:

$$P(\tau) = \begin{cases} \frac{1}{2\Delta\tau} & for \quad \tau_{cM}-\Delta\tau < \tau < \tau_{cM}+\Delta\tau \\ 0 & otherwise, \end{cases} \qquad (A_2.2)$$

where $\Delta\tau$ is the width of the distribution. By assuming the correlation time to have an exponential behavior: $\tau_c = \tau_0 \exp(\Delta/k_BT)$, the integration variable in $(A_2.1)$ can be changed ($\omega \rightarrow \Delta$), and an analytic solution of the integral can be found. In this case, $1/T_1$ becomes [2]:

$$\frac{1}{T_1\chi T} = \frac{A}{2\omega_L \ln(b)}\cdot\left\{arctg(b\omega_L\tau) - arctg\left(\frac{\omega_L\tau}{b}\right)\right\} \qquad (A_2.3)$$

where A is the fitting constant, independent of both magnetic field and temperature, that represents the strength of the hyperfine field fluctuations at the proton nuclear site; $b = \exp(\delta/T)$ where δ is the width of the rectangular distribution of the energy barrier Δ/k_B.

The second attempt was performed by using a Gaussian distribution of correlation times, τ_c-s. In this case $1/T_1$ becomes [3]:

$$\frac{1}{T_1\chi T} = A\int_{-\infty}^{+\infty} dE\,\frac{1}{\sqrt{2\pi\sigma}}\exp\left(-\frac{(E-E_c)}{2\sigma^2}\right)\frac{\omega_c}{\omega_c^2+\omega_L^2} \qquad (A_2.4)$$

where A is the arbitrary constant proportional to the square of the hyperfine fields fluctuations at the proton nuclear sites, E is the energy barrier, E_c and σ are the mean and the standard division of the energy distribution, and $\tau_c = \tau_0 \exp(\Delta/k_B T)$. Equation $(A_2.4)$ cannot be analytically solved and a numerical method to evaluate the integral must be used. The fitting curves according to the distribution models, i.e. Equations $(A_2.3)$ and $(A_2.4)$, are not displayed as the agreement with the experimental data is very poor.

Bibliography

Overview and Introduction:

[1] T. Lis, Acta Crystallogr. Sect. B **36** (1980) 2042-2046

[2] R. Sessoli, D. Gatteschi, A. Caneschi and M. A. Novak, Nature **365** (1993) 141-143.

[3]R. Sessoli, H.-L. Tsai, A. R. Shake, S. Wang, J. B. Vincent, K. Folting, D. Gatteschi, G. Christou and D. N. Hendrickson, J. Am. Chem. Soc. **115** (1993) 1804-1816.

[4] C. Delfs, D. Gatteschi, L. Pardi, R. Sessoli, K. Weighardt, and D. Hanke, Ingorg. Chem. **32** (1993) 3099-3103.

[5] D. Gatteschi, A. Caneschi, L. Pardi, and R. Sessoli, Since **265** (1994) 1054-8.

[6] P. C. E. Stamp, Nature (London) **383** (1996) 125-127.

[7] C. Sangregorio, T. Ohm, C. Paulsen, R. Sessoli and D. Gatteschi, Phys. Rev. Lett. **78** (1997) 4645-4648

[8] J. R. Friedman, M. P. Sarachik, J. Tejada and R. Ziolo, Phys. Rev. Lett. **76** (1996) 3830-3833 , see also L. Thomas, F. Lionti, R. Ballou, D. Gatteschi, R. Sessoli and B. Barbara, Nature (London) **383** (1996) 145-147.

[9] D. Gatteschi and R. Sessoli, *"Magnetism: Molecules to Material III"* edited by J. S. Miller and M. Drillon (Wiley-VHC, Verlag GmbH, Weinheim, 2002).

[10] D. Gatteschi, and R. Sessoli, Angew. Chem. Int. Ed **42** (2003) 268-297.

[11] I. Tupitsyn and B. Barbara, *"Magnetism: Molecules to Material III"* edited by J. S. Miller and M. Drillon (Wiley-VHC, Verlag GmbH, Weinheim, 2002).

[12] M. Luis, F. L. Mettes and L. Jos de Jongh, *"Magnetism: Molecules to Material III"* edited by J. S. Miller and M. Drillon (Wiley-VHC, Verlag GmbH, Weinheim, 2002).

[13] Y. Furukawa, K. Watanabe, K. Kumagai, F. Borsa, T. Sasaki, N. Kobayashi, and D. Gatteschi, Phys. Rev. B **67** (2003) 064426-7; K. Watanabe, Y. Furukawa, k. Kumagai, F. Borsa, D. Gatteschi, Mol. Cryst. Liq. Cryst. **379** (2002) 185-190

[14] W. Wernsdorfer, *"Handbook of Magnetism and advanced Materials"* Edited by H. Kronmüller and S. Parkin. Volume 4: Novel Materials (John Wiley & Sons, Ltd. ISBN: 978-0-470-02217-7, 2007)

[15] A. Chiolero, and D. Loss, Phys. Rev. Lett. **80** (1998) 169-172

[16] F. Meier, and D. Loss, Phys. Rev. Lett. **86** (2001) 5373-5376

[17] A. Honecker, F. Meir, D. Loss and B. Normand, Eur. Phys. J. B **27** (2002) 487-495

[18] P. Santini, S. Carretta, G. Amoretti, T. Guidi, R. Caciuffo, A. Caneschi, D. Rovai, Y. Qiu, J. R. D. Coley, Phys. Rev. B **71** (2005) 184405-7

[19] F. Borsa, A. Lascialfari, Y. Furukawa, "*In Novel NMR and EPR Techniques"*, edited by Dolinsek J, Vilfan M, Zumer S (Springer, New York, 2006) pp 304-355

Chapter 1:

[1] N. Gerbeleu, I. Struchkov, G. Timko, A. Batsanov, K. Indrichan and G. Popovich, Dokl. Akad. Nauk. SSSR, **313** (1990) 1459–1462.

[2] E. J. L. McInnes, S. Piligkos, G. A. Timco, and R. E. P. Winpenny, Coord. Chem. Rev. **249** (2005) 2577-2590.

[3] F. Meier and D. Loss, Phys. Rev. Lett., **86** (2001) 5373–5376.

[4] C.-F. Lee, D. A. Leigh, R. G. Pritchard, D. Schultz, S. J. Teat, G. A. Timco and R. E. P. Win- penny, Nature, **458** (2009) 314–318.

[5] B. Ballesteros, T. B. Faust, C.-F. Lee, D. A. Leigh, C. A. Muryn, R. G. Pritchard, D. Schultz, S. J. Teat, G. A. Timco and R. E. P. Winpenny, J. Am. Chem. Soc., **132** (2010) 15435–15444.

[6] A. Abragam, *"Principle of nuclear Magnetism"* Ed. Clarendon Press, Oxford (1961).

[7] S. Blundell *"Magnetism in condense matter"* Oxford, New York (2001)

[8] A. Messiah, *"Mècanique Quantique",* Dunod, Paris (1960)

[9] The energy states with different total-spin S are mixed because of many different contributions in the spin Hamiltonian. Therefore in order to diagonalize the full matrix of the system, one should exploit algorithms of parallel computing. However, since the information contained in the most experimental data involves only levels thermally occupied at very low temperatures this approach would be quite useless. So, Indeed a perturbative approach should employ because in AFM rings the exchange interaction is almost always the dominate interaction (see Chapter 2).

[10] J. Schnack, M. Luban, Phys. Rev. B **63** (2000) 014418-7

[11] O. waldmann, T. Guidi, S. Carretta, C. Mondelli, and A. L. Dearden, Phys. Rev. Lett. **91** (2003) 237202-4

[12] Y. Furukawa, K. Kiuchi, K. Kumagai, Y. Ajiro, Y. Narumi, M. Iwaki, K. Kindo, A. Bianchi, S. Carretta, G. A. Timco and R. E. P. Winpenny *Phys. Rev. B* **78** (2008) 092402-4. See also.,T. Guidi, B. Gillon, S. A. Mason, E. Garlatti, S. Carretta, P. Santini, A. Stunault, G. Caciuffo, J. V. Slageren, B. Klemke, A. Cousson, G. A. Timco and R. E. P. Winpenny, *Nature Communication* (2015) **6** 7061 . doi: 10.1038/ncomms8061.

[13] J. Van Slageren, R. Sessoli, D. Gatteschi, A. A. Smith, M. Helliwell, R. E. P. Winpenny, A. Cornia, A. barra, A. G. M. Jansen, E. Rentscheler and G. A. Timco, Chem.Eur. J. **8** (2002) 277-285

[14] B. Ballesteros, T. B. Faust, C-F Lee, D. A. Leigh, C. A. Muryn, R. G. Pritchard, D. Schultz, S. J. Teat, G. A. Timco, and R. E. P. Winpenny, J. AM. Chem. Soc **132** (2010) 15435-15444

[15] G. A. Timco, A. S. Batsanov, F. K. Larsen, C. A. Muryn, J. Overgaard, S. J. Teat and R. E. P. Winpenny, Royal Society of Chemistry, Chem. Commun., (2005) 3649-3651

[16] A. Bianchi, S. Carretta , P. Santini, G. Amoretti, T. Guidi, Y. Qiu, G. R. D Copley, G. Timco, C. Muryn and R. E. P Winpenny, Phys. Rev. B **79** (2009) 144422-6

[17] J-P. Boucher, M. Ahmed bakheit, M. Nechtschein, M. Villa, G. Bonera, and F. Borsa, Phys. Rev. B **13** (1976) 4098-13

[18] Mozzati M C et al., unpublished.

[19] F. Adelnia, L. Bordonali, M. Mariani, S. Bordignon. G. Timco, R. Winpenny, F. Borsa, and A. Lascialfari, J. Phys.: Condens. Matter **27** (2015) 506001 (8pp)

[20] E. Micotti, A. Lascialfari, F. Borsa, M. H. Julien, C. Berthier, M. Horvatić, J. van Slageren, and D. Gatteschi, Phys. Rev. B **72** (2005) 020405(R)

[21] M. Affronte, T. Guidi, R. Caciuffo, S. Carretta, G. Amoretti, J. Hinderer, I. Sheikin, A. G. M. Jansen, A. A. Smith, R. E. P. Winpenny, J. van Slageren, and D. Gatteschi, Phys. Rev. B **68** (2003) 104403-5

[22] F. Adelnia, A. Chiesa, S. Bordignon, S. carretta, A. Ghirri, A. Candini, C. Cervetti, M. Evangelisti, M. Affronte, I. Sheikin, R. Winpenny, G. Timco, F. Borsa, and A. Lascialfari, J. Chem. Phys **143** (2015) 244321-10

[23] J. P. Walsh, *"Anisotropy in molecular magnetism",* School of Chemistry, University of Manchester (2014) pp: 95-100

[24] F. Troiani, A. Ghirri, M. Affronte, S. Carretta, P. Santini, G. Amoretti, S. Piligkos, G. Timco, and R. E. P. Winpenny, Phys. Rev. Lett. **94** (2005), 207208-4

[25] PHI is a computer program designed for the calculation of the magnetic properties, of paramagnetic coordination complexes. It is based on the construction and diagonalization of the Hamiltonian matrix that describes the system under study, from which it is possible to obtain different variables of physical interest such as susceptibility, magnetization, heat capacity, energy levels, etc. see also, N. F. Chilton, R. P. Anderson, L. D. Turner, A. Soncini, and K. S. Murray, J. Comput. Chem. **34** (2013) 1164-1175

[26] A. Radaelli, "*Magnetic properties and spin dynamics of integer-spin AFM rings"*, Università degli studi di Milano (2015). Codice P.A.C.S: **76.60.-k**

Chapter 2:

[1] C. P. Slichter, *"Principles of Magnetic Resonance",* Springer-Verlag Berlin Heidelberg, (1990) pp: 145-218.

[2] E. Fukushima, S. B. W. Roeder *"experimental Pulse NMR; a Nuts and Bolts Approach",* Addison-Wesley Company, Inc. (1981) pp: 47-96

[3] E. M. Haacke, R. W. Brown, M. R. Thompson and R. Venkatesan, *"Magnetic Resonance Imaging: Physical Principle and sequence design"* Wily-Liss, New York (1999)

[4] A. G. Redfield IBM. Res. Dev. **1** (1957) 19

[5] R. C. Tolman *"The Principle of Statistical Mechanics",* Oxford University Press, New York (1946)

[6] T. Moriya, Prog. Theor. Phys. **16** (1956) 23-44. See also, e.g., T. Moriya Prog. Theor. Phys. **28** (1962) 371-400

[7] S. Alexander and A. Tzalmona Phys. Rev. 138 (1965) A845; see also A. Rigamonti and J. R. Brookman, Phys. Rev. B **21** (1980) 2681

[8] C. P. Slichter and D. Ailion, Phys. Rev, (1964) A1099; see also D. Ailion and C. P. Slichter, Phys. Rev. **137** (1965) A235

[9] S. H. Baek, F. Borsa, Y. Furukawa, Y. Hatanaka, S. Kawakami, K. Kumagai, B. J. Suh and A. Cornia, Phys. Rev. B **71** (2005) 214436

[10] The spin-spin Correlation Function (CF) describes how the random spin fluctuations of a spin affect the temporal fluctuations of another spin in a different site or the spin in the same site (auto-correlation). These correlations are a consequence of the various interactions (exchange, dipolar, hyperfine and etc.) which couple different spins in a spin system. The investigation of the spin dynamics of the system is essentially the issue of studying the time evolution of the spin-spin correlation function. One of the aims of the NMR investigation is to study how the spin-spin CF changes as a

function of the external magnetic field H_0 and the temperature T. R. Sessoli, D. Gatteschi, A. Caneschi and M. A. Novak, Nature **365** (1993) 141.

[11] A. Abragam, "Principle of nuclear Magnetism" Ed. Clarendon Press, Oxford (1961)

[12] F. Borsa, A. Lascialfari, Y Furukawa, "*In Novel NMR and EPR Techniques"*, edited by J. Dolinsek, M. Vilfan, S. Zumer (Springer, New York) 2006 pp 304-355

[13] F. Borsa, M. Mali, Phys. Rev. B, **9**, 2215, (1974)

[14] L. P. Kadanofi, P. C. Martin, Ann. Phys., **49**, 419, (1963)

[15] J. P. Boucher, M. Ahmed Bakheit, M. Nechtschein, M. Villa, G. Bonera, and F. Borsa, Phys. Rev. B **13**, 4098 (1976).

[16] M. Takigawa, T. Asano, Y. Ajiro, M. Mekata, and Y. J. Uemura, Phys. Rev. Lett. **76** (1996) 2173-2176

[17] J. Tang, S. N. Dikshit and J. R. Norris, J. Chem. Phys **103** (1995) 2873-2881

[18] A. Abragam, *"Principle of nuclear Magnetism"* Ed. Clarendon Press, Oxford (1961) pp: 541-583

[19] I. Rousochatzakis, A. Lauchli, F. Borsa, and M. Luban, Phys. Rev. B **79** (2009) 064421-5

[20] Robert M. White *"Quantum Theory of Magnetism",* Springer-Verlag, Berlin (2007) 237-274

[21] M. Belesi, F. Borsa, and A. K. Powell, Phys. Rev. B **74** (2006) 184408-6

[22] A. Cornia, A. Fort, M. G. Pini and A. Rettori, EuroPhys. Lett., **50** (1) (2000) pp. 88-93

[23] F. Carboni and P. M. Richards, Phys. Rev., **117** (1969) 889

[24] A. Bencini and D. Gatteschi., *"EPR of Exchange Coupled Systems",* Springer-Verlag, Berlin (1990)

Chapter 3:

[1] L. Bordonali, E. Garlatti, C. M. Casadei, Y. Furukawa, A. Lascialfari, S. Carreta, F. Troiani, G. Timco, R. E. P. Winpenny and F. Borsa, J Chem Phys , **140** (2014) 144306-13.

[2] F. Carboni and M. Richards, Phys. Rev. **177** (1969) 889-904.

[3] D. G. McFadden, R. A. Tahir-Kheli and G. Bruce Taggart, Phys. Rev. **185** (1969) 854-859.

[4] F. B. McLean and M. Blume, Phys. Rev. B **7** (1973) 1149-1179.

[5] G. Müller, Phys. Rev. Lett. **60** (1988) 2785-2788.

[6] F. Borsa, A. Lascialfari, Y. Furukawa, "*In Novel NMR and EPR Techniques"*, edited by Dolinsek J, Vilfan M, Zumer S (Springer, New York, 2006) pp 304-355.

[7] F. Borsa and M. Mali, Phys. Rev. B **9** (1974) 2215-2219

[8] F. Adelnia, M. Mariani, L. Ammannato, A. Cneschi, D. Rovai, R. Winpenny, G. Timco, M. Corti, A. Lascialfari and F. Borsa, Journal of Applied Physics **117** (2015) 17B308-4.

[9] F. Haldane, Phys. Lett. **93A** (1983) 464

[10] M. P. Nightingale and H. W. J. Blote, Phys. Rev. B **33** (1986) 659-661. M. Takahashi, Phys. Rev. Lett. **62** (1989) 2313-2316

[11] O. Golinelli, Th. Jolicceurt and R. Lacazet, J. Phys: Condens. Matter **5** (1993) 1397-1410.

[12] M. Takigawa, T. Asano, Y. Ajiro, M. Mekata, and Y. J. Uemura, Phys. Rev. Lett. **76** (1996) 2173-2176

[13] H. Mutka, C. Payen, P. Molinie, J. L. Soubeyrou, P. Colombet, Phys. Rev. Lett. **67** (1991) 497-500.

[14] M. Takigawa, T. Asano, Y. Ajiro and M. Mekata, Phys. Rev. B **52** (1995) R13087-90.

[15] A Lorentzian expression for $1/T_1$, often called a BPP formula, is widely used in NMR. See e.g., A. Abragam, "*The principle of Nuclear Magnetism"*, (Clarendon, Oxford, 1961), pp 457.

[16] F. Adelnia, L. Bordonali, M. Mariani, S. Bordignon, G. Timco, R. Winpenny, F. Borsa, and A. Lascialfari, J. Phys.: Condens. Matter **27** (2015) 506001-8

[17] H. Amiri, A. Lascialfari, Y. Furukawa, F. Borsa, G. A. Timco, and R. E. P. Winpenny, Phys. Rev. B **82** (2010) 144421-13

[18] C. P. Slichter, "*Principle of Magnetic Resonance"*, Springer, (Verlag, New York, 1996), pp: 65-80

[19] P. Khuntia, M. Mariani, A. V. Mahajan, A. Lascialfari, F. Borsa, T.D. Pasatoiu, and M. Andruh, Phys. Rev. B, **84** (2011) 184439-9

[20] A. Kumar and C. S. J. Johnson, J. Chem. Phys. **60** (1974) 137, see also; J. Humphreys *"A Broad-Line NMR Investigation of Methyl Motion in Poly (Methylmethacrylate)"* polymer **25** (1984) 1227-1234

[21] S-H. Baek, M. Luban, A. Lascialfari, E. Micotti, Y. Furukawa, F. Borsa, J. V. Slageren, and A. Cornia, Phys. Rev. B **70** (2004) 134434-5

[22] N. Bloembergen, E. M. Purcell, and R. V. Pound, Phys. Rev **73** (1948) 679-714

[23] T. Moriya, Prog. Theor. Phys. **16** (1656) 23-44. See, also, e.g., T. Moriya, Prog. Theor. Phys. **28** (1962) 371-400

[24] P. Santini, S. Carretta, E. Liviotti, P. Carretta, M. Filibian, A. Lascialfari, and E. Micotti, *Phys. Rev. Lett* **94** (2005) 077203-4

[25] I. Rousochatzakis, A. Lauchli, F. Borsa, and M. Luban, Phys. Rev. B **79** (2009) 064421-5

[26] A. Bianchi, S. Carretta, P. Santini, G. Amoretti, J. Lago, M. Corti, A. Lascialfari, P. Arosio, G. Timco, and R. E. P. Winpenny, Phys. Rev. B **82** (2010) 134403-7

[27] C. Kittel, "*Introduction to solid state physics"* (John Wiley & Sons, Inc 2005) chapter 13 pp 366-370

[28] M. Belesi, A. Lascialfari, D. Procissi, Z. H. Jang, and F. Borsa, Phys Rev B **72**, (2005) 014440.

[29] (a) A. Radaelli, "*Magnetic properties and spin dynamics of integer-spin AFM rings"*, Università degli studi di Milano (2015). Codice P.A.C.S: **76.60.-k.** (b) J. P. Walsh, *"Anisotropy in molecular magnetism",* School of Chemistry, University of Manchester (2014) pp: 95-100

[30] E. Garlatti, S. Bordignon, S. Carretta, G. Allodi, G. Amoretti, R. De Renzi, A. Lascialfari, Y. Furukawa, G. A. Timco, R. Woolfsan, R. E. P. Winpenny, and P. Santini, Phys. Rev. B. **93**, (2016) 024424-9.

[31] D. Procissi, P. Arosio, F. Orsini, M. Marinone, A. Corenia, and A. Lascialfari, Phys. Rev. B **80** (2009) 094421-6

[32] T. Orlando, A. Capozzi, E. Umut, L. Bordonali, M. Mariani, P. Galinetto, F. Pineider, C. Innocenti, P. Masala, F. Tabak, M. Scavini, P. Santini, M. Corti, C. Sangregorio, P. Ghigna, and A. Lascialfari, J. Phys. Chem. C **119** (2015) 1224-1233

[33] A. Bianchi, S. Carretta, P. Santini, G. Amoretti, Y. Furukawa, K. Kiuchi, Y. Ajiro, Y. Narumi, K. Kindo, J. Lago, E. Micotti, P. Arosio, A. Lascialfari, F. Borsa, G. Timco, and R. E. P. Winpenny, J. MMM **322** (2010) 1262-1264

[34] E. Micotti, A. Lascialfari, F. Borsa, M. H. Julien, C. Berthier, M. Horvatić, J. van Slageren, and D. Gatteschi, Phys. Rev. B **72** (2005) 020405(R)-4

[35] A. Cornia, A. Fort, M. G. Pini and A. Rettori, EuroPhys. Lett., **50** (1) (2000) pp. 88-93

[36] M. Luban, F. Borsa, S. Bud'ko, S. Jun, J. K. Jung, P. Kögerler, D. Mentrup, A. Müller, R. Modler, D. Procissi, B. J. Sun and M. Torikachvili, Phys. Rev B **66** (2002) 054407

[37] F. Adelnia, A. Chesa, S. Bordignon, S. Carretta, A. Ghirri, A. Candini, C. Cervetti, M. Evangelisti, M. Affronte, I. Sheikin, R. Winpenny, G. Timco, F. Borsa and A. Lascialfari, J. Chem. Phys. **143** (2015) 244321-10

[38] S. Carretta, P. Santini, G. Amoretti, T. Guidi, J. R. D. Copley, Y. Qiu, R. Caciuffo, G. Timco and R. E. P. Winpenny, Phys. Rev. Lett, **98** (2007) 167401-4

[39] A. Abragam, The Principles of Nuclear Magnetism (Clarendon, Oxford, 1961).

[40] C. P. Slichter, Principle of Magnetic Resonance, (Springer-Verlag, Berlin, 1989).

Appendix 1:

[1] F. Borsa and A. Rigamonti, "Magnetic Resonance at Phase Transition", edited by *Frank J. Owens, Charles P. Poole and Horacio A. Farach,* Academic Press, New York (1986) Page: 79-136

[2] G. Grosso and G. Pastori Parravicini, Solid State Physics, Academic Press, Cambridge (200).

Appendix 2:

[1] A. Radaelli, "*Magnetic properties and spin dynamics of integer-spin AFM rings"*, Università degli studi di Milano (2015). Codice P.A.C.S: **76.60.-k**

[2] D. Procissi, P. Arosio, F. Orsini, M. Marinone, A. Corenia, and A. Lascialfari, Phys. Rev. B **80** (2009) 094421-6

[3] T. Orlando, A. Capozzi, E. Umut, L. Bordonali, M. Mariani, P. Galinetto, F. Pineider, C. Innocenti, P. Masala, F. Tabak, M. Scavini, P. Santini, M. Corti, C. Sangregorio, P. Ghigna, and A. Lascialfari, J. Phys. Chem. C **119** (2015) 1224-1233

Publications

- F. Adelnia, L. Bordonali, M. Mariani, S. Bordignon, G. Timco, R. Winpenny, F. Borsa, A. Lascialfari., J. phys.: Condens. Matter 27 (2015) 506001.

"Comparison of spin dynamics and magnetic properties in antiferromagnetic closed and open molecular Cr-based ring"

- F. Adelnia, A. Chiesa, S. Bordignon, S. Carretta, A. Ghirri, A. Candini, C. Cervetti, M. Evangelisti, M. Affronte, I. Sheikin, R. Winpenny, G. Timco, F. Borsa, A. Lascialfari, J. Chem. Phys. 143 (2015) 244321.

"Low temperature magnetic properties and spin dynamics in single crystals of Cr_8Zn antiferromagnetic molecular rings"

- F. Adelnia, M. Mariani, L. Ammannato, A. Caneschi, D. Rovai, R. Winpenny, G. Timco, M. Corti, A. Lascialfari, F. Borsa,. Journal of Applied Physics 117, 17B308 (2015).

"High temperature spin dynamics in linear magnetic chains, molecular rings and segments by NMR".

Acknowledgements

I would like to take the opportunity to express my deep appreciation to everyone who contributed and helped me in various ways during the years I have spent in Italy.

First and foremost, I wish to express my most sincere gratitude to my PhD advisor, Prof. Alessandro Lascialfari. Needless to say, without his guidance, I would not be able to successfully accomplish my PhD. He was at my side at every step of the way, doing everything in his power to advance the project as best as he could. I used to call him my God-father and indeed it is a right statement thanks to his incredible supports and helps since the first day, 13th January, 2013. I do know very well that no words are capable of expressing my deep appreciation. So, please accept my sincerest apologies for incapability of my words. Many many special thanks to Prof. Ferdinando Borsa for his incredible scientific knowledge, brilliant ideas, insightful comments, constructive feedbacks, immense enthusiasm, as well as endless supports. Without his assistance throughout these years, I would not be such proud of my PhD as I am now. I will forever be thankful to him because of his patience for teaching me NMR.

My sincere thanks also go for Prof. Maurizio Corti as well as members of the NMR group in the University of Pavia for their great hospitality and kindness within my experimental times. Furthermore, I would also like to thank Dr. Andrea Zanzani from the University of Milan because of his endless administrative support.

My parents always watched me closely from a distance while I was working towards my degree. The completion of this thesis will mean a lot to them, particularly "seeing more of me". Therefore, I dedicate this project to my beloved parents, whose loves, affections, and encouragements, made this work possible.

Finally, I would like to thank my family and friends who supported me constantly to reach my goals.

Pavia, April 11th 2016